Master's thesis

NTNU
Norwegian University of Science and Technology
Faculty of Information Technology and Electrical Engineering
Department of Computer Science

Tore Bergebakken

HoloNeoDoppler

Augmented Reality Training Application for Monitoring Cerebral Blood Flow in Infants

Master's thesis in Computer Science
Supervisor: Gabriel Kiss
Co-supervisor: Shubham Jain and Frank Lindseth
June 2023

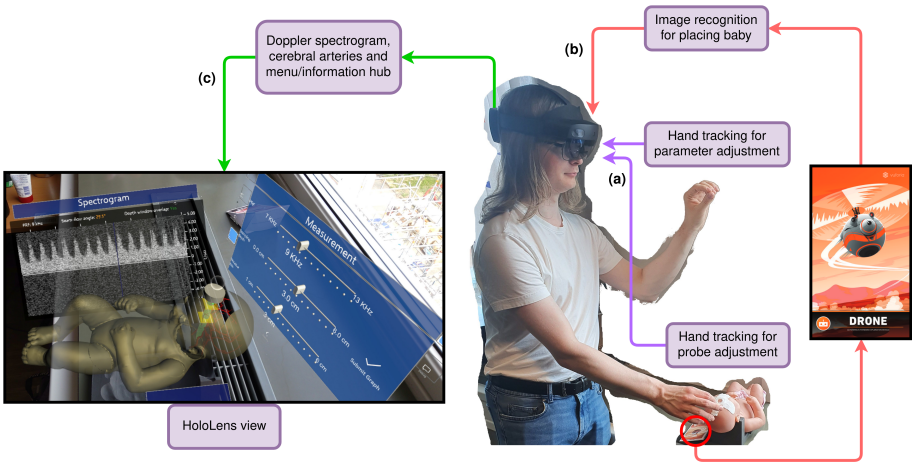

NTNU
Norwegian University of Science and Technology

Tore Bergebakken

HoloNeoDoppler

Augmented Reality Training Application for Monitoring Cerebral Blood Flow in Infants

Master's thesis in Computer Science
Supervisor: Gabriel Kiss
Co-supervisor: Shubham Jain and Frank Lindseth
June 2023

Norwegian University of Science and Technology
Faculty of Information Technology and Electrical Engineering
Department of Computer Science

NTNU
Norwegian University of
Science and Technology

Abstract

In this master thesis, we developed HoloNeoDoppler, a simulation of the NeoDoppler probe that is used to monitor cerebral blood flow (CBF) in infants. Fluctuations in CBF are related to intraventricular hemorrhage (IVH) and other severe problems in the brains of babies that are born too early.

HoloNeoDoppler aims to train medical students and personnel in the proper placement of the NeoDoppler probe while educating them on fundamental concepts of pulsed wave (PW) Doppler ultrasound. It builds upon HoloUmoja, a simulation for obstetric Doppler ultrasound by Nylund.

Before interacting with the simulation, users are provided with information on various aspects of Doppler ultrasound. Within the simulation, users control a virtual probe using their hands, targeting the cerebral arteries through the anterior fontanelle. The cerebral arteries are modeled using Bézier curves and tested for intersection with a ray projected from the probe to determine the insonation angle, while accounting for the adjustable depth window. Unlike HoloUmoja, this simulation uses hand tracking and a purely virtual model of the subject, which *can* be superimposed onto a physical model (see Figure 1). The ultrasound beam responds to changes in signal and angle by changing color, while simulated ultrasound signals are displayed on a realistic spectrogram that changes resolution based on the chosen pulse repetition frequency (PRF). The spectrogram is generated from a snippet of an actual blood velocity curve and has background and signal noise to appear like a real spectrogram.

To evaluate the effectiveness of the project, user tests with medical students (n=14) were conducted. These tests verified the simulation's usefulness and revealed some points of improvement. All participants were able to capture Doppler spectrograms that were considered clinically relevant by an expert sonographer, with 12 out of 14 succeeding on both attempts. The tests also confirmed that the ultrasound information provided in the application was useful.

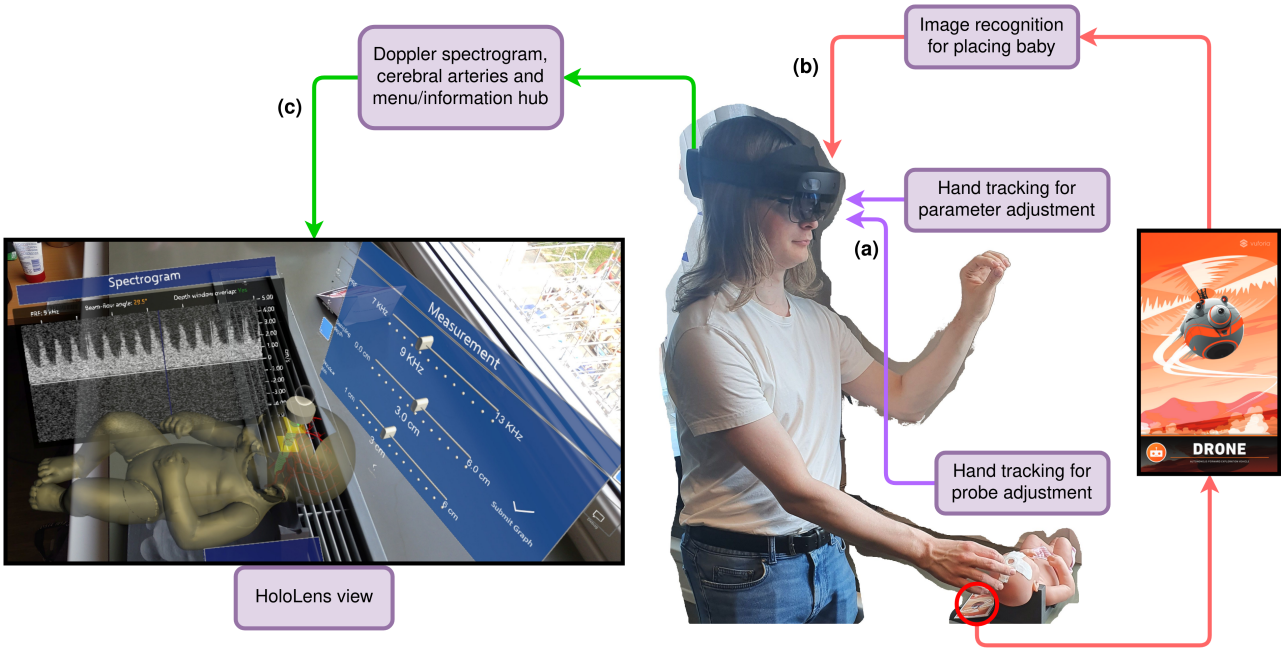

Figure 1: Overview of HoloNeoDoppler.
(a) Hand tracking enables users to interact with the probe and the menu.
(b) Image tracking anchors the baby model to a surface. Here shown together with the 3D printed stand for the baby doll.
(c) The user's interactions affect the holograms that they see: A Doppler spectrogram, an immaterial baby model with cerebral arteries, and a menu with information and adjustable parameters.

Sammendrag

I denne masteroppgaven utviklet vi HoloNeoDoppler, en simulering av NeoDoppler-proben, en ultralydprobe som brukes til å overvåke blodstrømmen i hjernen til nyfødte barn. Kraftige svingninger i denne blodstrømmen har blitt knyttet til intraventrikulære blødninger (IVH) og andre problemer i hjernene til for tidlig fødte barn. Formålet med HoloNeoDoppler er å lære opp medisinstudenter og medisinsk personell i å plassere NeoDoppler-proben korrekt, samtidig som de lærer grunnleggende konsepter for pulset (PW) Doppler-ultralyd. Prosjektet bygger på HoloUmoja, en tidligere masteroppgave skrevet av Nylund for simulering av obstetrisk Doppler-ultralyd.

Før brukerne interagerer med simuleringen får de servert informasjon om pulset Doppler-ultralyd. I selve simuleringen kan brukerne flytte på en etterligning av NeoDoppler-proben med fingrene sine for å treffe blodårer gjennom pannefontanellen. Blodårene er modellert med Bézier-kurver og innfallsvinkelen beregnes ved å finne skjæringspunkt mellom blodårene og en stråle sendt fra proben, samtidig som det tas hensyn til det justerbare dybdevinduet. I motsetning til HoloUmoja bruker denne simuleringen håndsporing og en fullstendig virtuell modell av subjektet, som *kan* legges oppå en fysisk modell (se Figure 2). Ultralydstrålen endrer farge basert på innfallsvinkelen, og simulerte signaler vises på et realistisk spektrogram som endrer oppløsning basert på den justerbare pulsrepetisjonsfrekvensen (PRF). Spektrogrammet blir generert ved å legge til støy på en hastighetskurve for en reell blodstrøm, med bakgrunnsstøy for å få spektrogrammet til å se ekte ut.

Det ble avholdt brukertester med medisinstudenter (n=14) for å evaluere prosjektet. Testene verifiserte brukbarheten til simuleringen og åpenbarte noen områder som kunne forbedres i fremtiden. Alle deltakerne klarte å få Doppler-spektrogrammer som ble ansett som klinisk relevante av en sonografiekspert, og 12 av 14 fikk begge forsøkene sine godkjent. Testene bekreftet også at den pedagogiske ultralydinformasjonen hadde god læringsverdi.

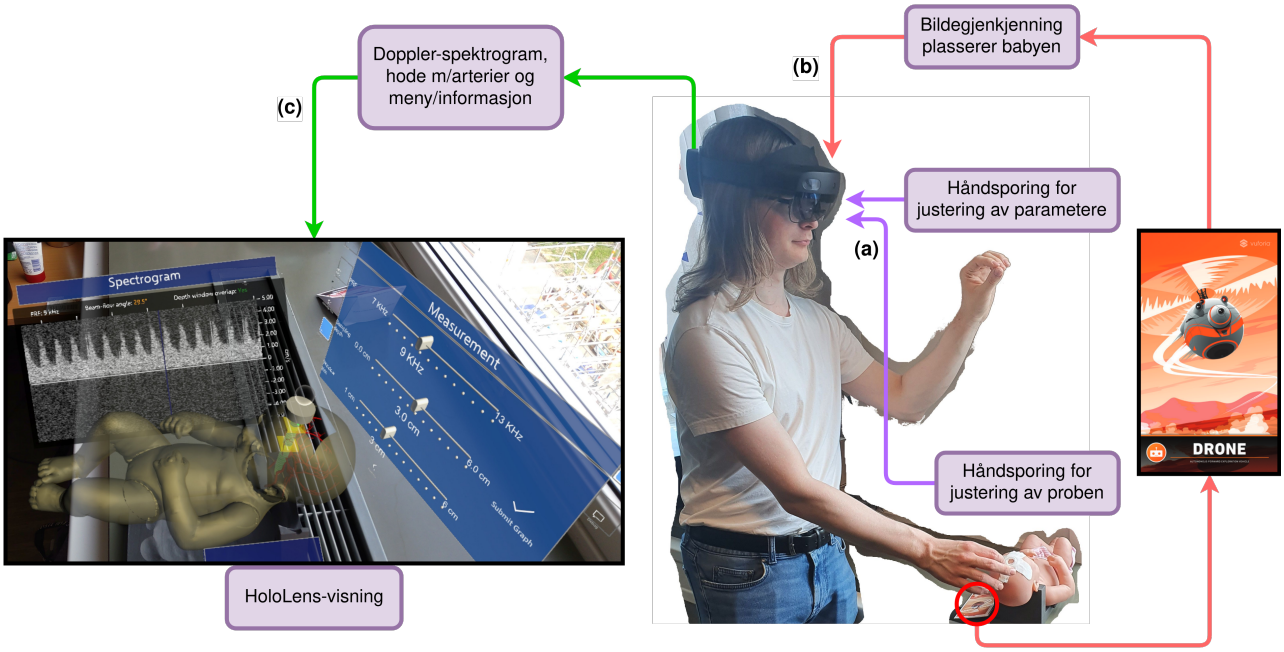

Figure 2: Oversikt over HoloNeoDoppler.
(a) Håndsporing lar brukerne interagere med proben og menyen.
(b) Bildesporing forankrer den virtuelle babymodellen til et punkt i den virkelige verden. Her ser vi også den 3D-printede holderen til den fysiske babydukken.
(c) Brukernes bevegelser påvirker hologrammene de ser: Et Doppler-spektrogram, en babymodell med blodårer i hjernen og en meny med informasjon og justerbare parametere.

Acknowledgements

I would like to thank

- Gabriel Kiss, my main supervisor, for helpful advice and reassuring statements
- Hans Torp and Siri Ann Nyrnes, for creating NeoDoppler and answering my medical questions
- Shubham Jain, my secondary supervisor, for assistance with planning and conducting user tests
- Frank Lindseth, my other secondary supervisor, for providing feedback and advice
- Maria Nylund, who wrote the HoloUmoja project, for help with getting the project up and running, as well as miscellaneous advice on Unity and HoloLens
- Fredrik Eiding, for Unity advice and the suggestion to use Bézier curves for blood flow direction
- The rest of the game project group in Hackerspace NTNU, for sharing their knowledge about Unity
- Thomas Bakken Moe, Helene Yuee Jonson and others for emotional support

Contents

Figures

Tables

Code Listings

Acronyms

AR Augmented Reality. xiv, xv, 1, 5, 6, 30, 33, 53, 65, 75, 86, 90

ASQ After Scenario Questionnaire. xiv, xv, 34, 71, 73, 75–78, 85, 86

BLE Bluetooth Low Energy. 16, 18, 31, 33, 54, 83

CBF Cerebral Blood Flow. iii, 4, 5, 13

FFT Fast Fourier Transform. 20, 22, 23

HMD Head-Mounted (stereoscopic) Display. 5, 15

IVH IntraVentricular Hemorrhage. iii, v, 7, 30

MRTK Mixed Reality ToolKit. 33, 39

PRF Pulse Repetition Frequency. iii, v, xiv, 12, 13, 16, 32, 52, 53, 55, 57, 61, 71, 73, 82–84, 90

PW Pulsed Wave. iii, v, 11, 12, 52, 87

TAM Technology Acceptance Model. xiv, 34, 70

UI User Interface. 33, 73

VR Virtual Reality. 5, 79, 90

XR Extended Reality. 5, 33

Glossary

anterior Frontal. iii, 1, 6, 32

artery Blood vessel that transports oxygen-rich blood out to organs. High pressure. iii, 1, 6, 11, 31

construct Concept that is investigated in a survey, preferably represented in multiple questions. 34, 35

fontanelle Soft gap in the less developed skull of an infant [2]. iii, 1, 6, 32, 37

gizmo Visual indicators for developers that can be added to Unity objects and only show up in the editor. 40

Likert scale Ordinal scale that measures attitude in surveys. Created by Likert [3, 4]. 34, 107

retroreflective Reflects light directly back to the light source [5]. 15, 53, 87, 88

spectrogram Graph of signal frequencies per time. 16

Chapter 1

Introduction

1.1 Motivation

Babies born prematurely are at a high risk of cerebral damage due to low or variable blood flow [6–8]. NeoDoppler uses Doppler ultrasound to monitor blood flow [6, 9]. Ultrasound waves are transmitted through the anterior fontanelle and must hit an artery at a near-parallel angle to get a decent signal, making the correct placement of the probe crucial for successful usage of NeoDoppler. Other procedures for measuring blood flow in infants' brains have turned out to be difficult and time-consuming [10, 11]. Medical staff with no prior experience must be trained to use this device, as placing the ultrasound probe correctly is quite difficult.

Augmented reality has been shown to be useful in improving training for medical procedures [12]. AR technology enables enhancing real-world interactions with additional visual information, e.g., displaying internal organs in a patient's body during surgery or training [12, 13], or the cerebral arteries of an infant while placing an ultrasound probe.

This paper details the development of an augmented reality training application for NeoDoppler. Our work is based on a previous master's project (HoloUmoja) with a similar case; simulation of Doppler ultrasound on cerebral blood flow in fetuses [1]. As in the older project, we will create an application for HoloLens 2 and use a physical model of the subject to enhance the learning value of the simulation. We will strive to improve some important aspects of the previous project, namely:

- Detail in arterial blood flow direction
- Realism in simulated Doppler spectrogram

- Accuracy of probe tracking
- Clarity and amount of technical information

Since this project will improve on HoloUmoja as part of the development of a NeoDoppler training application, we will evaluate the quality of our NeoDoppler simulation *and* the impact of our enhancements on HoloUmoja.

1.2 Problem Description

Monitoring cerebral blood flow, especially in pre-term births, is crucial to avoid brain damage. Preterm births affect 10% of all newborns, exposing them to an increased risk of brain damage in their first months of life. A novel technology, NeoDoppler, was developed for continuous measurement of brain blood flow in infants by Cimon Medical. They aim for wide adoption by clinical personnel, not only experts that have prior knowledge of Doppler acquisitions. For that purpose, we wanted to test the hypothesis that XR can be used to simulate the procedure and allow the users to learn the correct placement of the ultrasound probe. In addition, it is highly desirable to be able to adjust PW-Doppler related parameters such as pulse repetition frequency, sample depth, window size, and probe angle and see their effects on the resulting Doppler spectrum in real time. A combination of 3D printed artifacts and XR visualization is envisioned for the task at hand, building further on HoloUmoja, which has shown that it is possible to simulate the measurement process for fetal ultrasound purposes if one assumes a well-defined area of measurement.

1.3 Stakeholders

In this project, the stakeholders were the author's supervisors, customers (employees at St. Olav's hospital in Trondheim) and end-users (medical students and personnel).

Supervisors Gabriel Kiss, Shubham Jain, Frank Lindseth

Customers Hans Torp, Siri Ann Nyrnes

End-users Medical students and intensive care nurses with no prior knowledge of ultrasound that would like to use the NeoDoppler device

1.4 Research Questions

Our goals with this project were to adapt HoloUmoja for NeoDoppler, make it possible to model blood flow direction through the twists and turns of cerebral arteries, make the spectrogram more realistic, as well as improve and evaluate the overall user experience of the application. Thus, our research questions are:

RQ1. How can we merge a real-life model of the subjects with a digital model of cerebral arteries?

RQ2. How can we simulate the directional and temporal pattern of arterial blood flow in a virtual environment?

RQ3. How can we efficiently generate a realistic Doppler spectrogram based on artery interactions?

RQ4. How well do the intended users perform a clinically relevant Doppler examination with our application?

RQ5. To what degree can users understand the technical details of Doppler ultrasound through our application?

1.5 Main Contributions

The main contributions of this project are:

- Completely reworked and much more realistic spectrogram based on real velocity data
- Spline-modeled arteries that allow for any curve imaginable to be measured
- Visible cerebral arteries within the virtual baby's head
- Realistic ultrasound-blocking baby head model, with a fontanelle that lets ultrasound beams through
- A more precise probe tracking approach that utilizes the hand tracking capabilities of the HoloLens
- Pedagogical material about Doppler ultrasound, embedded in the simulation

1.6 Thesis Outline

The remaining chapters of this thesis are structured as follows:

Chapter 2 explains concepts that are relevant to our implementation or give context to the ultrasound terminology, as well as related papers on CBF monitoring and ultrasound simulation on the HoloLens.

Chapter 3 conveys the methodologies for research, development, and evaluation in this project.

Chapter 4 dives into implementation details.

Chapter 5 describes our results, in terms of simulation content and user tests.

Chapter 6 discusses new features, how the simulation was improved compared to HoloUmoja, how the user test results turned out, and lists possible improvements in future work.

Chapter 7 summarizes and concludes the thesis.

Appendix A shows the task board that was used in the development process.

Appendix B contains notes from meetings with stakeholders.

Appendix C describes the questionnaires that were used in the user tests.

Appendix D includes various statistical calculations that were not strictly necessary to include in Chapter 5.

Chapter 2

Background

In this chapter, we will explain some concepts that are important to this project, related papers on CBF in infants, and previous attempts at ultrasound simulation on the HoloLens. Some paragraphs are based on text from the preparatory project.

2.1 Augmented Reality

Milgram *et al.* developed a categorization of extended reality called the *reality-virtuality continuum* [14]. As depicted in Figure 2.1, *Virtual Reality (VR)* is at the opposite end of *reality* (which simply means mundane interactions with the physical world). VR is typically accessed through a Head-Mounted (stereoscopic) Display (HMD) that envelops users in a fully virtual world, whereas *Augmented Reality (AR)* enhances real-world environments with virtual elements like 3D models overlaid on a phone's camera or holograms displayed on the HoloLens' visor [15].

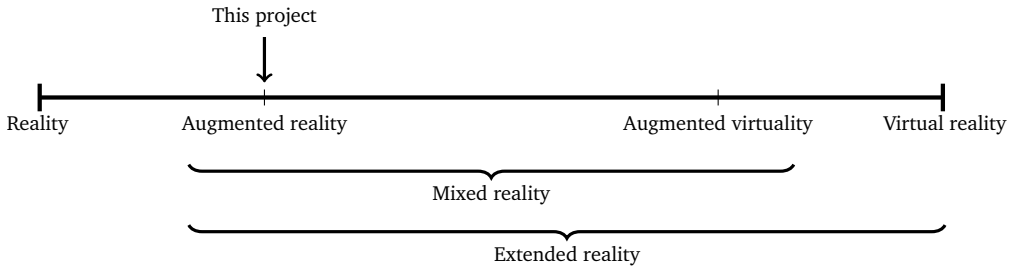

Figure 2.1: Reality-virtuality continuum, modified to use consistent phrasing and show the XR area as the widely encompassing category that it is [15], as well as the alignment of our project.

Many experiments with extended reality for learning have been conducted.

Some examples include demonstrating the impact of climate change [16], training assembly line workers [17], explaining nuclear power plant safety to the public [18], and providing training for medical procedures [12, 13, 19].

In the medical field, AR proves particularly valuable. For instance, surgical procedures often involve operating on organs that are obscured by the patient's body, requiring the use of small cameras and other monitoring devices. Displaying this monitoring information closer to the surgeon's work area, e.g., through overlays on the corresponding body parts, can significantly enhance its usefulness. This can be achieved with AR technology, as the paper by Chen *et al.* provides examples of [13].

2.2 Cerebral Arteries

The NeoDoppler probe can reach the anterior cerebral artery through the anterior fontanelle, a patch without skull on the heads of infants. This artery supplies the upper front of the brain and is connected to other brain arteries through the circle of Willis [10, 20], shown in Figure 2.2, which connects the main arteries of the brain and ensures sustained blood flow even if an artery is blocked [21].

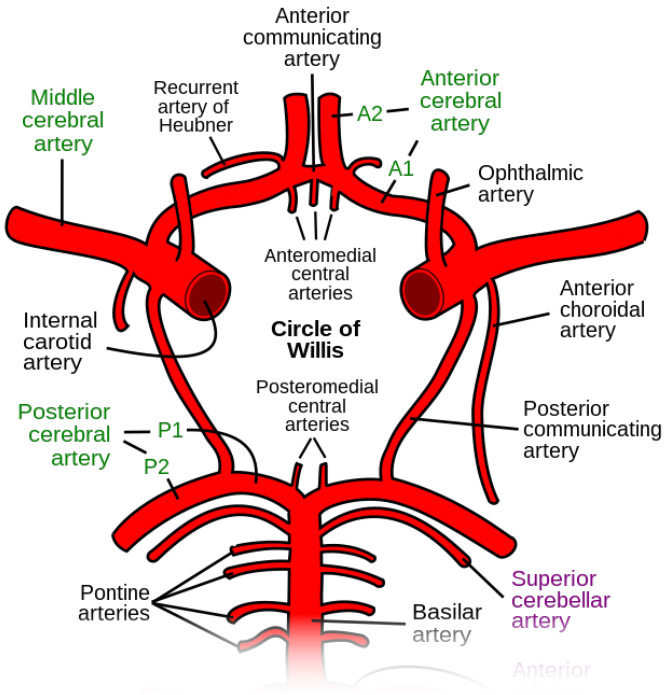

Figure 2.2: The circle of Willis. Created by Rhcastilhos [22]. Cropped.

Extreme fluctuations of cerebral blood pressure have been associated with bleeding into the fluid-filled gaps in the brain, a condition known as IntraVentricular Hemorrhage (IVH) [7]. In one experiment, infants with IVH were found to have both low and high blood pressure leading up to their conception [23].

2.3 Doppler Ultrasound

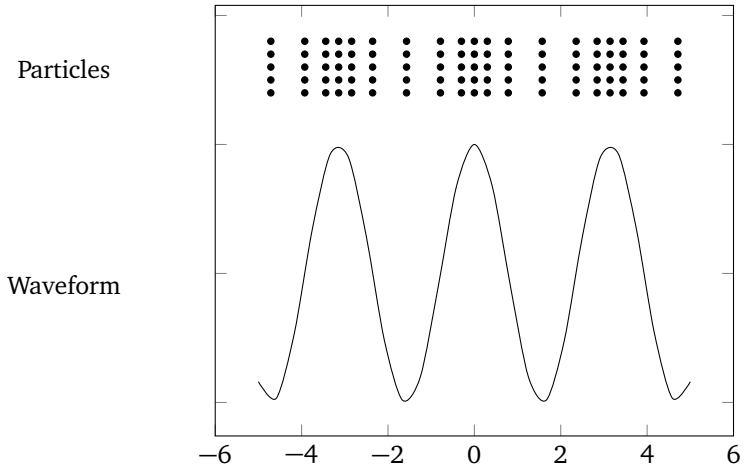

Figure 2.3: Sound wave depicted as ripples in particles (above) and a sine wave (below).

Sound waves are compressions and rarefactions of particles in the air and other materials [24, 25], as illustrated in Figure 2.3. Like other waves, they have frequency (f), amplitude, period (T), and wavelength (λ).

Sound of frequencies beyond what humans can hear, known as *ultrasound* [26], can reverberate through tissue with minimal risk of injury [27]. This makes ultrasound useful in medical examinations, where inspecting inner organs through the soft tissue of human bodies is especially important. Ultrasound waves bounce off certain materials in the body, and their reflections can be measure by devices called ultrasound probes. In this context, *depth* means the distance that a wave traveled away from the ultrasound probe before being reflected.

NeoDoppler monitors cerebral blood flow velocity by determining the speed at which red blood cells move away from or towards the probe [6]. It utilizes the Doppler effect, which states that waves that bounce off an object moving *away* from the observer will have a longer wavelength, while waves reflected off an object that moves *towards* the observer will have a shorter wavelength [28], see

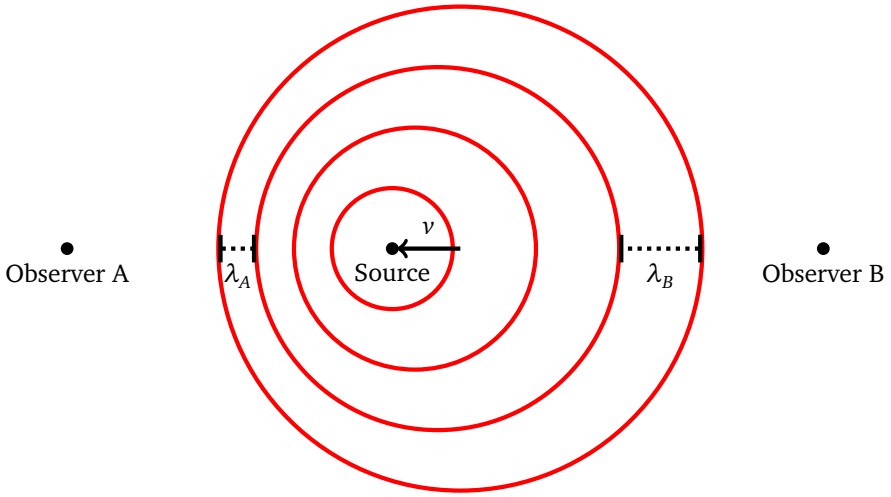

Figure 2.4: The Doppler effect. Here, the source moves towards observer A and shifts the wavelength of the sound it makes from λ_0 to λ_A, while observer B measures λ_B as the source moves away from it. Note that $\lambda_A < \lambda_0 < \lambda_B$.

Figure 2.4.

If we observe incoming waves with wavelength λ (λ_A or λ_B in Figure 2.4) after having sent waves with wavelength λ_0, the wavelength has been shifted by Δs due to velocity $v = \frac{\Delta s}{\Delta t}$. $\lambda = \frac{c}{f}$ and $\Delta t = \frac{1}{f_0}$ since we inspect the situation at wavelength scale, and we can solve this wavelength shift in terms of $f_d = f - f_0$:

$$
\begin{aligned}
\lambda_0 &= \lambda + \Delta s \\
\lambda &= \lambda_0 - \Delta s \\
\frac{c}{f} &= \frac{c}{f_0} - v\Delta t, \quad \lambda = \frac{c}{f}, \quad \Delta s = v\Delta t \\
\frac{c}{f} &= \frac{c}{f_0} - \frac{v}{f_0}, \quad \Delta t = \frac{1}{f0} \\
\frac{v}{f_0} &= \frac{c}{f_0} - \frac{c}{f} \quad | \cdot f_0 \\
v &= c - \frac{cf_0}{f} \\
v &= c\left(1 - \frac{f_0}{f}\right) \quad | \cdot f \\
vf &= c(f - f_0) \\
f - f_0 &= f\frac{v}{c} \\
f_d &= f\frac{v}{c}
\end{aligned}
$$

In the ultrasound case, we are both sending and receiving sound waves, so the effect is *doubled* [28]. To turn the equation into a more useful form, we use the fact that $v << c$ (some cm/s vs 299 Mm/s) makes $f \approx f_0$ to input the transmitted frequency f_0 instead of f:

$$f_d = 2f_0\frac{v}{c} \tag{2.1}$$

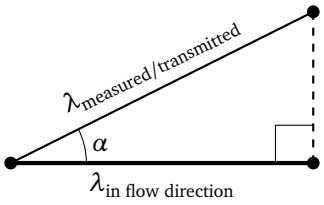

Figure 2.5: Angular relationship between beam and flow direction. α is the beam-flow angle.

Since the ultrasound beam is likely not parallel to the blood flow's direction, we should take into account another parameter: The angle between the flow and beam direction (α), called the beam-flow angle or insonation angle. To arrive at the formula for Doppler shift, we start with the difference in wavelengths. The angle affects the sound waves that the probe transmits and measures, as illustrated

in Figure 2.5. We may rephrase the starting equation in terms of the *hypothetical* λ and λ_0 if we measured at a parallel angle:

$$
\begin{aligned}
\lambda &= \lambda_0 - \Delta s \\
\lambda &:= \frac{\lambda}{\cos\alpha} && (2.2)\\
\lambda_0 &:= \frac{\lambda_0}{\cos\alpha} && (2.3)\\
\frac{\lambda}{\cos\alpha} &= \frac{\lambda_0}{\cos\alpha} - \Delta s \quad | \cdot \cos\alpha \\
\lambda &= \lambda_0 - \Delta s \cos\alpha \\
\frac{c}{f} &= \frac{c}{f_0} - \frac{v}{f_0}\cos\alpha \quad | \cdot \frac{f f_0}{c} \\
f_0 &= f - f\frac{v}{c}\cos\alpha \\
f_d = f - f_0 &= f\frac{v}{c}\cos\alpha
\end{aligned}
\tag{2.4}
$$

As before, we use $f \approx f_0$ and know that the effect is twice as strong in our case:

$$f_d = 2f_0\frac{v}{c}\cos\alpha \tag{2.5}$$

From the nature of the cosine function, we see that small angle deviations give Doppler shifts close to the actual shift ($\cos 0 = 1$), while large deviations may make the Doppler shift seem smaller or nonexistent ($\cos 90° = 0$). This matches with the intuitive reasoning that if we observe at a close to parallel angle, we see approximately correct motion, while at close to 90° we won't see much motion since the blood isn't moving away from or towards us.

As for how the measured velocity is affected by the beam-flow angle: We have two perspectives on the Doppler equation. Let the v in Equation (2.1) be the measured velocity v_{measured}, while the v in Equation (2.5) is the real blood flow velocity, which determines v_{measured} together with the beam-flow angle α. The Doppler shift f_d is the same from both perspectives.

$$
\begin{aligned}
f_d &= 2f_0 \frac{v_{\text{measured}}}{c} \\
f_d &= 2f_0 \frac{v}{c} \cos\alpha \\
\cancel{2f_0} \frac{v_{\text{measured}}}{\cancel{c}} &= \cancel{2f_0} \frac{v}{\cancel{c}} \cos\alpha \\
v_{\text{measured}} &= v \cos\alpha
\end{aligned} \tag{2.6}
$$

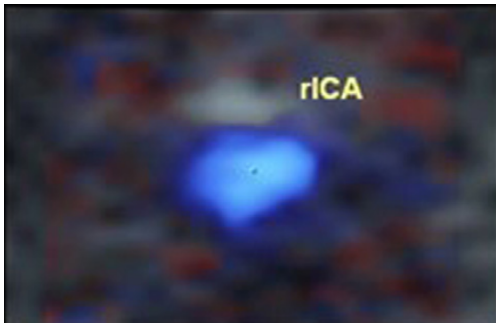

Figure 2.6: Color Doppler image of a cerebral artery, taken from Rubin *et al.*'s article [10]. The major artery shows up as blue, since the blood inside is moving away from the observing probe.

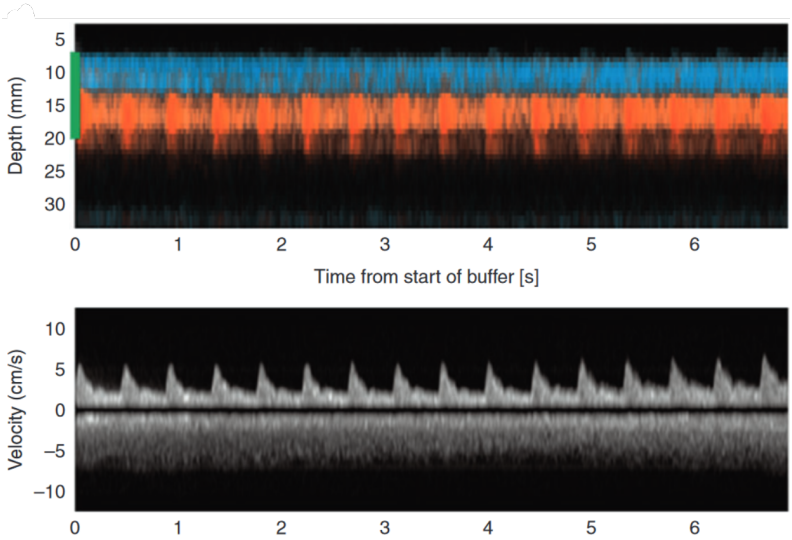

Figure 2.7: Pulsed Wave Doppler spectrogram for specific depths measured by the NeoDoppler probe, plotted below a graph of all monitored depths. The green line indicates the depths that are monitored to generate the spectrogram. Taken from the original NeoDoppler paper by Vik *et al.* [6]

In continuous wave Doppler ultrasound, signals are sent and received simultaneously, which makes the procedure collect signals from the full depth it is able to detect [29]. In color Doppler ultrasound, movement away from/towards the probe is displayed as blue/red areas (see Figure 2.6). In Pulsed Wave (PW) Doppler ultrasound, on the other hand, signals are sent and subsequently analyzed. This makes it possible to focus on a specific range of depths and only analyze reflections from that area [30], called depth window or sample volume. NeoDoppler uses PW Doppler ultrasound with a wide beam (see Figure 2.9) and several sample volumes at different depths [6], as demonstrated in Figure 2.7. Users set a depth window that the system should start monitoring [31].

The Pulse Repetition Frequency (PRF) is the rate at which a PW ultrasound probe sends pulses of signals. It functions as the sampling rate for the procedure [30]. By Nyquist's theorem, a PRF twice as great as the Doppler shift is required in order to avoid aliasing [28, 32]:

$$\text{PRF} \geq 2f_d \tag{2.7}$$

To find the maximal detectable velocity, consider that the Doppler shift would be half of the current PRF, following Nyquist's theorem. The angle should be 0 to maximize the cosine value ($\cos 0 = 1$). With this information, the maximal velocity $v_{\max}$ becomes:

$$\begin{aligned} f_d &:= \frac{1}{2}\text{PRF} \\ \alpha &:= 0 \\ f_d &= 2f_0 \frac{v_{\max}}{c} \cos\alpha \\ \frac{1}{2}\text{PRF} &= 2f_0 \frac{v_{\max}}{c} \cdot 1 \quad \mid \cdot \frac{c}{2f_0} \\ v_{\max} &= \frac{c \cdot \text{PRF}}{4f_0} \end{aligned} \tag{2.8}$$

2.4 Ultrasound Devices

In practice, ultrasound devices may expose most of the parameters explained in Section 2.3. Figure 2.8 shows the interface of an ultrasound device that supports ultrasound imaging as well as Doppler ultrasound. PRF is adjusted by turning a knob on the device [33], angle correction (compensating for insonation angle,

which users can determine from the image mode) is adjusted through a button that gives access to a slider, and the depth window (or *sampling gate*) is adjusted by interacting with the yellow lines on the upper image [34].

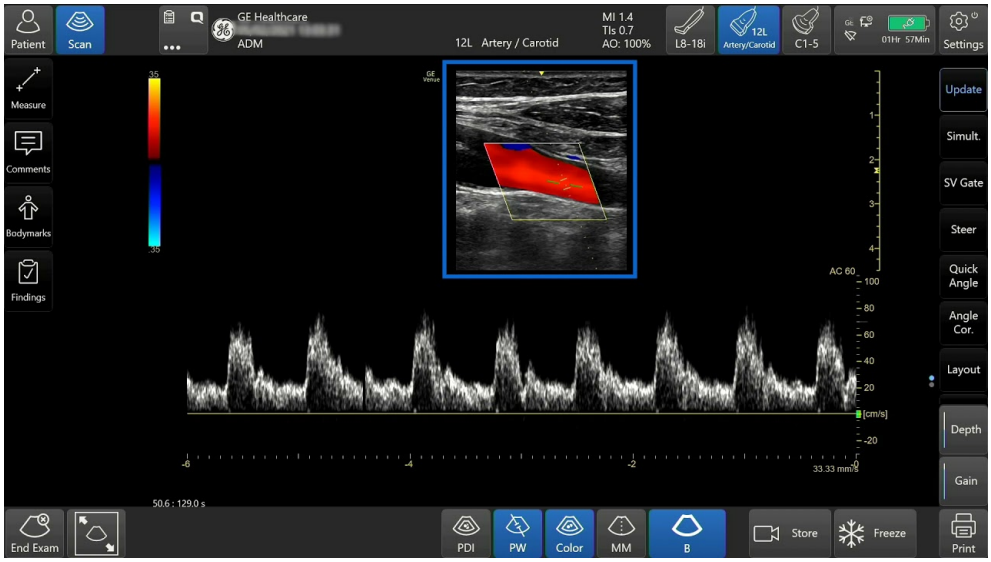

Figure 2.8: Interface of the *Venue Family R3* ultrasound device. Captured from a video by GE HealthCare [34].

NeoDoppler does not expose nearly as many parameters as other ultrasound devices. In normal usage, users are able to affix the probe at a position and angle of their choosing, by placing the probe in different locations on the infant's head. See Figure 2.9 for a possible placement of the probe. The digital interface shown in Figure 2.10 allows the user to choose the depth that the device monitors, as well as angle correction and other settings in the advanced mode [31]. One advanced setting is the vertical scale of the graph, which changes the maximum velocity displayed. Changing it corresponds to changing the PRF, but the resolution is only altered in the vertical direction, as the real PRF is unchanged.

2.5 Ultrasound of Cerebral Blood Flow in Infants

Ultrasound has been a viable option for measuring cerebral blood flow in infants for many years, but with NeoDoppler it is possible to use it for continuous monitoring. There was no usable method for continuous CBF monitoring of *any* kind before NeoDoppler [6]. However, ultrasound has been used for singular measurements of CBF in the past, though with methods that were relatively slow and

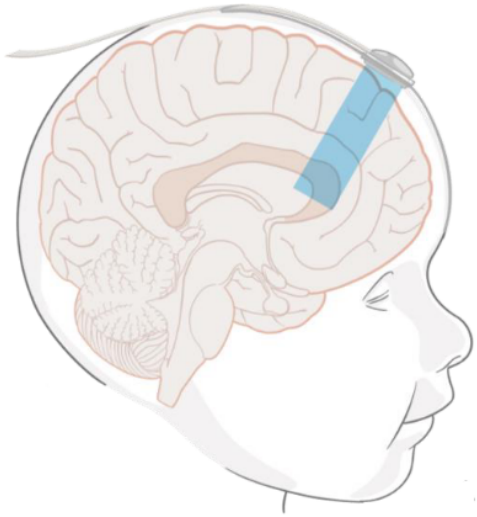

Figure 2.9: NeoDoppler probe affixed to an infant's head. Taken from the NeoDoppler manual [31]

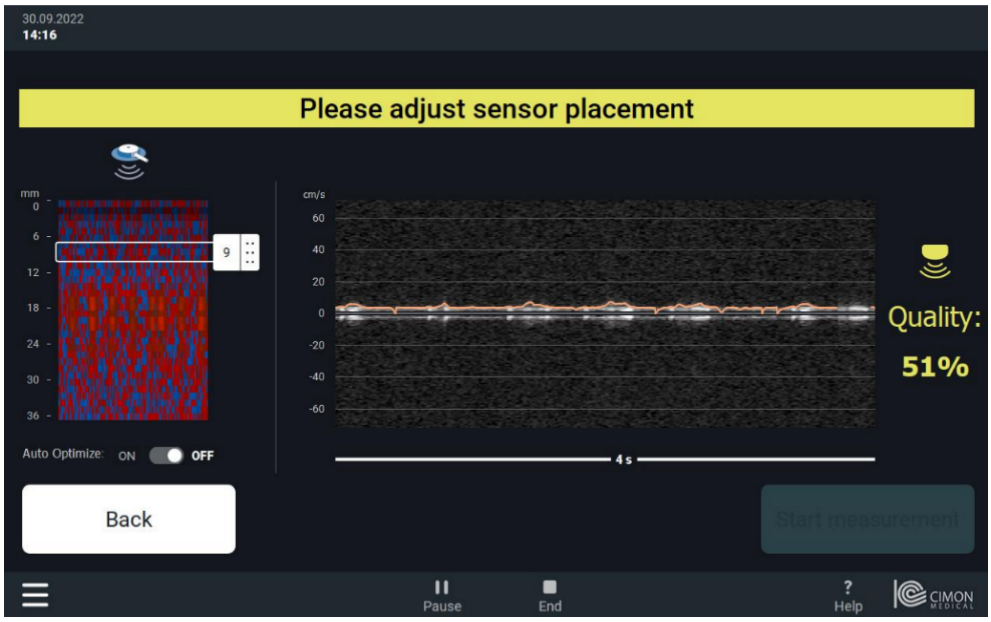

Figure 2.10: NeoDoppler depth selection interface. Taken from the NeoDoppler manual [31]

difficult to perform.

In one instance, measuring blood flow volume took between 12 ± 4 and 24 ± 6 minutes, depending on the practitioner's skill [11]. Spending *this* much time per measurement is not practical for continuous monitoring.

A more recent study by Rubin *et al.* focused on ultrasound imaging of the major blood vessels in the circle of Willis [10]. The authors measured blood flow volume and found that their results were consistent with other methods that were not based on ultrasound. However, the article did not mention the duration of the procedure, indicating that efficiency was not a priority.

2.6 Ultrasound Simulation on HoloLens

There have been several prior attempts to simulate or enhance ultrasound using the HoloLens.

Nguyen *et al.* developed and tested an application that displayed ultrasound images on top of a real ultrasound probe. This application tracked black-and-white pixelated patterns on the probe. The results seemed promising, with a latency of 80 milliseconds and a frame rate of 25 on the first-generation HoloLens [35].

Costa *et al.* found that the tracking accuracy for another application, which used a custom QR-code tracker for an ultrasound imaging simulator, was comparable to a specific electromagnetic orientation measurement device [36].

In a recent project by von Haxthausen *et al.*, an ultrasound probe was tracked using retroreflective spheres [37]. The probe's position was determined based on captured images of spheres surrounding the probe, and a Kalman filter was used to reduce noise from the HoloLens' camera. The authors evaluated the position and pose estimation with and without the Kalman filter and found that it had a positive impact on position accuracy. The application was able to track the probe 20 times per second, while ultrasound images were streamed with a delay of 16 milliseconds on average. The authors considered the HoloLens to be promising for ultrasound training, at least if accuracy below 1 millimeter was not required. However, they did not test their application while the HMD moved, which meant that their accuracy was incomparable to our case. Though this application did not require keeping an image marker in focus at all times, the authors did acknowledge that the retroreflective sphere tracking likely had blind spots.

In summary, previous projects have achieved performant and accurate orientation tracking. Considering the project we are basing our work on, our probe

tracking will be limited by what Vuforia has achieved unless we explore alternative solutions.

2.7 HoloUmoja

HoloUmoja, the project by Nylund which our work is based upon, aimed to be a training simulator for fetal Doppler ultrasound. Its physical components were a 3D printed model of a pregnant stomach and another 3D print of an ultrasound probe with an Arduino strapped to the back, as shown in Figure 2.11. The purpose of these elements was to enhance the realism of the training simulator, where holograms were laid on top of the real-world components, and their position in the virtual world was found using Vuforia image tracking [1].

There were a few problems with the outcome of this project that we will focus on improving:

- Measurement of blood flow was possible only on a single cylindrical segment of the umbilical cord, as shown in Figure 2.12. This was a surprise to some users during tests.
- The Doppler spectrogram that responded to the angle at which the probe beam hit the vein, see Figure 2.13, was not realistic. The spectrogram showed a very simple curve compared to that of real-world fluctuations in blood flow. This curve graph was displayed in plain white, without any imitation of the noise that would show up on a real spectrogram.
- In HoloUmoja, probe orientation was determined through a combination of image tracking and input from a BLE gyroscope that was mounted on the probe. Many testers complained about low accuracy on the probe tracking [33], and the gyroscope did not compensate well enough for the loss of tracking when the image marker fell out of view.
- HoloUmoja's tutorial lacked information about Doppler ultrasound. It explained a few specific interactions that were used in the application (how to pin the menu and reset its position, how to pinch and adjust sliders), and went on to show detailed information about the connection to the BLE device (see Figure 2.14), which was a little too technical for the users. In addition to a menu with sliders for PRF, sampling depth and arterial velocity, the application's last page was devoted to a quiz where users had to calculate velocity based on depth and PRF, shown in Figure 2.15, which seemed more likely to confuse than enlighten users.

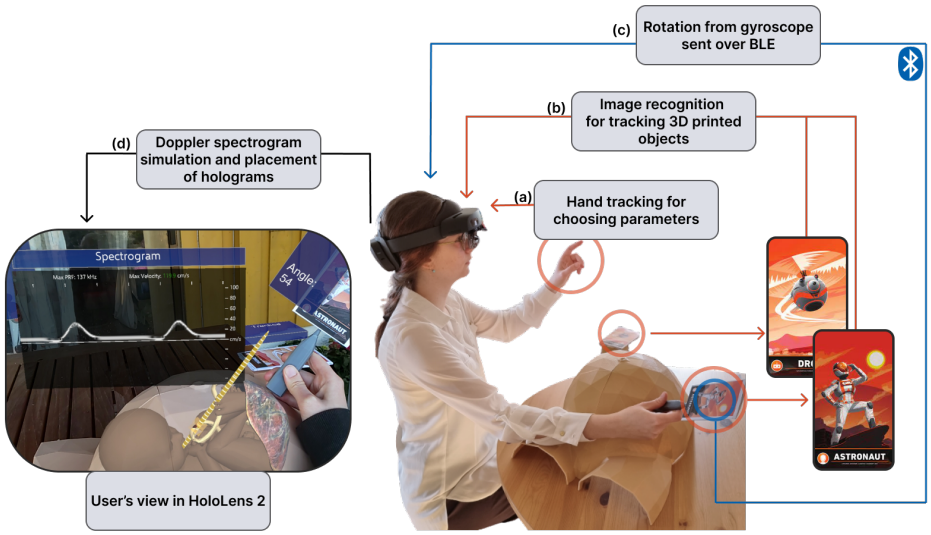

Figure 2.11: Diagram showing the overall setup of HoloUmoja. Taken from Nylund's master thesis [1]

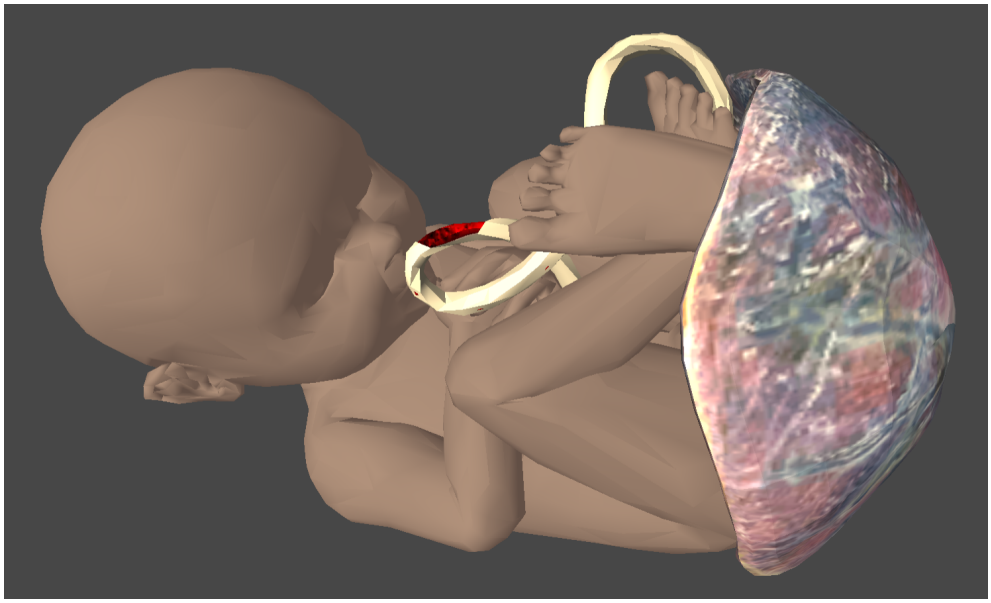

Figure 2.12: Fetus and placenta model used in HoloUmoja. Note that the red segment of the umbilical cord is the only part of the vein that the probe may hit.

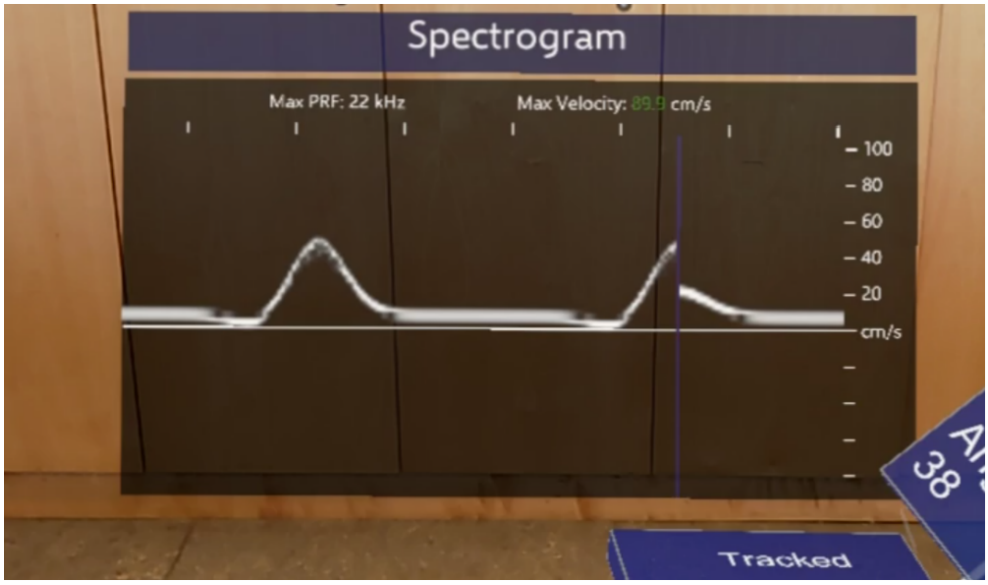

Figure 2.13: Spectrogram generated in HoloUmoja. Low-resolution and based on a very simple wave. Taken from Nylund's master thesis [1]

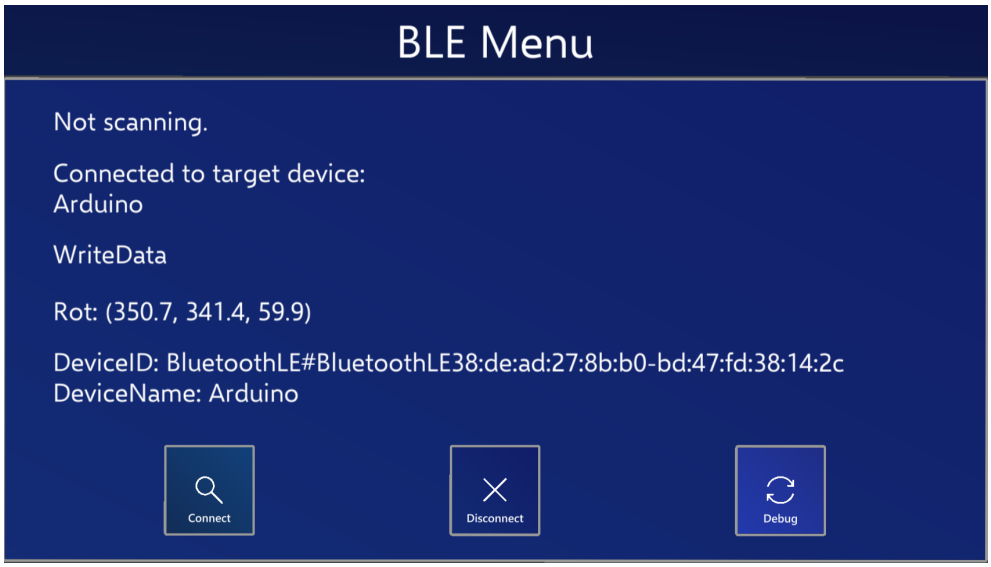

Figure 2.14: BLE page in HoloUmoja. Taken from Nylund's master thesis [1]

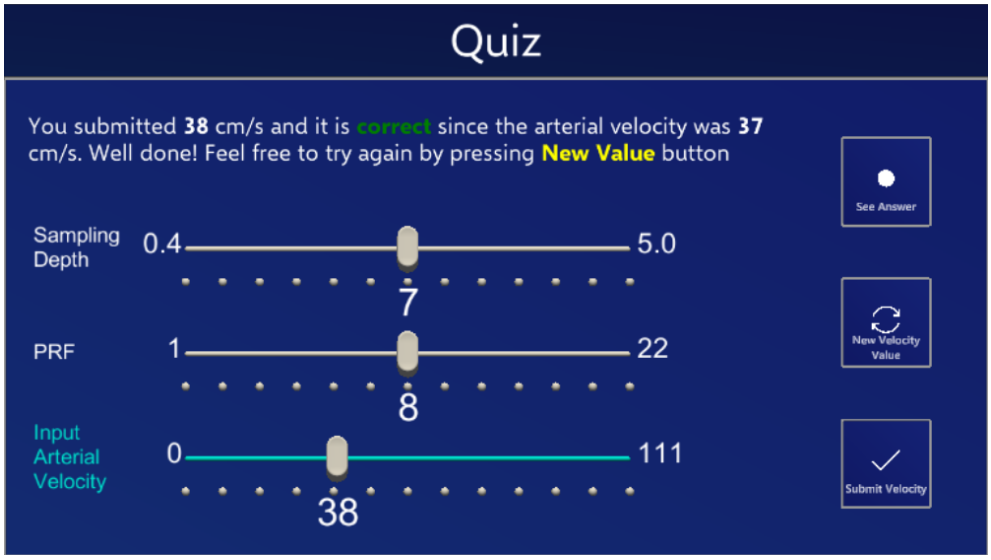

Figure 2.15: Quiz page in HoloUmoja. Taken from Nylund's master thesis [1]

2.8 Signal Processing

2.8.1 Fourier Transform

In signal processing, it is very useful to know the wave frequencies that make up a signal. Continuous signals can be approximated as possibly infinite sums of sine and cosine terms, called Fourier series. The following formula describes the general Fourier series for a signal $f(t)$ defined on the interval $[-L, L]$ [38, p. 6]:

$$f(t) \approx \frac{a_0}{2} + \sum_{n=1}^{\infty} a_n \cos\left(\frac{n\pi}{L}t\right) + b_n \sin\left(\frac{n\pi}{L}t\right)$$

$$a_n = \frac{1}{L}\int_{-L}^{L} f(t)\cos(\frac{n\pi}{L}t)dt$$

$$b_n = \frac{1}{L}\int_{-L}^{L} f(t)\sin(\frac{n\pi}{L}t)dt$$

Creating the Fourier series representation of a signal requires knowing the coefficients a_n and b_n. These coefficients may be represented quite efficiently as a vector of complex numbers. With the use of a_n and b_n as cosine and sine amplitudes, we may utilize Euler's formula,

$$e^{ix} = \cos x + i \sin x,$$

to express the coefficients a_n and b_n as complex numbers [38, p. 20-21]. With this in mind, we can derive them by integrating the function times an exponential function. This way of finding the coefficients of a Fourier series is called a Fourier transform. Given a signal $f(t)$, it transforms the signal to a sequence of frequency values (the complex coefficients). Its mathematical definition is as follows [38, p. 22]:

$$F(\omega) = \int_{-\infty}^{\infty} f(t) e^{i\omega t} dt$$

A discrete version of this transformation is used in digital signal processing, commonly in the form of the Fast Fourier Transform (FFT). Figure 2.16 shows the transformation from a signal (shown as its components) to discretized frequency values. It is possible to reverse this process using the *inverse* transform.

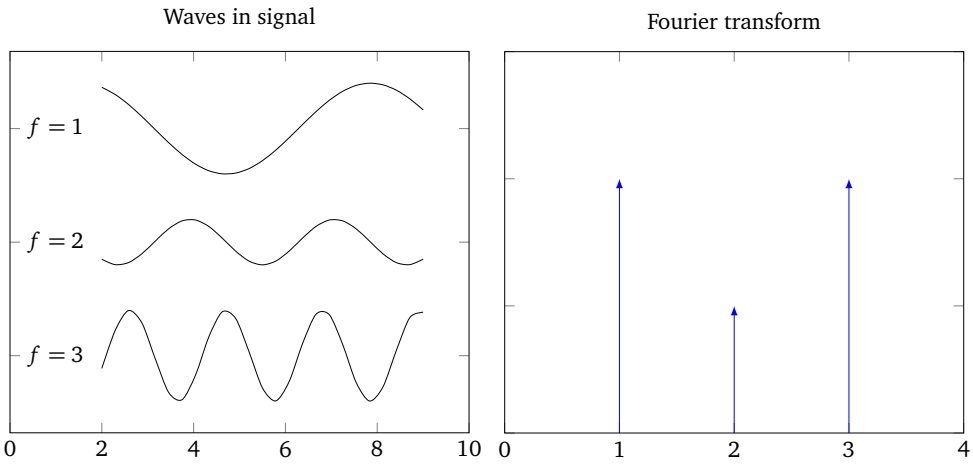

Figure 2.16: Fourier transform of a simple signal. *Left:* The sinusoidal waves that constitute a signal. The frequencies are there for illustration purposes and thus not to scale. *Right:* The discrete Fourier transform of the signal. Note that the frequency of each component of the signal is represented.

2.8.2 Window Functions

Window functions are typically bell-shaped curves centered at some point b, that a signal is multiplied with before it is put through a Fourier transform [38, p. 246-247]:

$$\int_{-\infty}^{\infty} f(t) g(t-b) e^{i\omega t} dt,$$

where g is a window function centered at $t = b$.

These functions are primarily used to avoid *spectral leakage* — frequencies blending into one another due to short, imperfectly aligned signals. The discrete Fourier transform assumes infinite repetitions of the input signal, which poses an issue when applying the transform to small input signals with endpoints that do not match up, see Figure 2.17 [39]. Window functions diminish the contribution of the edges of a signal on the resulting spectrum, by tapering off the values at the edges and leaving only the center part intact [38, 39], as demonstrated in Figure 2.18.

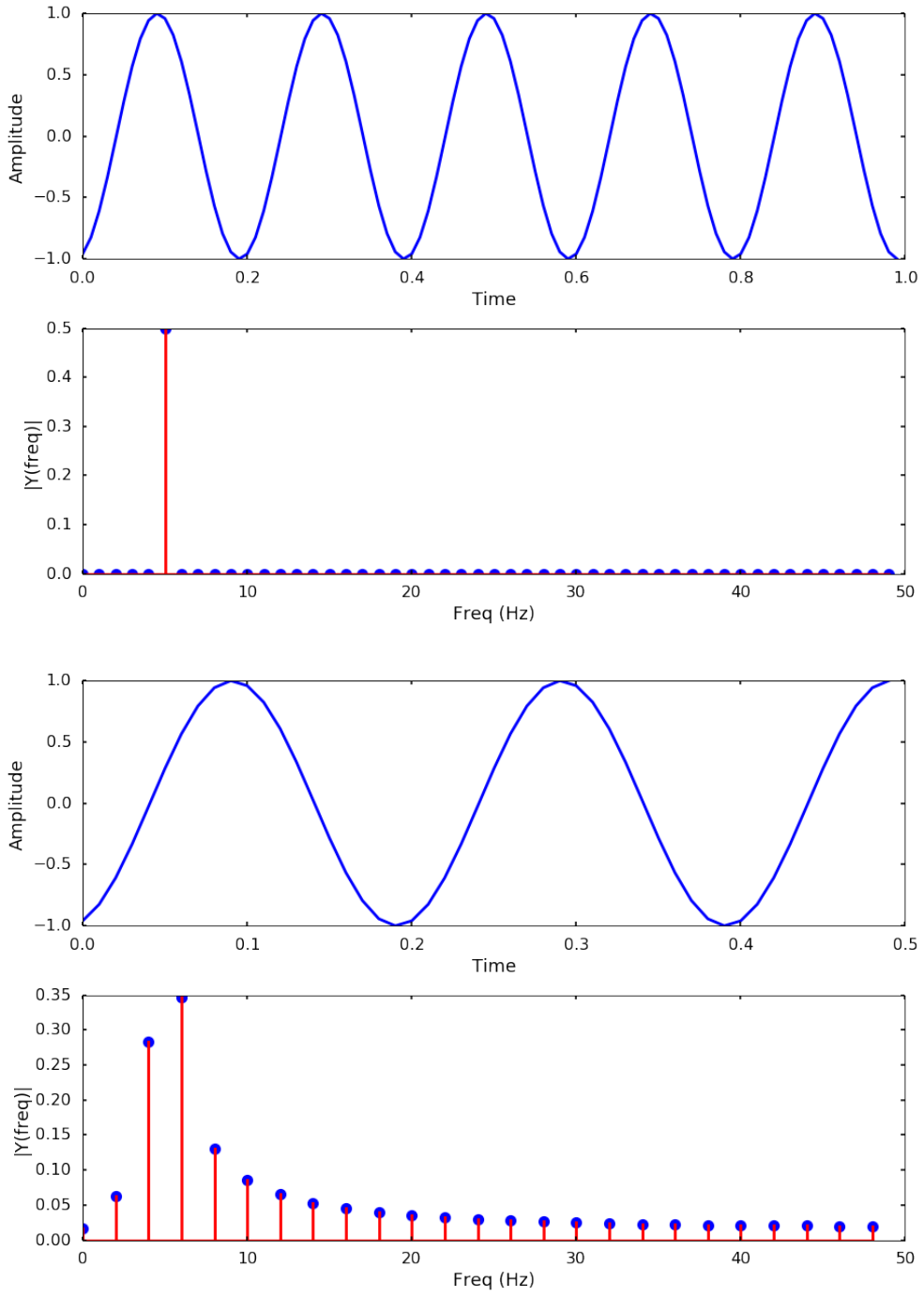

Figure 2.17: *Top:* Perfectly aligned signal and its FFT. *Bottom:* Same signal with misaligned cropping and lots of leakage to other frequency bins in its FFT. Taken from a blog post by Kong [40].

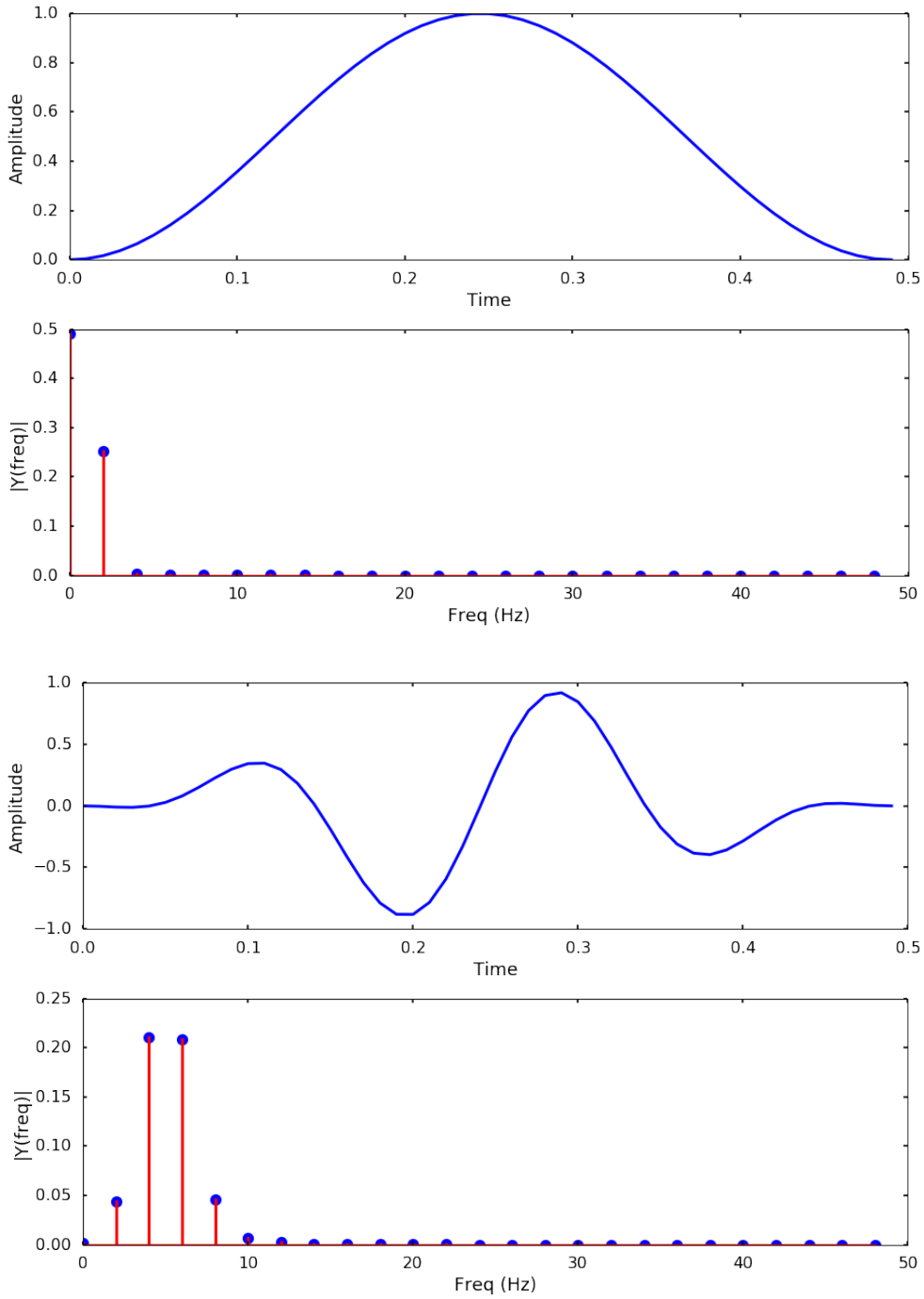

Figure 2.18: *Top:* Hanning window and its FFT. *Bottom:* Hanning window applied to the misaligned signal from Section 2.8.2. Note that the FFT is much closer to the one for the perfectly continuous version of the signal. Taken from a blog post by Kong [40].

2.9 Bézier Curves

To simulate the network of curves and intersections that constitutes the cerebral arteries, we need to model them. A common way to encode complex curves is to define Bézier curves that fit them. Bézier curves are defined by sets of control points that are evaluated with what is effectively recursive linear interpolation.

Let

$$\text{lerp}(\mathbf{a}, \mathbf{b}, t) = (1-t) \cdot \mathbf{a} + t \cdot \mathbf{b}$$

in the following, to shorten linear interpolation notation.

With the recursive rule of the De Casteljau algorithm, *any* higher-order Bèzier curve can be defined as follows [41, p. 194][42, p. 120][43]:

$$\begin{aligned} B^0_{\mathbf{p_i}}(t) &= \mathbf{p_i} \\ B^r_{\mathbf{p_0},\mathbf{p_1},\dots,\mathbf{p_n}}(t) &= \text{lerp}(B^{r-1}_{\mathbf{p_0},\mathbf{p_1},\dots,\mathbf{p_{n-1}}}, B^{r-1}_{\mathbf{p_1},\mathbf{p_2},\dots,\mathbf{p_n}}, t) \end{aligned}$$

and this recursive nature implies that higher-order curves can be split into several lower-order segments.

From here on, we derive the explicit formula for cubic Bézier curves and their first derivative from the recursive rule.

Linear Bézier curve:

$$\begin{aligned} B^1_{\mathbf{p_0},\mathbf{p_1}}(t) &= \text{lerp}(B^0_{\mathbf{p_0}}(t), B^0_{\mathbf{p_1}}(t), t) = \text{lerp}(\mathbf{p_0}, \mathbf{p_1}, t) \\ &= (1-t)\mathbf{p_0} + t\mathbf{p_1} \end{aligned}$$

Quadratic Bézier curve:

$$\begin{aligned} B^2_{\mathbf{p_0},\mathbf{p_1},\mathbf{p_2}}(t) &= \text{lerp}(\text{lerp}(\mathbf{p_0}, \mathbf{p_1}, t), \text{lerp}(\mathbf{p_1}, \mathbf{p_2}, t), t) \\ &= \text{lerp}((1-t)\mathbf{p_0} + t\mathbf{p_1}, (1-t)\mathbf{p_1} + t\mathbf{p_2}, t) \\ &= (1-t)((1-t)\mathbf{p_0} + t\mathbf{p_1}) + t((1-t)\mathbf{p_1} + t\mathbf{p_2})) \\ &= (1-t)^2\mathbf{p_0} + 2(1-t)t\mathbf{p_1} + t^2\mathbf{p_2} \end{aligned}$$

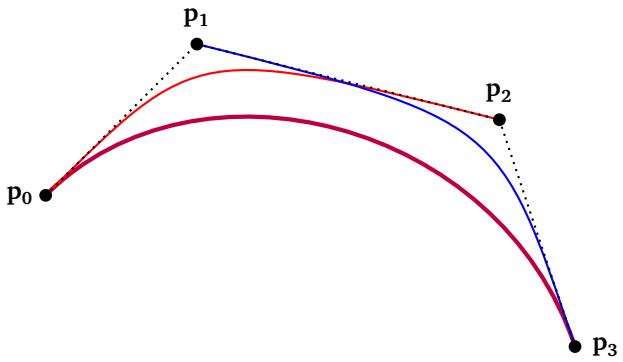

Figure 2.19: Bézier curve with subdivision illustrated. Red curve is $B^2_{\mathbf{p_0},\mathbf{p_1},\mathbf{p_2}}(t)$, blue curve is $B^2_{\mathbf{p_1},\mathbf{p_2},\mathbf{p_3}}(t)$, purple curve is $B^3_{\mathbf{p_0},\mathbf{p_1},\mathbf{p_2},\mathbf{p_3}}(t)$.

Cubic Bézier curve, shown in Figure 2.19:

$$\begin{aligned}
B^3_{\mathbf{p_0},\mathbf{p_1},\mathbf{p_2},\mathbf{p_3}}(t) &= \text{lerp}(B^2_{\mathbf{p_0},\mathbf{p_1},\mathbf{p_2}}(t), B^2_{\mathbf{p_1},\mathbf{p_2},\mathbf{p_3}}(t), t) \\
&= \text{lerp}(\\
&\quad (1-t)^2\mathbf{p_0} + 2(1-t)t\mathbf{p_1} + t^2\mathbf{p_2}, \\
&\quad (1-t)^2\mathbf{p_1} + 2(1-t)t\mathbf{p_2} + t^2\mathbf{p_3}, \\
&\quad t) \\
&= (1-t)((1-t)^2\mathbf{p_0} + 2(1-t)t\mathbf{p_1} + t^2\mathbf{p_2}) \\
&\quad + t((1-t)^2\mathbf{p_1} + 2(1-t)t\mathbf{p_2} + t^2\mathbf{p_3}) \\
B^3_{\mathbf{p_0},\mathbf{p_1},\mathbf{p_2},\mathbf{p_3}}(t) &= (1-t)^3\mathbf{p_0} + 3(1-t)^2t\mathbf{p_1} + 3(1-t)t^2\mathbf{p_2} + t^3\mathbf{p_3} \qquad (2.9)
\end{aligned}$$

First derivative of cubic Bèzier curve:

$$\begin{aligned}
B^{3\prime}_{\mathbf{p_0},\mathbf{p_1},\mathbf{p_2},\mathbf{p_3}}(t) &= ((1-t)^3\mathbf{p_0} + 3(1-t)^2t\mathbf{p_1} + 3(1-t)t^2\mathbf{p_2} + t^3\mathbf{p_3})' \\
&= (-1)\cdot 3(1-t)^2\mathbf{p_0} + (3(1-t)^2t\mathbf{p_1} + 3(1-t)t^2\mathbf{p_2})' + 3t^2\mathbf{p_3} \\
&= -3(1-t)^2\mathbf{p_0} + 3((1-t)^2 + (-1)\cdot 2(1-t)t)\mathbf{p_1} \\
&\quad + 3(2(1-t)t + (-1)t^2)\mathbf{p_2} + 3t^2\mathbf{p_3} \\
&= -3(1-t)^2\mathbf{p_0} + 3(1-t)^2\mathbf{p_1} - 6(1-t)t\mathbf{p_1} \\
&\quad + 6(1-t)t\mathbf{p_2} - 3t^2\mathbf{p_2} + 3t^2\mathbf{p_3} \\
B^{3\prime}_{\mathbf{p_0},\mathbf{p_1},\mathbf{p_2},\mathbf{p_3}}(t) &= 3(1-t)^2(\mathbf{p_1}-\mathbf{p_0}) + 6(1-t)t(\mathbf{p_2}-\mathbf{p_1}) + 3t^2(\mathbf{p_3}-\mathbf{p_2}) \qquad (2.10)
\end{aligned}$$

2.10 Unity

For greater clarity in the coming chapters, we will explain some important Unity concepts.

Unity *scenes* can be thought of as trees with several *game objects* [44] as nodes, see Figure 2.20. Each game object has a *transform* that stores its scale, rotation, and translation relative to its parent. When the parent object's transform changes, the child will inherit the new transform and end up oriented or scaled differently in world space, given the new base transform from the parent [45]. Transform objects provide information like the vector that points forward (*forward vector*) in the local coordinate space of the objects that they apply to [46].

The behavior of each game object is defined by the *components* that are attached to it [47]. Components are implemented with *scripts* written in C#. These scripts are regular C# classes that inherit from *MonoBehaviour*. This Unity-specific class has methods that are called at specific points in the application's runtime and can be overridden by developers to make the object behave in specific ways, as well as references to the game object's transform and methods that grant access to other components [48].

Unity includes a physics engine with collision detection [49] and support for casting arbitrary rays through the scene and checking which colliders they hit [50].

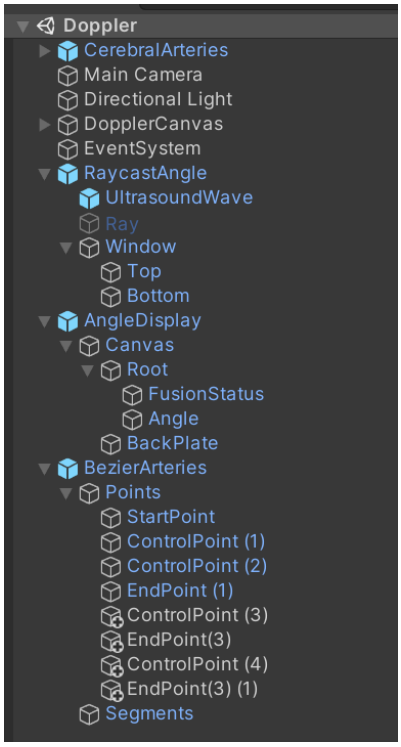

Figure 2.20: Scene tree for test scene in HoloNeoDoppler

Chapter 3

Method

This chapter explains different aspects of the methodology of this thesis. Section 3.1 describes the research and development process, Section 3.2 lists the set of requirements we added on top of HoloUmoja, Section 3.4 briefly explores the technologies used in HoloNeoDoppler, Section 3.5 details the plan for the user tests and Section 3.6 describes the way we analyzed our results.

Some paragraphs in Section 3.1 and Section 3.4 were reused and heavily rewritten from the preparatory project.

3.1 Research and Development Process

Figure 3.1: Rough illustration of the research and development process in the preparatory project

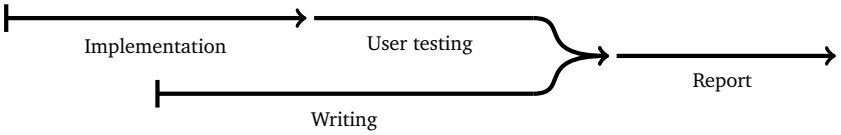

Figure 3.2: Rough illustration of the development and evaluation process in master thesis semester

In the preparatory project, we focused on doing research, gathering requirements, and starting development, with these parts culminating in a report as

shown in Figure 3.1. During the master thesis semester, we focused on development and evaluation through user tests and expert interviews. The overall process during this semester is illustrated in Figure 3.2.

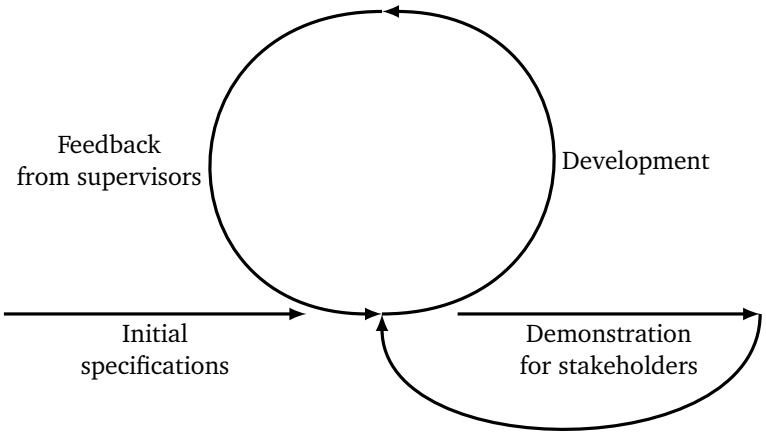

Figure 3.3: Development feedback loop. The middle loop was repeated multiple times before transitioning to demonstration, after which the loop starts over again.

The development process consisted of several iterations of the core of agile processes: Implementing features and receiving feedback that affects future implementation periods. After several iterations of this core loop, we would hold demonstrations for stakeholders and alter the course of development based on this feedback. We received the initial specifications from the problem statement and conversations with stakeholders during the preparatory project. This whole process is illustrated in Figure 3.3.

We used a task board in Notion to track planned and implemented features and fixes, as larger tasks with several subtasks. Figure A.1 shows a snapshot of this board after the preparatory project, while Figure A.2 shows its state at the end of the master thesis.

In the preparatory project, we conducted research starting from the references used in HoloUmoja, and supplemented these with papers and articles related to NeoDoppler, ultrasound, and the use of AR in medical training. We used these keywords in the prompts of our literature searches: ‘augmented reality’, ‘hololens’, ‘ultrasound’, ‘training’, ‘surgery’, ‘medical education’, ‘hypotension’, ‘ivh’ (Intra-Ventricular Hemorrhage).

3.2 Functional Requirements

With NeoDoppler, we had a case that differed significantly from HoloUmoja in several ways.

- The probe is a tiny, flat disc that is fastened to the head, as shown in Figure 2.9. A physical imitation of the probe would need to be very small if physical. A virtual probe should stick to the head, whereas a physical probe should only work if pressed down to the head.
- While HoloUmoja dealt with the umbilical cord as a single vein with a known flow pattern, there are several arteries in the brain that flow in different directions.
- Cerebral arteries are thinner than the arteries and veins in the umbilical cord, and need better precision to aim towards.
- Hitting arteries should be a lot easier in practice than with obstetric Doppler ultrasound, as long as the beam is aimed through the fontanelle. The NeoDoppler probe uses a single element and a broad ultrasound beam, since it is designed for use by non-experts [6].

Because of these facts, the simulation needed some changes. We also needed to improve upon HoloUmoja, since several aspects of it were less optimal:

- There was no way to model more complex arteries.
- The spectrogram was based on a very simple curve, rendered in very low resolution and did not look much like an actual spectrogram (see Figure 2.7).
- The menu confused users by showing debug information about the BLE connection, and did not explain Doppler ultrasound concepts.

We summarized these needs in the following list of functional requirements. These requirements *supplement* the ones in HoloUmoja [1].

FRQ1. **Display cerebral arteries inside the doll head**
This will give users a visual aid to determine what they can hit.

FRQ2. **Find correct angle between ultrasound ray and *curved* blood flow**
Angle should be derived from the simulated direction of blood flow in the artery segment that is hit.

FRQ3. **Simulate that the infant's skull can block ultrasound**
It should be impossible to get a signal from parts of the head that are fully

formed skull. The ultrasound beam should only be able to penetrate the anterior fontanelle.

FRQ4. **Restrict ultrasound beam to receive signals from an adjustable depth window**
Another important aspect of real-world NeoDoppler usage. The existing but malfunctioning implementation in HoloUmoja should be fixed.

FRQ5. **Track the probe accurately enough to reliably hit cerebral arteries**
Probe tracking precision was a common complaint among the midwives that tested HoloUmoja [33]. This needs to be improved.

FRQ6. **It should be quite easy to hit the arteries**
Since the real-world use of the probe is relatively simple, as stated in Appendix B.2, we should strive to make the simulation easy to complete as well.

FRQ7. **Doppler spectrogram should show a more realistic curve**
HoloUmoja used a simple sine wave for its spectrogram. Realistic graphs are more complex.

FRQ8. **Add background and signal noise on the Doppler spectrogram**
The previous iteration had a very simple spectrogram that only showed an envelope without any noise around.

FRQ9. **PRF should affect resolution of Doppler spectrogram**
In HoloUmoja, the PRF only affected the frequency of the displayed signal, whereas, in reality, it should affect the density of data points on the spectrogram.

FRQ10. **The application should teach users basic Doppler ultrasound concepts**
HoloUmoja's tutorial should be expanded with more details so that users can comprehend what happens in the application.

FRQ11. **Users should be able to submit the current spectrogram for evaluation**
For quantifiable test results, we want to check how the spectrogram that each tester creates looks, so it should be possible to save the current spectrogram as an image.

3.3 Non-Functional Requriements

We also made a major addition to the nonfunctional requirements, and kept the two nonfunctional requirements from HoloUmoja, though slightly modified:

NFRQ1. **The application should be educational for medical students**
Since HoloNeoDoppler was intended to function as an educational tool for NeoDoppler, it was important to ensure that users were, in fact, educated by this simulation.

NFRQ2. **Performance should meet HoloLens 2 recommendations**
For a positive user experience, it is important to ascertain that an application performs well. This is crucial in AR, where virtual elements are expected to follow interactions in the real world closely. Microsoft has published a set of criteria regarding frame rate, hologram stability, holograms on real surfaces, viewing zone and interaction that HoloNeoDoppler should meet [51].

NFRQ3. **The code should be readable and easy to develop on**
We wanted to improve upon the code in HoloUmoja, which had some clear signs of being hastily added to at the end of the project.

3.4 Technology

Our technology choices were limited since this project builds on prior work, and most of our choices were forced to stay in line with the previous project.

We used Unity Engine (see Section 2.10) to create the training application, with the following packages:

- Vuforia for tracking of image markers that anchor real-world elements in the simulation [52].
- Mixed Reality Toolkit (MRTK) for UI elements on the XR device [53].

Like HoloUmoja, we used Microsoft HoloLens 2 as our AR device. It displays 3D graphics on real-world surroundings by projecting images onto its visor. The device supports hand tracking [54] for tangible interactions with real and virtual elements.

For probe tracking, we no longer needed the BLE Arduino device, as explained in Section 4.6.

3.5 Evaluation

The application was evaluated in expert interviews with our customers at several points in the process, see Appendix B. Feedback from these interviews was used to improve all aspects of HoloNeoDoppler and prevent the project from straying off its course.

After the project was largely finished, we conducted user tests with medical students who had no prior experience with NeoDoppler. The aim was to gather information about the product's usability, how well the users performed, how well the users *thought* they performed, and how capable the users felt about using NeoDoppler in real life after trying the simulation.

We created a questionnaire to find data on these constructs, with three questions per construct, all on a seven-point Likert scale. One part of the questionnaire was based on the Technology Acceptance Model (TAM), which describes the motivational relationship between the features of a system and the way users employ it [55], with questions adapted from the survey by Venkatesh *et al.* [56]. There was an instance of the ASQ for each task the users were supposed to complete. We added some questions of our own about the constructs perceived learning and technical understanding. See Appendix C.3 for the final version of this questionnaire. Before the main part of the tests, we had our participants sign a consent form, see Appendix C.1, and answer a demographics questionnaire, see Appendix C.2.

The user tests had the following schedule:

1. Introduction of HoloNeoDoppler and the test (2 minutes)
2. User signs the consent form and answers the demographics questionnaire (3 minutes)
3. User goes through the tutorial and knowledge base (5 minutes, tests FRQ10)
4. User performs the tasks (5 minutes, repeated twice)
    a. Get *any* Doppler signal (tests FRQ1, FRQ3, FRQ4, FRQ5, FRQ6)
    b. Find a good ($< 30°$) beam-flow angle (tests FRQ2)
    c. Adjust the PRF to get a clear spectrogram (tests FRQ9)
    d. Submit a spectrogram they are satisfied with (tests FRQ11)
5. User answers the post-tasks questionnaire (5 minutes, tests NFRQ1)

We recorded time spent going through the tutorial, performing the tasks, and filling out the final questionnaire. The task timing was cross-checked with the timestamps on the saved spectrograms and angle data that the users submitted.

After all the tests were complete, we sent the spectrograms and angles to a medical professional for scoring.

3.6 Statistical Analysis

Data from the tests was collected into a spreadsheet and transformed into more usable forms (timestamps to seconds, Likert scale items to discrete numbers, etc.). Simple statistics like average and standard deviation were performed in the spreadsheet. We used a Python library called Seaborn to create a box plot of construct scores.

SPSS Statistics [57] was used for independent t-tests and linear regression analysis. The t-tests were performed with various grouping variables from the demographics questionnaire and timing, angle, and questionnaire construct results as test variables. Linear regression was used on some dependent variables from the timing, angle, and questionnaire results, with a smattering of independent variables that we inspected for statistical significance.

Chapter 4

Implementation

4.1 Augmented Reality Scene

The original plan for HoloNeoDoppler was to replace the physical stomach model from HoloUmoja with a baby doll and use a smaller physical probe model that was more like the NeoDoppler probe. For reasons explored in Section 4.6, the physical probe was abandoned in favor of a virtual probe built with the HoloLens' hand tracking features.

The most important improvements from the preparatory project were that we replaced the fetus model with a cerebral artery model, wrote a new system for spline arteries (Section 4.2), and used that system to model some arteries.

The following semester was spent rewriting the Doppler spectrogram (Section 4.5), adding a CT-scanned model of a baby doll, placing the arteries correctly inside the head of said doll to satisfy FRQ1, modeling more arteries, fixing the depth window implementation (Section 4.3), cutting a hole for the fontanelle in the baby model and making only the fontanelle let ultrasound signals pass through (Section 4.4), reworking the probe tracking method (Section 4.6), adding NeoDoppler-specific information to the menu (Section 4.7), and creating utilities for user tests (Section 4.8).

All the different components were wired up in one Unity scene. Most of what was needed for HoloNeoDoppler could be used in HoloUmoja as well, so objects were abstracted into new prefabs and existing ones were modified for shared functionality. Figure 4.1 shows how the various components of HoloNeoDoppler were related in the final version. Figure 4.2 shows the scene view of HoloUmoja compared to the HoloNeoDoppler scene.

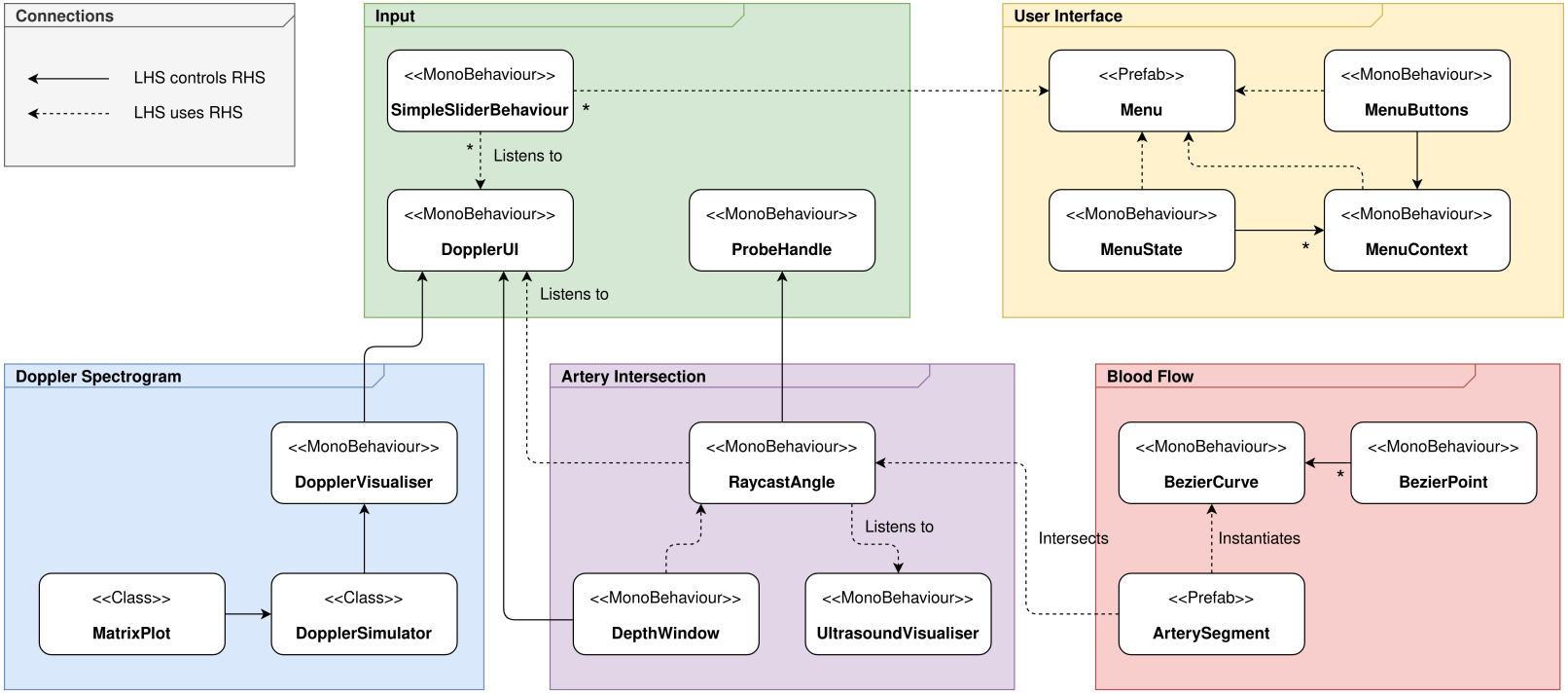

Figure 4.1: Relationship between components in the HoloNeoDoppler implementation.

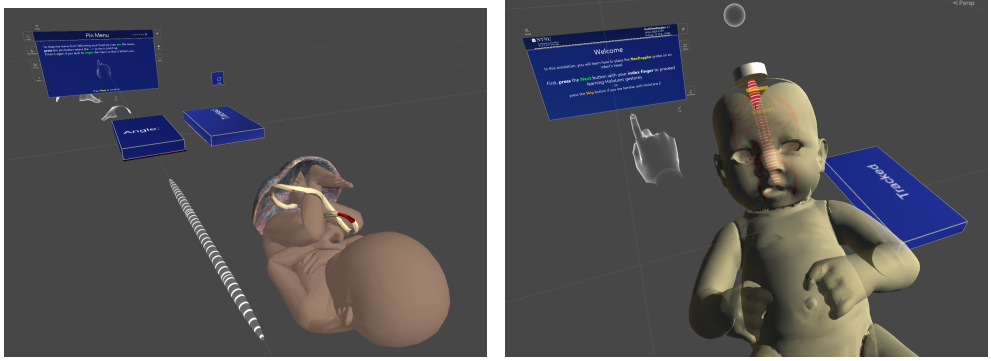

(a) Original HoloUmoja scene. Fetus with umbilical cord and ultrasound beam attached to the image marker.

(b) HoloNeoDoppler scene. An infant with cerebral arteries and a hole serving as the fontanelle. The probe is stuck to the skull.

Figure 4.2: Unity scene before and after NeoDoppler customization.
The blue boxes are MRTK panels. One sticks to the probe and shows the beam-to-flow angle (only in HoloUmoja), and the other sticks to the subject model's marker.

4.2 Artery Modeling

In HoloUmoja, the beam-flow angle was found through ray intersection with a *single* collider (see Figure 2.12) that modeled a unidirectional part of a vein in the umbilical cord. This made the simulated ultrasound beam unable to register signals from the entire umbilical cord, and there was no solution in place to model blood flow through complex networks of blood vessels. Another issue was that the beam-flow angle was restricted to stay between 0° and 90°, with negative Doppler signals being flipped and displayed as if they were positive.

To answer RQ2 and fulfill FRQ2, we had to improve on the artery handling in HoloUmoja. In the preparatory project, several possible solutions were investigated for finding the direction of blood flow along a 3D mesh of cerebral arteries:

1. Find the slope of the artery model at the point of intersection
2. Use a special texture that maps texture coordinates to blood flow direction
3. Instantiate segments along the curves of the arteries that point in the direction of blood flow

Solution 1 was eschewed because of its excessive complexity, and because the limited polygon count supported by the HoloLens 2 [58] could make a gradient less accurate.

Solution 2 would involve too much manual work to be worth attempting, as

one would have to add direction vectors as colors to a texture in some convoluted process.

The third solution could be implemented fairly easily by modeling the arteries with Bézier curves (see Section 2.9) and instantiating cylindrical colliders along the path of each curve. We chose cubic Béziers since they provide a good balance between performance and versatility. Higher-order Bézier curves take more time to evaluate. Because of the recursive nature of Bézier curves, it is possible to create the same curves with cubic Béziers as with higher-order Béziers. With this solution, it would not be necessary to store any more additional data about the arteries than some two-digit number of control points.

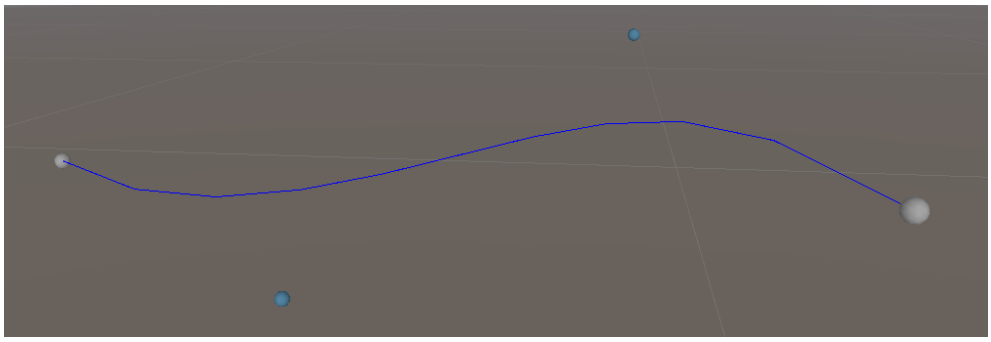

(a) Bézier curve with gizmos showing control points and curve. Grey endpoints, blue middle points.

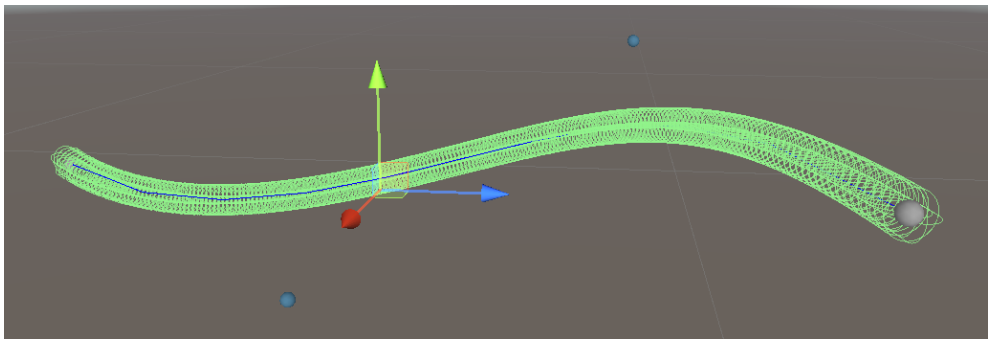

(b) Colliders instanced along this Bézier curve.

Figure 4.3: Bézier curve with/without collider instances

Empty Unity objects were used as control points and made visible with gizmos. The curves were displayed with gizmos in development and cylindrical colliders were instantiated at steps of Δt along their path at runtime using Equation (2.9), see Figure 4.3 and Figure 4.4. The direction of each segment was found by calculating the first derivative of the curve using Equation (2.10). For modeling long arteries, curves could be extended by adding two additional points for $\mathbf{p}_2$ and $\mathbf{p}_3$

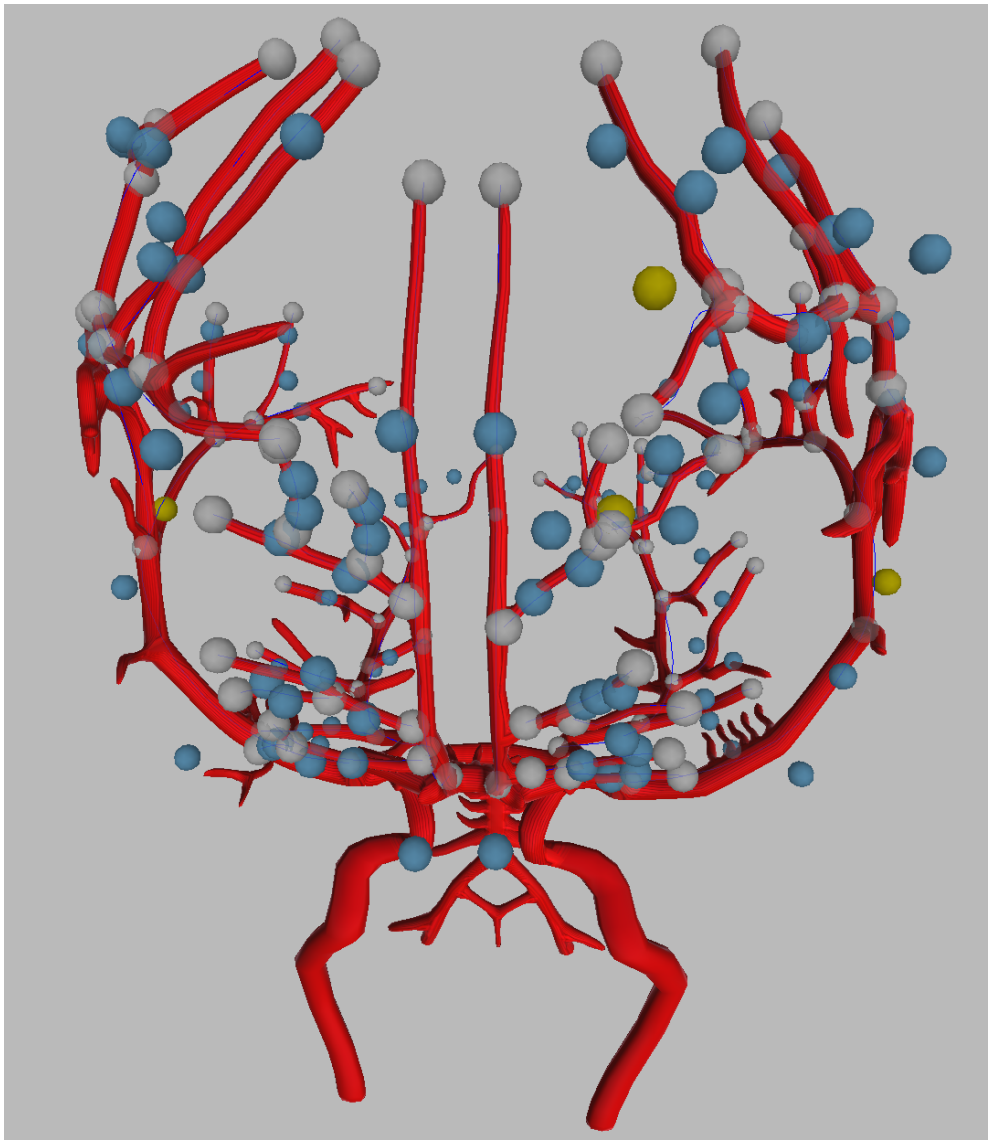

Figure 4.4: Bézier control points (blue, yellow, grey) on artery mesh. Generated curves are shown as thin, blue lines. The yellow control points are mirrored, which makes composite curves smooth.

of additional segments. $\mathbf{p}_3$ of the previous segment became $\mathbf{p}_0$ in the next, and the final control point mirrored $\mathbf{p}_{2'}$ from the last segment:

$$\mathbf{p}_1 = \mathbf{p}_{2'} + 2(\mathbf{p}_0 - \mathbf{p}_{2'}) \tag{4.1}$$

This mirroring is demonstrated in Figure 4.5.

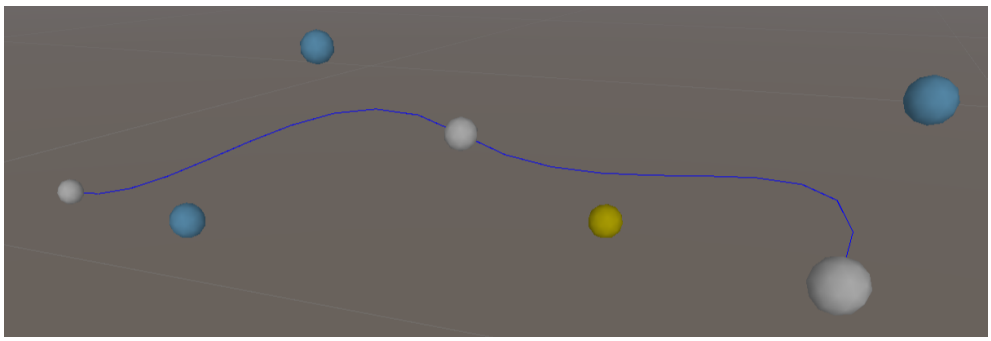

Figure 4.5: Mirrored control point on extended curve. The yellow point is a mirrored version of the blue one to the left of it, mirrored through the middle grey control point.

In order to restrict the number of segments, which would help avoid performance issues on the HoloLens, the step length Δt was based on an estimate of the arc length and the desired number of colliders per unit length, k, like this:

$$\Delta t = \frac{1}{k \cdot |\mathbf{p}_3 - \mathbf{p}_0|}. \tag{4.2}$$

$|\mathbf{p}_3 - \mathbf{p}_0|$ was chosen as the estimate of the arc length since most of the curves were likely to be relatively straight. Algorithm 1 shows how the instantiation process works.

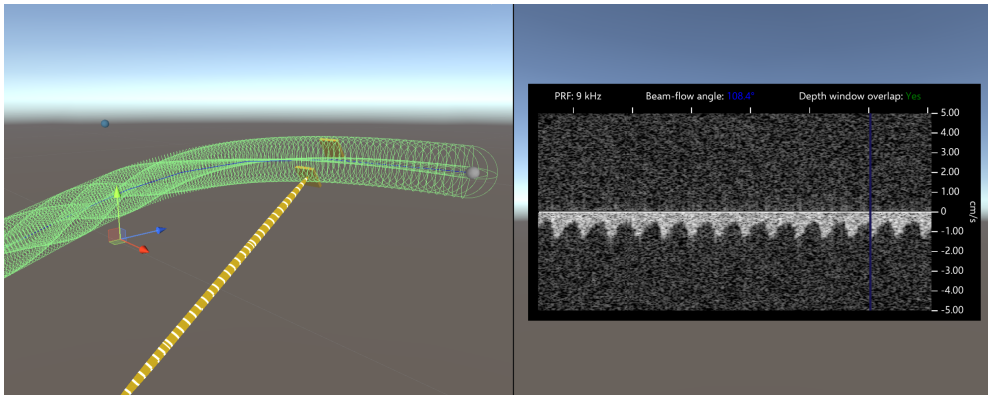

Figure 4.6: Demonstration of ray intersection with Bézier curve-modeled artery. In this case, the beam-to-flow angle is $> 90°$, so the spectrogram dips below 0.

Algorithm 1 Bézier curve instantiation algorithm

Require: $k > 0$
Require: List of control points for segments
  $\mathbf{p}_0, \mathbf{p}_1, \mathbf{p}_2, \mathbf{p}_3 \leftarrow$ first segment
  $\Delta t \leftarrow \frac{1}{k \cdot |\mathbf{p}_3 - \mathbf{p}_0|}$ ▷ Equation (4.2)
  Instantiate colliders along Bézier curve $\mathbf{p}_0, \mathbf{p}_1, \mathbf{p}_2, \mathbf{p}_3$
  with step distance Δt ▷ Equations (2.9) and (2.10)
  $\mathbf{p}_0 \leftarrow \mathbf{p}_3$
  $\mathbf{p}_{2'} \leftarrow \mathbf{p}_2$
  for $\mathbf{p}_2, \mathbf{p}_3 \in$ remaining segments **do**
    $\mathbf{p}_1 = \mathbf{p}_{2'} + 2(\mathbf{p}_0 - \mathbf{p}_{2'})$ ▷ Equation (4.1)
    $\Delta t \leftarrow \frac{1}{k \cdot |\mathbf{p}_3 - \mathbf{p}_0|}$ ▷ Equation (4.2)
    Instantiate colliders along Bézier curve $\mathbf{p}_0, \mathbf{p}_1, \mathbf{p}_2, \mathbf{p}_3$
    with step distance Δt ▷ Equations (2.9) and (2.10)
    $\mathbf{p}_{2'} \leftarrow \mathbf{p}_2$
    $\mathbf{p}_0 \leftarrow \mathbf{p}_3$
  end for

Regarding the restricted angle in HoloUmoja, we removed the transformation from the full range of $[0°, 180°]$ to $[0°, 90°]$. This made it possible to see negative values in the Doppler spectrogram, see Figure 4.6.

4.3 Depth Window

NeoDoppler excludes signals outside a certain range (window size) from a certain depth (sampling depth). HoloUmoja had an unfinished implementation of a version of this feature, where users could only adjust sampling depth and the depth

window itself did not work. In HoloNeoDoppler, we wanted to make it possible to adjust both window size and depth, which would resolve FRQ4.

In the depth window code from HoloUmoja, The `CalculateOverlap` method shown in Code listing 4.1 performed some complicated-looking calculations before returning 1 by default.

Code listing 4.1: Previous overlap calculation

```
public float CalculateOverlap(Vector3 i1, Vector3 i2)
{
    Vector3 p1 = top.position;
    Vector3 p2 = bottom.position;
    var pos = transform.position;

    float distToP1 = Vector3.Distance(pos, p1);
    // distToP2, distToI1, distToI2 calculated similarily

    bool p1Outside = (distToP1 < distToI1 && distToP1 < distToI2)
                  || (distToP1 > distToI1 && distToP1 > distToI2);
    // and p2Outside similarily
    bool p1Inside = distToP1 >= distToI1 && distToP1 <= distToI2;
    bool p2Inside = distToP2 >= distToI1 && distToP2 <= distToI2;

    float overlap = 0f;
    if (p1Outside && p2Outside)
    {
        overlap = 0f;
    } else if (p1Inside && p2Inside)
    {
        overlap = 1f;
    }
    else
    {
        if (p1Inside && p2Outside)
        {
            overlap = (distToI2 - distToP1)/_windowSize;
        }
        else if(p1Outside && p2Inside)
        {
            overlap = (distToP2 - distToI1)/_windowSize;
        }
    }

    Overlap = overlap;
    return 1.0f;//overlap;
}
```

After discussions with the stakeholders, we decided to treat the overlap as an

on/off state [33]. Instead of calculating exactly how much of the artery was encapsulated in the depth window, we simply wanted to know whether the artery was inside the depth window at all. We rewrote the code to the point where it worked and was a substantial improvement over the previous code, see Code listing 4.2.

Code listing 4.2: Rewritten and simplified overlap check

```
private bool IsInsideWindow(Vector3 point)
{
    // Inside if distances to both endpoints are within size
    return Vector3.Distance(point, top.position) <= windowSize &&
           Vector3.Distance(point, bottom.position) <= windowSize;
}

public float CalculateOverlap(Vector3 hit)
{
    return IsInsideWindow(hit) ? 1 : 0;
}
```

However, in the end, we incorporated the depth window check into the intersection test by casting a ray from the start of the depth window, as described in the following section. This way we could avoid cases where the ray hit something outside the depth window and thus reported no overlap, while there actually *was* an artery segment inside the window that the ray had not reached.

In HoloUmoja's measurement menu, the depth window was only controlled by one slider (sampling depth), whereas on a high-end ultrasound scanner, the window would have adjustable depth *and* size [33]. We added another slider for the window size and adjusted the scale to match what we wanted. The expert interview in Appendix B.3 helped define the depth range.

4.4 Artery and Cranium Intersection

In order to simulate that the users must aim the probe down the fontanelle in order to get a signal at all, for FRQ3, a hole approximately equal to the fontanelle was cut into the skull of the baby doll, see Figure 4.7. It was initially a very rough approximation and was refined after the third expert interview, see Appendix B.3. The model with the hole was then used as the visual appearance of the baby in the simulation, with a collider that should stop the ultrasound beam.

The artery intersection procedure was revised to consist of two steps: First, a ray was shot from the probe. If it hit the skull or nothing, no hit was reported. If not, a ray would be cast from the top to the bottom of the depth window. To

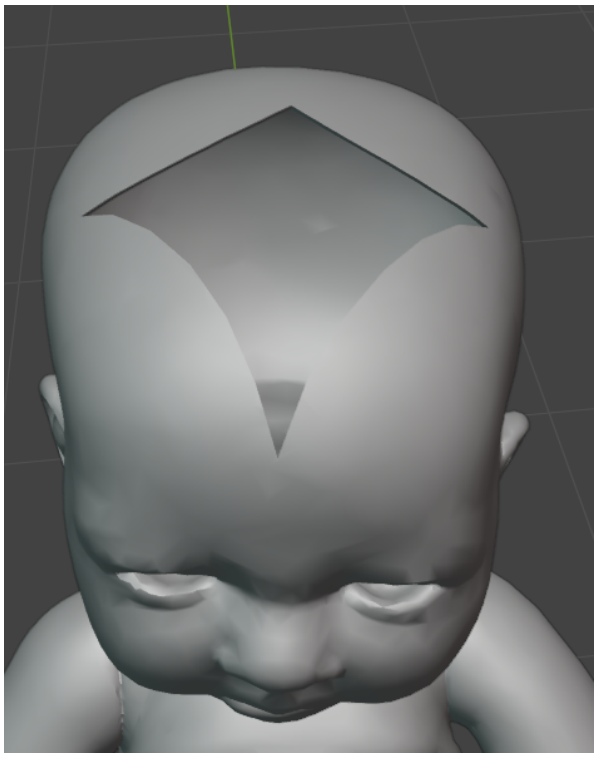

Figure 4.7: Fontanelle cut into baby model

safeguard against errors in the window placement, the skull also blocked this ray. If the ray hit an artery inside the depth window, a hit would be reported at the average angle to all segments that were found inside the depth window. See Figure 4.8 for a demonstration of the rays that are cast, and Figure 4.9 for the three different cases the algorithm could find — except for no intersection with anything.

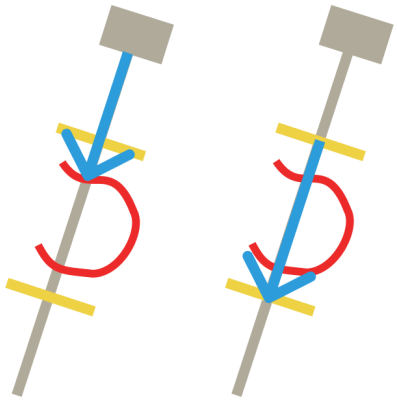

Figure 4.8: The two rays that determine beam-flow angle

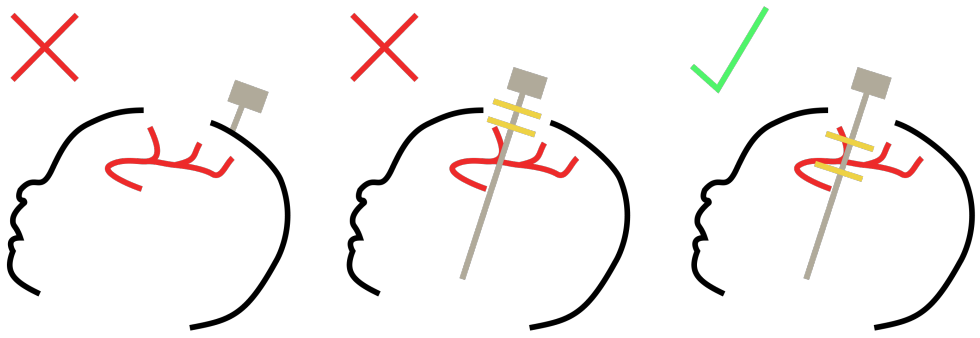

Figure 4.9: The three cases of artery intersection. Skull hit, no overlap with depth window, and a successful measurement.

See Algorithm 2 for a full view of this revised algorithm.

Algorithm 2 Artery intersection algorithm

```
Angle ← 90°                                   ▷ Makes the angle factor cos 90° = 0
Overlap ← 0
Cast ray from probe
if No intersection or ray hit the skull then
    Abort
end if
Cast ray from top to bottom point in depth window
if No intersection or ray hit the skull then
    Abort
end if
Angle ← average angle between ray and all intersected colliders
Overlap ← 1
```

With all components of the probe, the ultrasound beam, and the cerebral arteries in place, the arteries could be oriented and then given a center point such that it was fairly simple to hit the arteries with the probe beam and get a decent angle quickly, which could resolve FRQ6. The two final expert interviews (Appendix B.3 and Appendix B.4) were helpful in adjusting this. The depth window was adjusted to a very shallow initial sampling depth, to force users to adjust the depth window in order to have the probe at a sufficiently parallel angle to the blood flow. Figure 4.10 shows the three cases of intersection on the actual baby model.

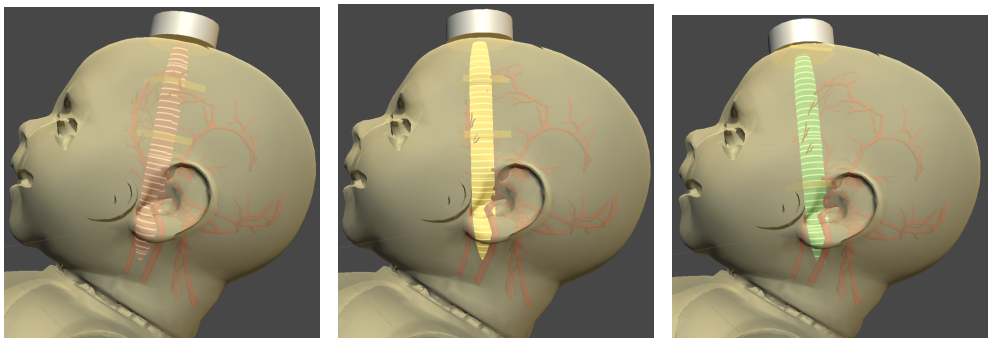

(a) No signal **(b)** Decent signal **(c)** Good signal

Figure 4.10: Intersection cases demonstrated on the baby head

4.5 Improved Spectrogram

For displaying a realistic spectrogram, which would answer RQ3, we ported Matlab code written by Hans Torp to the HoloLens 2. This code simulated a Doppler spectrogram by adding noise to a real velocity sample, shown in Figure 4.11a, and running it through a Fourier transform to generate what looked like a spectrogram, shown in Figure 4.11b. Compare this to the spectrogram from HoloUmoja (Figure 2.13), which showed an unrealistic and low-quality rendition of a simple wave.

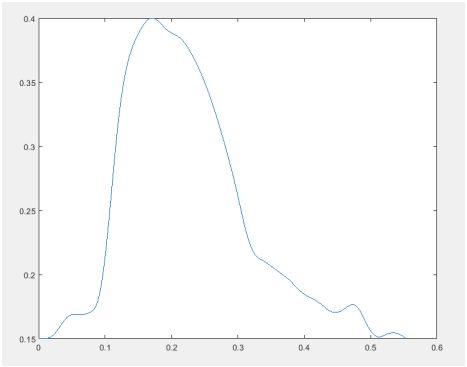

(a) Velocity trace

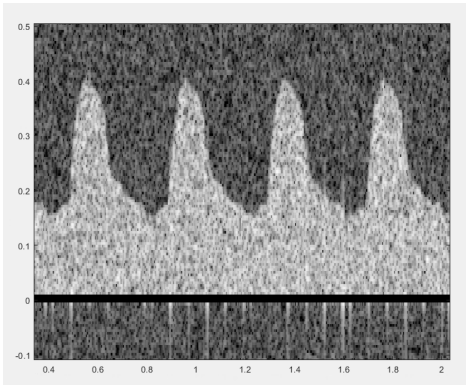

(b) Spectrogram corresponding to repeated copies of the velocity trace

Figure 4.11: Velocity trace and spectrogram in Matlab

Since Matlab has data types and operations from linear algebra in its standard library, and implementing various linear algebra primitives ourselves would be time-consuming and error-prone, we looked at linear algebra libraries for C# that would work on the HoloLens. We chose Math.NET since it was actively developed, open source, and had been used on the HoloLens before. What we did not know at the time was that this library's 2D Fourier implementation only ran on x86 architectures, which posed a problem since HoloLens has an ARM64 processor [54].

Equivalents for the majority of built-in functions in Matlab were identified, but certain operations necessitated a more roundabout coding approach. One example was the `interp1` Matlab function, which interpolated a defined sequence at a list of query points in a simple function call, which in C# had to be written as interpolation followed by queries.

The underlying velocity data that was fed to the spectrogram generation, was a snippet of a real velocity trace that could be repeated seamlessly, shown in Fig-

ure 4.11a with repetitions in spectrogram form in Figure 4.11b. This curve was decidedly more complex than the simple wave used in HoloUmoja, thus fulfilling FRQ7 and contributing to the goal of RQ2. In order to make the Matlab code, which operated on the entire signal at once, work for real-time generation of a spectrogram based on changing parameters, the signal had to be processed in smaller slices. This required saving some signal values from the preceding slice to feed into the generation along with the values for the currently processed slice. We first made a version of the original Matlab code with the input data sliced and verified that this approach functioned, and then wrote C# code that fed slices of the same data into the generation process.

To make the beam-flow angle, which we explored in the previous sections, affect the signal strength on the spectrogram, we used Equation (2.6) and multiplied each velocity data point with the cosine of the angle.

In HoloUmoja, the spectrogram was generated on the same thread as where the engine code ran. With the more expensive operations of the improved spectrogram code, we had to delegate the task to a different thread, which was achieved with C#'s `System.Task` threading library and an asynchronous coroutine that waited for the completion of each slice. To make the slice generation flow evenly in time, we added a delay of

$$|\text{intended duration} - \text{generation time}|$$

seconds to account for varying time spent generating each slice.

To make the spectrogram more realistic and thus fulfill FRQ8, we revised the entire spectrogram generation to add noise to the signal and fill the area under the curve. The improved spectrogram consisted of two layers: Background noise as shown in Figure 4.12, simply created as normal-distributed random values, and a noisy version of the underlying signal. For the noisy signal, the signal's average velocity was used to determine the length of a Tukey window function curve with $r = 0.1$ (almost rectangular) that was zero-padded and multiplied element-wise with random values, to create a spectrum of frequencies up to the frequency corresponding to the current velocity, see Figure 4.13. This spectrum was then run through an inverse Fourier transform to create a random signal with the correct frequencies. The random signal was modified to have an amplitude that made it stand out well enough from the background noise, conjugated if the velocity was negative, and then added to the background noise to create a signal that gave a spectrogram like in Figure 4.14.

Figure 4.12: Background noise

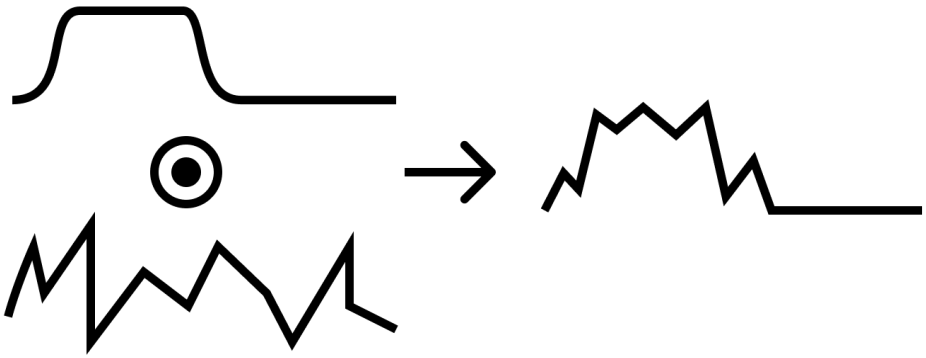

Figure 4.13: Creation of spectrum for signal noise. The Tukey window and the random values are multiplied element-wise to create a combined signal.

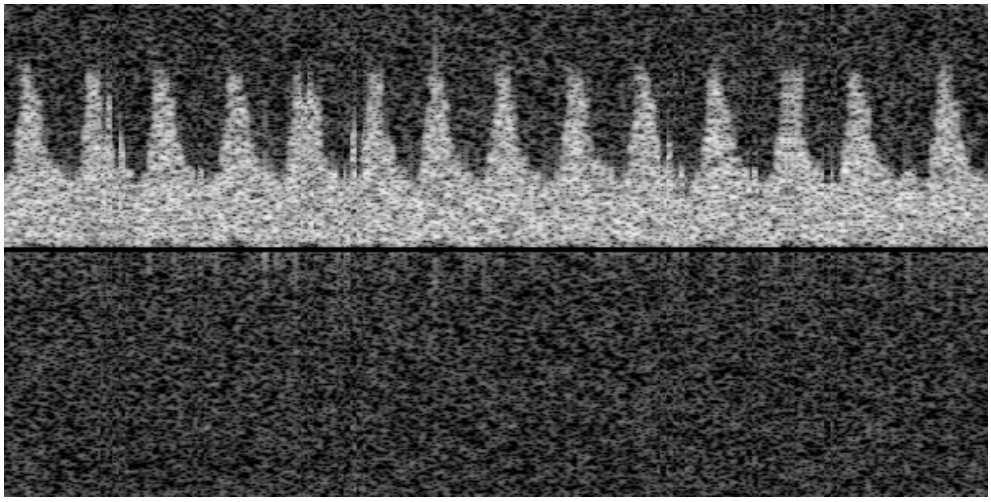

Figure 4.14: Full spectrogram with background noise and signal noise

This combined signal of layered noise was split into overlapping chunks that were treated as rows in a matrix, where the column dimension corresponded to time. Each row was multiplied with a Hamming window to prevent spectral leakage (see Section 2.8.2), then run through a Fourier transform to generate a spectrum for each row, effectively giving a spectrogram corresponding to the changes in signal frequencies over time. This final transform was found to be the most expensive operation in the simulation, causing a massive slowdown in the initial implementation. Parallelizing the loop of Fourier transforms on each row was enough to solve this major performance issue.

In PW Doppler, the PRF determines the sampling rate for the ultrasound signal. At lower PRFs, the spectrogram should show a lower-resolution slice, to resolve FRQ9. This was reflected in HoloNeoDoppler by upscaling the generated spectrogram slices on lower PRFs so that each slice occupied the same horizontal space on the spectrogram. We implemented a simple nearest-neighbor upscaling, as showcased in Figure 4.15, which worked well given the high horizontal resolution of the plot. Although PRF is not adjustable in NeoDoppler (see Section 2.4), it was an important principle to demonstrate, and something that would be configurable in other ultrasound devices.

The y axis of the spectrogram was for velocity. In Section 2.3, we found the maximal velocity based on the Nyquist frequency as Equation (2.8). We labeled the y axis with ticks on the range $[-v_{\max}, v_{\max}]$. Figure 4.15 shows the spectrogram as it was presented to the user, with ticks on the y axis and information about angle, PRF and overlap above it.

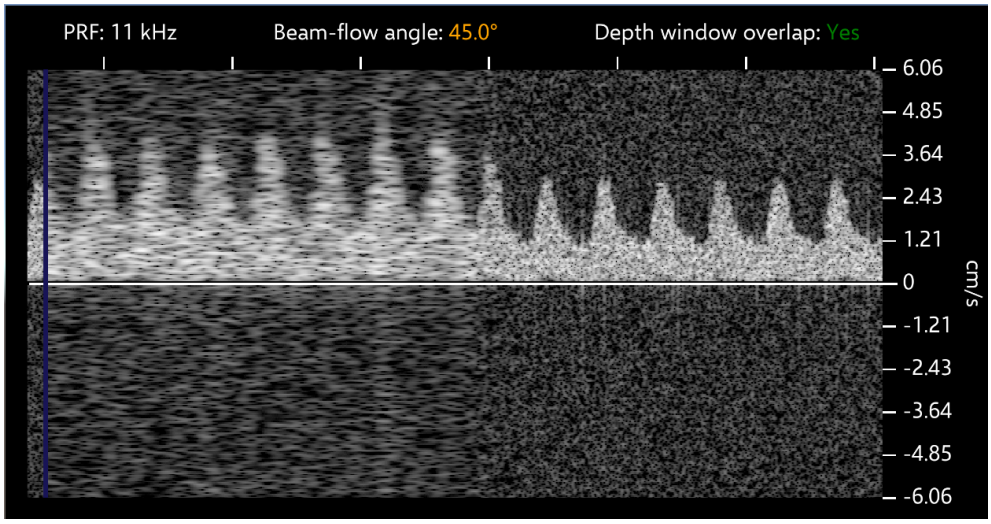

Figure 4.15: Spectrogram where the PRF has been adjusted from low to high, giving a transition between low and high resolution.

4.6 Probe Tracking

The previous marker- and gyroscope-based probe tracking was deemed too slow and imprecise for the more fine-grained movements required to hit arteries in the brain. We considered several solutions for FRQ5:

- Improve the previous tracking, where there *was* a tangible probe, but precision and performance was much worse than desired. A major issue with this what that the attached image marker would make a smaller probe rather unwieldy.
- Track retroreflective spheres mounted on the probe, see Section 2.6. This would also be against the goal of showing a smaller probe, since the probe would need four spheres mounted at different distances from it. The performance of this technique seemed dubious as well: In a paper where the technique was tested, the HoloLens was mounted at a fixed point at all times [37], which might indicate worse performance in cases where the AR device moves with a user.
- Use the native finger tracking support of the HoloLens, which seemed more precise and responsive. However, the HoloLens' grab gesture requires the grabbed objects to be virtual, as the user has to pinch their fingers together within the object, which would make it impossible to use a physical probe.

In tests of the previous project as well as in demonstrations for stakeholders

in this project (see Appendix B.2), users frequently ignored instructions to keep the marker on the probe in their vision at all times, sometimes flipping the probe around so the marker faced the other way. Additionally, the image tracking had some performance issues that made the tracked point lag behind where the marker was for unpredictable durations. This issue was not alleviated by the rotation input from the BLE gyroscope. Lastly, since the NeoDoppler probe was a small, flat device, a physical imitation of it would likely topple or fall with an image marker attached. Retroreflective spheres would have the same issue, as well as requiring special materials and having unknown performance. With all these issues in mind, using finger tracking was the natural choice.

We removed the need for a physical probe with a marker in the NeoDoppler simulation, and added a grabbable flat cylinder that was the new incarnation of the probe. It could be moved by pinching its hitbox and dragging it around, or using the transparent, floating orb that functioned as a grabbable handle that would work without the user needing to hold onto the probe itself at all times, as the probe was stuck to the surface of the baby's head. This was accomplished by projecting a ray from the floating orb handle to the center of the head and moving the probe model to where this ray hit the head. See Figure 4.16 for a demonstration of the pinching gesture.

The direction of the probe underwent a few iterations. It was initially based on the direction to the center of the baby's head, but after a meeting with our supervisor, we decided to add a separate, default mode of free rotation of the probe. Based on feedback from the demonstration for Cimon Medical (see Appendix B.3), we decided to revert to the first version, since the real NeoDoppler probe did not support rotational adjustments. The probe was scaled down and adjusted to fit the new context, and its raycast visualizer was updated to be a little more manageable. The previous ultrasound beam had weird behavior when scaling or rotating it, as its children were oddly transformed.

4.7 Improved Tutorial

HoloUmoja's menu had a Bluetooth connection page (see Figure 2.14) appear after the user finished a basic HoloLens tutorial. This confused most users, and it did not seem necessary to include it. With the new probe tracking, there was no need to check the status of the BLE connection.

The other pages were for image tracking, adjusting parameters, and answering

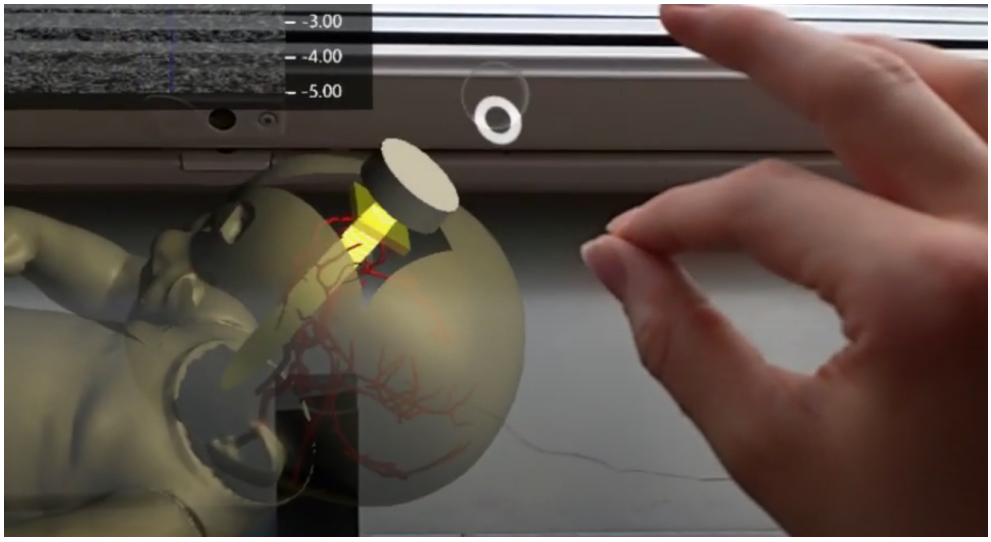

Figure 4.16: A user's hand pinching the probe. Note that HoloLens screenshots display holograms at a significant offset from their real-world position. The pinch was actually performed close to the probe, contrary to what this screenshot makes it seem like.

a quiz that was more akin to a math problem (see Figure 2.15). The quiz was removed since it did not seem to add any value to the simulation.

To help users understand what went on in the simulation regardless of prior knowledge and thus fulfilling FRQ10, we added several pages with custom illustrations that explained the interactions between the ultrasound probe and the cerebral arteries (see Figure 4.17 and Figure 4.18), as well as what the parameters (depth window in Figure 4.19 and PRF in Figure 4.20) actually controlled. Parts of the menu code were reworked to make adding additional menus easier, but since the menu state was based on enums, it was necessary to update all subsequent menus when we added a new page.

4.8 Evaluation Support

In order to have more quantifiable results from user tests and thus satisfy FRQ11, we wanted to have an ultrasound expert grade the spectrograms and positioning that our testers ended up with. We added a button in the estimation menu (shown in Figure 4.21) that saved the current spectrogram to a file, along with beam-flow angle, overlap, and position and rotation of the probe.

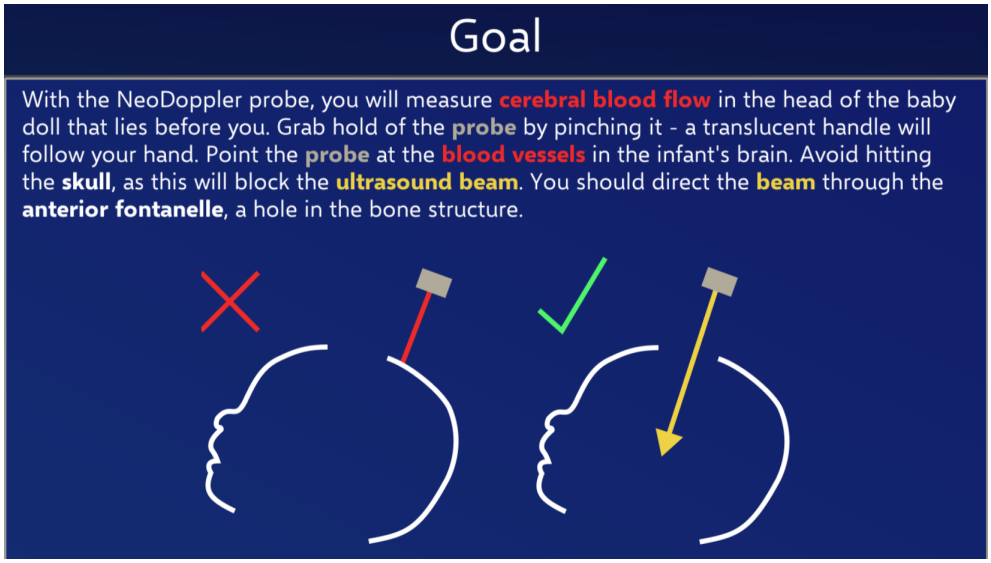

Figure 4.17: Doppler ultrasound information, page 1: Introduction and fontanelle

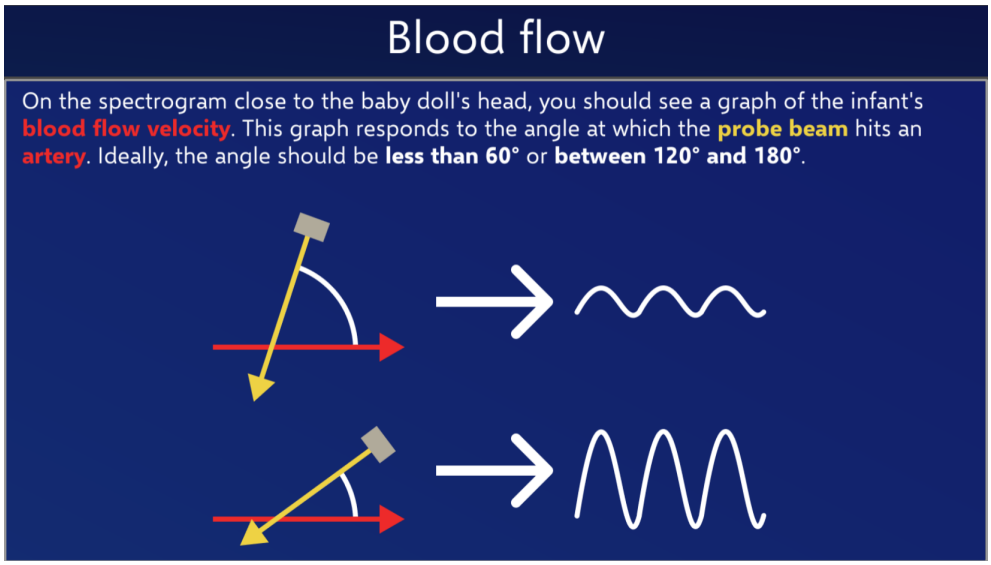

Figure 4.18: Doppler ultrasound information, page 2: Angle

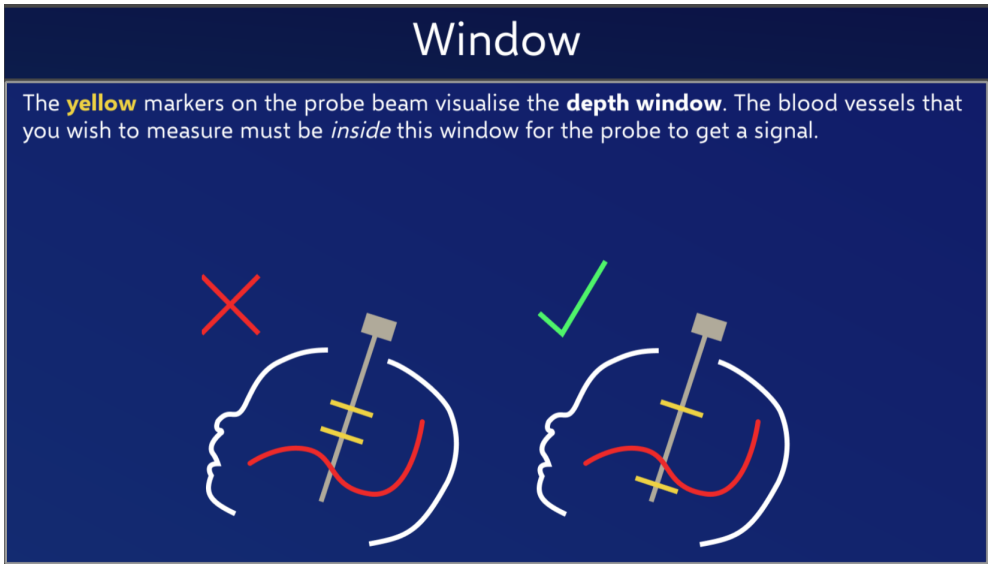

Figure 4.19: Doppler ultrasound information, page 3: Depth window

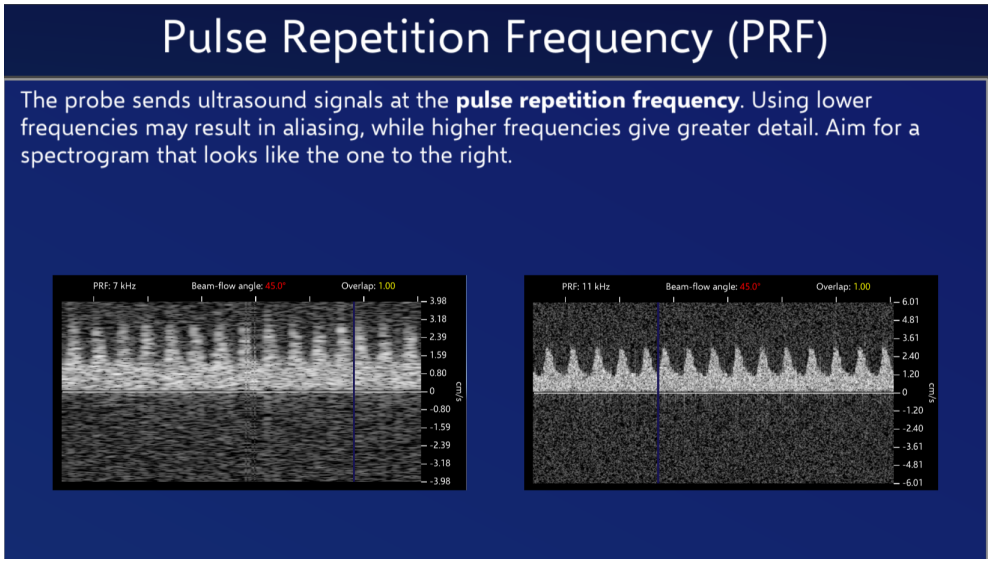

Figure 4.20: Doppler ultrasound information, page 4: PRF

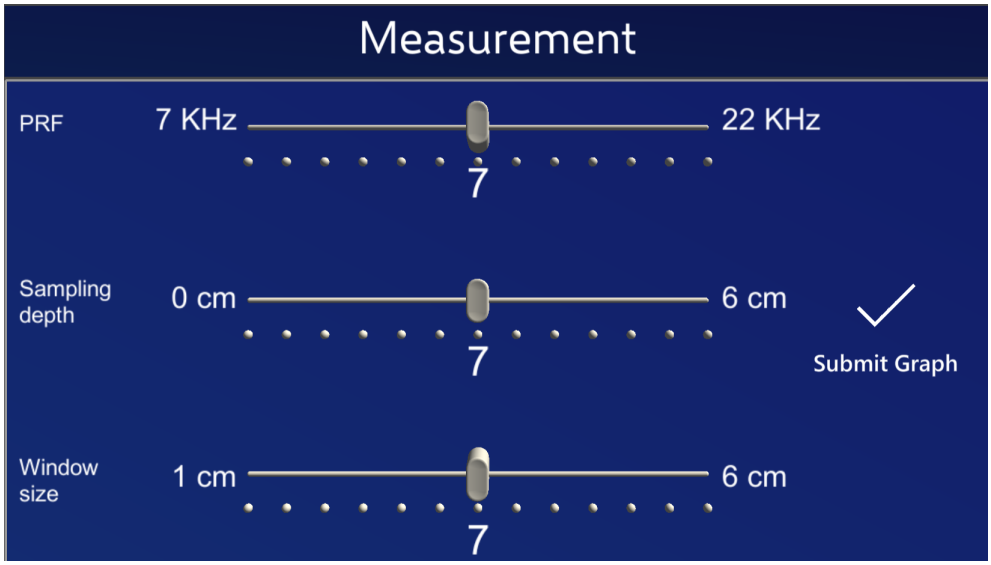

Figure 4.21: Measurement menu with sliders

4.9 Refactor

We strove to improve the code quality of the project as we added features that touched on old code of dubious quality, which we stated as NFRQ3.

A recurring problem was the lack of useful inputs to delegate functions. The following is an example of this.

Originally, the `OnValueUpdate` delegate in the `SimplifiedSliderBehaviour` class did not supply a value when invoked; the value had to be fetched from its `CurrentValue` property. This made changing the slider update code an error-prone affair, as one had to update both the LHS and RHS of the assignment if a slider was changed to mean something else.

Code listing 4.3: Original PRFSliderUpdate

```
private void PRFSliderUpdate()
{
    _dopplerVisualiser.PulseRepetitionFrequency = prfSlider.CurrentValue;
    _dopplerVisualiser.UpdateDoppler();
}
```

In the rewritten code, the delegate supplied the current slider value itself when invoked, and there was no need to manually call `UpdateDoppler` as that was incorporated into the `PulseRepetitionFrequency` property setter.

Code listing 4.4: New PRFSliderUpdate

```
private void PRFSliderUpdate(float value)
{
    dopplerVisualiser.PulseRepetitionFrequency = value;
}
```

Implementing the improved spectrogram involved rewriting the existing spectrogram code almost from scratch, with heavy refactoring of the `DopplerVisualiser` class that was responsible for displaying the generated result.

The raycast class originally controlled the class that adjusted the color of the ultrasound beam. We inverted this coupling and made the coloring class listen to changes in angle and overlap, like what was done in all the other components that responded to those changes.

We overhauled parts of the file structure so that the scripts were less cluttered. As mentioned before, we extracted some reusable objects into prefabs to make future alternate scenes easier to create.

This section has covered only *some* aspects of the refactoring, we refer to the history in the GitHub repository at `https://github.com/toberge/holoneodoppler`.

Chapter 5

Results

In this chapter, we present the results of this project. Section 5.1 summarizes the implemented application, while the remaining sections describe the results gathered from the user tests.

5.1 Implemented Simulation

In the final version of HoloNeoDoppler, shown in Figure 5.1 which is referred to in **(bold)** from here on, users are first presented with the same tutorial as in HoloUmoja, which goes through basics like pinching sliders and grabbing menus. After the technical tutorial come a few pages with information about Doppler ultrasound, to prepare users for the main part of the simulation. With newfound or reaffirmed knowledge about ultrasound, users are all set to track the image marker **(a)** for the baby model and proceed to interact with the probe **(b)**. The menu becomes a set of sliders that adjust PRF and depth window **(c)**. By pinching the probe, shown as a gray disc on top of the infant's head **(b)**, users can adjust its position and orientation to aim at cerebral arteries **(d)** through the fontanelle. The probe will be red as long as it has no signal, and turn yellow or green depending on the insonation angle when it intersects an artery. The spectrogram **(e)**, which hovers around the baby, will respond to a successful intersection with a signal. The amplitude of the signal varies depending on the beam-flow angle that users adjust by moving the probe. The depth window is shown as two yellow boxes on the probe beam **(f)**. After capturing a satisfactory spectrogram, users can press the submit button **(g)** to save it. These stored spectrograms were among the results we describe later in this chapter.

Compare to the result from the preparatory project shown in Figure 5.2.

For a full visual demonstration of the final product, watch the demonstration video here: `https://youtu.be/yTsN4qUqkss`

Note that in the video, the baby is present from the start, since it was already tracked. This made it possible to demonstrate some concepts while going through the knowledge base. Also note that screenshots and videos captured on the HoloLens show all virtual elements above the real-world capture, while the user actually sees their hands in front of the holograms and so on. The real-world elements are shifted from their position in hologram space as well.

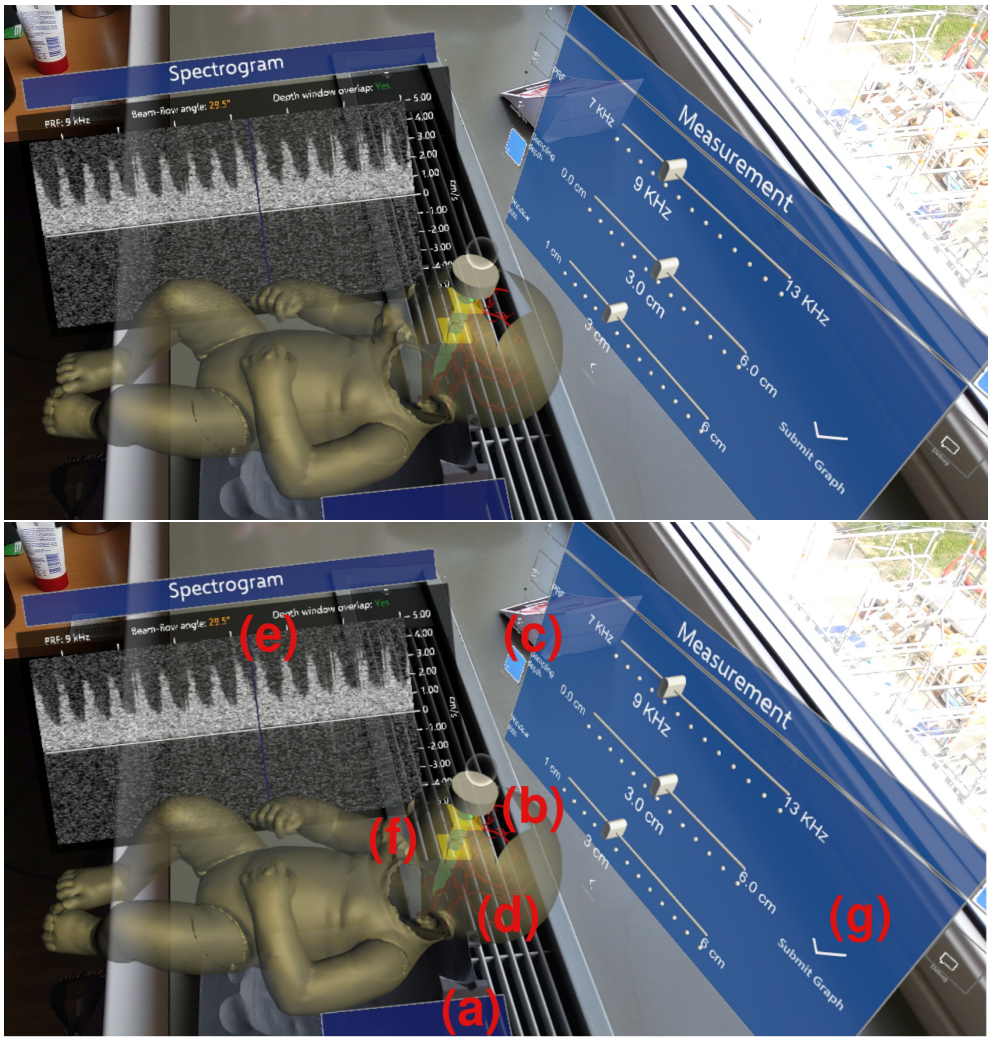

Figure 5.1: Result near completion of the master thesis. This version was evaluated in the user tests. Displayed with and without annotations.

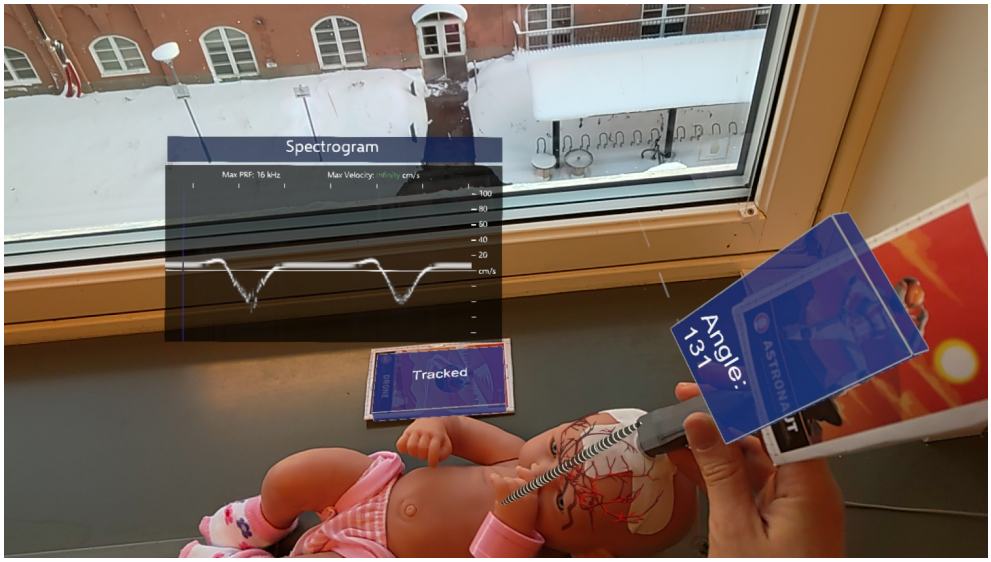

Figure 5.2: Result after preparatory project. The old probe tracking was still in use.

5.2 User Tests

We gathered results as described in Section 3.5 from $n = 14$ participants, all medical students.

5.3 Demographics

These results are answers to the questionnaire shown in Appendix C.2.

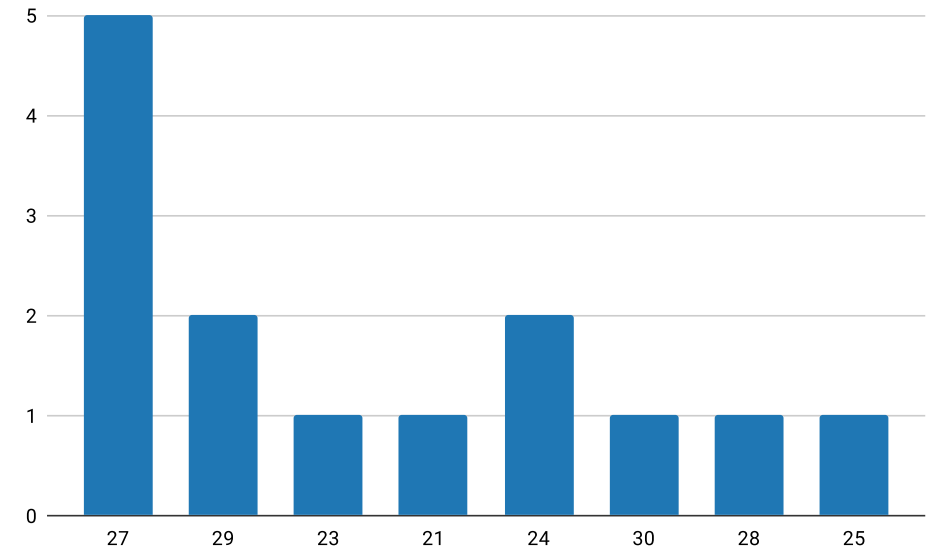

Figure 5.3: Age distribution of the participants

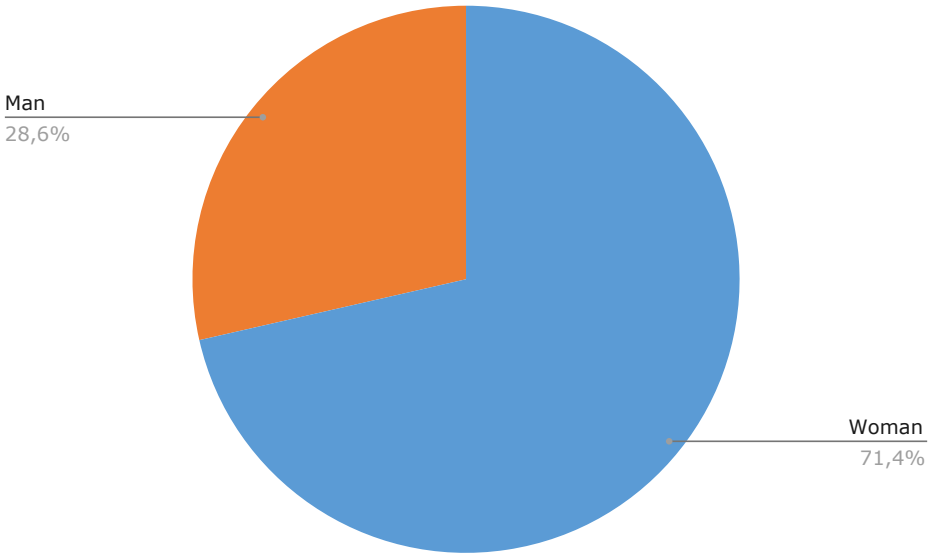

Figure 5.4: Gender distribution of the participants

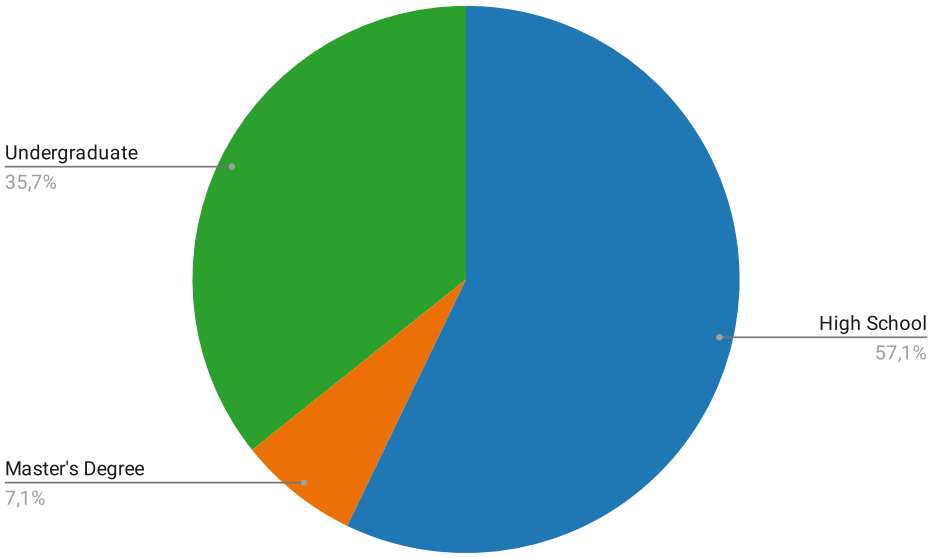

Figure 5.5: Highest level of education achieved by the participants

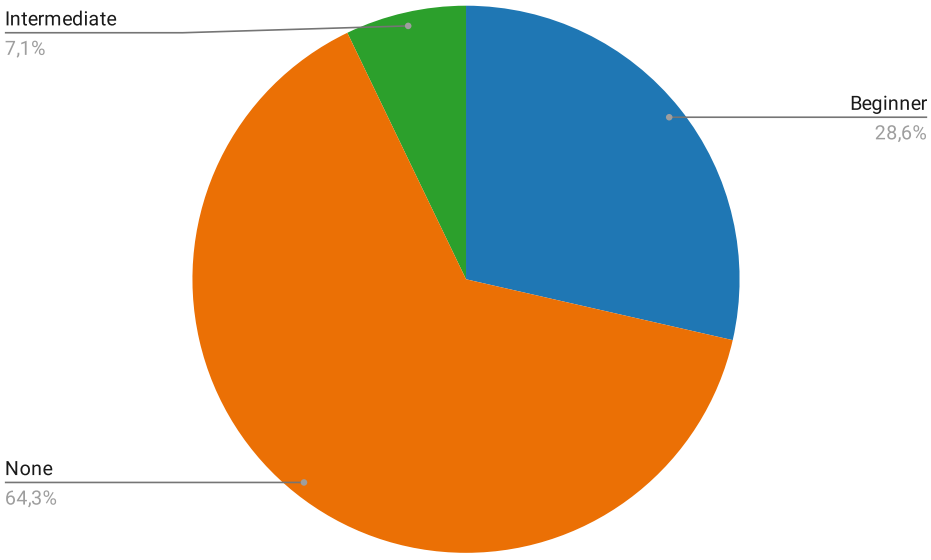

Figure 5.6: Experience with mobile AR

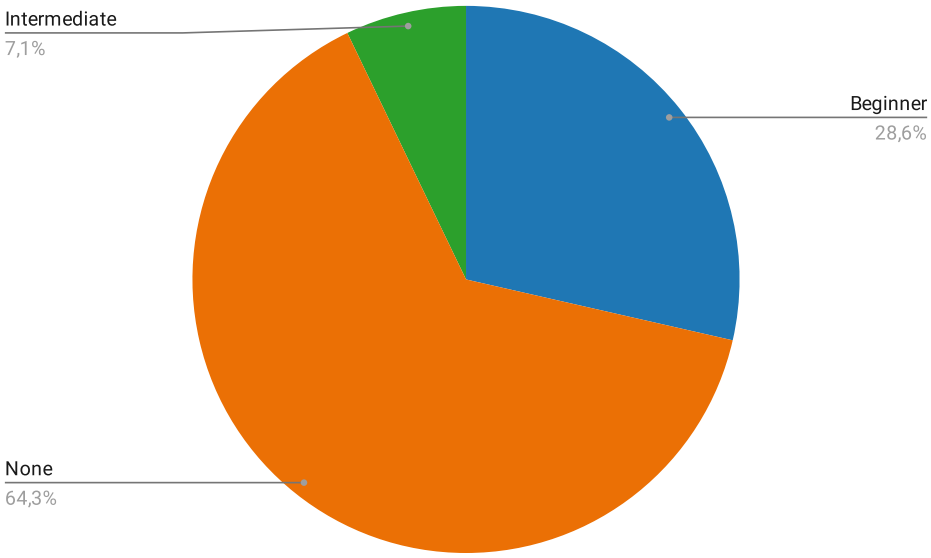

Figure 5.7: Experience with head-mounted displays

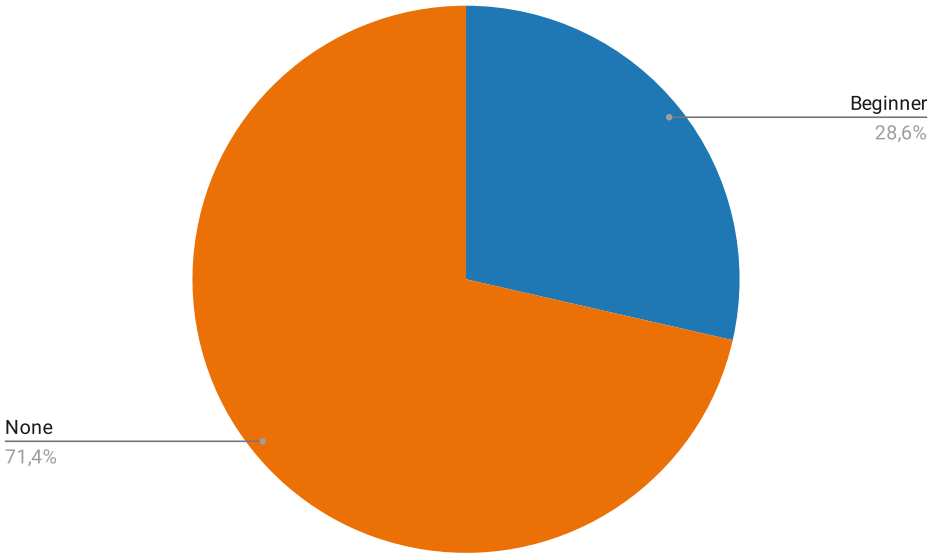

Figure 5.8: Experience with HoloLens 1/2

5.4 Simulation Tasks

We recorded the time each user spent on their two attempts, as well as going through the tutorial and filling out the questionnaire. Since the timing could differ by several seconds depending on how quickly we responded during testing, we rounded the values to the nearest fifth second. These times are shown in Table 5.2 along with the angle of the spectrograms submitted at the end of each attempt. In some instances, we did not time the users in the tutorial and questionnaire, and in one case the second attempt was not submitted by the user. This missing data is indicated with N/A in the table.

The results were scored on the scale defined in Table 5.1:

Criteria	**Score**
No signal	0
Stable signal, angle $> 60°$	1
Stable signal, angle $50° - 60°$	2
Stable signal, angle $40° - 50°$	3
Stable signal, angle $30° - 40°$	4
Stable signal, angle $25° - 30°$	5
Stable signal, angle $20° - 25°$	6

Table 5.1: Scoring system for spectrogram evaluation

Tutorial	**First attempt**			**Second attempt**			**Delta**	**Questionnaire**
time	**Time**	**Angle**	**Score**	**Time**	**Angle**	**Score**	**time**	**time**
N/A	3:55	22.4	6	1:40	26.7	6	2:15	N/A
10:00	3:50	20.8	6	1:45	N/A	N/A	2:50	N/A
6:20	5:40	58.5	2	3:10	57.4	2	2:30	4:00
7:00	8:20	49.2	3	2:00	54.8	3	6:20	4:00
4:00	9:40	29.6	5	1:30	29.6	5	8:10	5:30
5:00	4:05	56.4	2	1:45	75.8	1	2:20	5:30
N/A	4:30	54.3	2	1:15	53.9	2	3:15	6:30
8:00	5:40	23.6	6	1:05	23.1	6	4:35	4:20
4:20	8:55	25.6	5	1:50	28.0	5	7:50	4:20
5:05	4:20	41.0	3	2:00	46.0	3	2:20	5:10
2:20	4:00	55.2	2	3:25	56.3	2	0:35	4:20
5:20	6:35	21.5	6	7:45	26.7	5	-2:50	2:50
4:00	5:15	55.4	2	1:00	55.5	2	4:15	5:00
4:23	4:50	58.1	2	1:25	57.5	2	3:25	5:10
Mean and standard deviation								
5:29	5:41	40.8	3.71	2:15	45.5	3.38	3:25	4:43
±2:04	±1:57	±15.9	±1.82	±1:43	±16.7	±1.76	±2:30	±0:56

Table 5.2: Time, angles, and scores for the user tests

To illustrate the variance in submitted spectrograms, Figure 5.9 shows the worst user's results and Figure 5.10 shows the best user's results.

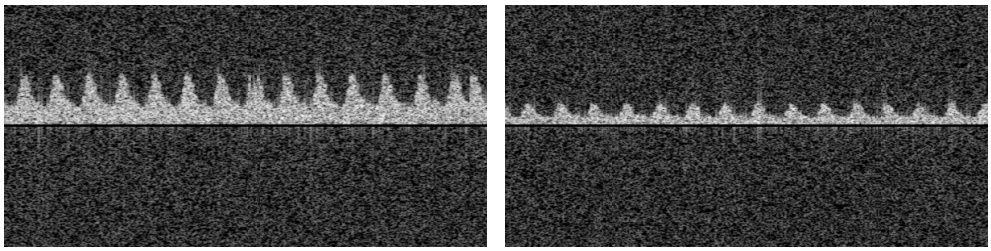

(a) First attempt **(b)** Second attempt

Figure 5.9: The worst set of submitted spectrograms

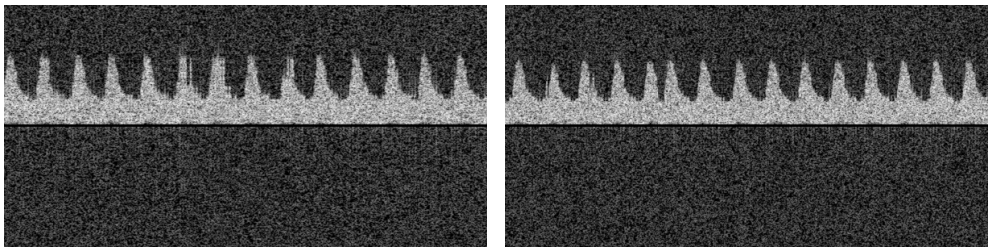

(a) First attempt **(b)** Second attempt

Figure 5.10: The best set of submitted spectrograms

We made some quantifiable observations that we summarize in Table 5.3. 5 users had trouble pressing buttons, 3 found pinching the probe to be quite hard, and 3 others needed the lights to be off in order to see the holograms. 9 users expressly stated that they found testing HoloNeoDoppler to be "cool" or "fun".

Trouble with pressing buttons	**Trouble with pinching the probe**	**Found the holograms hard to see**	**Stated that the project was "cool" or "fun"**
X	-	-	-
-	-	-	-
-	-	-	-
-	-	**X**	**X**
X	-	**X**	**X**
X	-	-	**X**
-	-	-	**X**
X	-	**X**	**X**
-	**X**	-	-
-	-	-	-
-	**X**	-	**X**
-	-	-	**X**
-	**X**	-	**X**
-	-	-	**X**
X	-	-	-
5	3	3	9

Table 5.3: Quantified observations. **X** marks instances.

5.5 Questionnaire

The results for the post-test questionnaire described in Appendix C.3 were as follows:

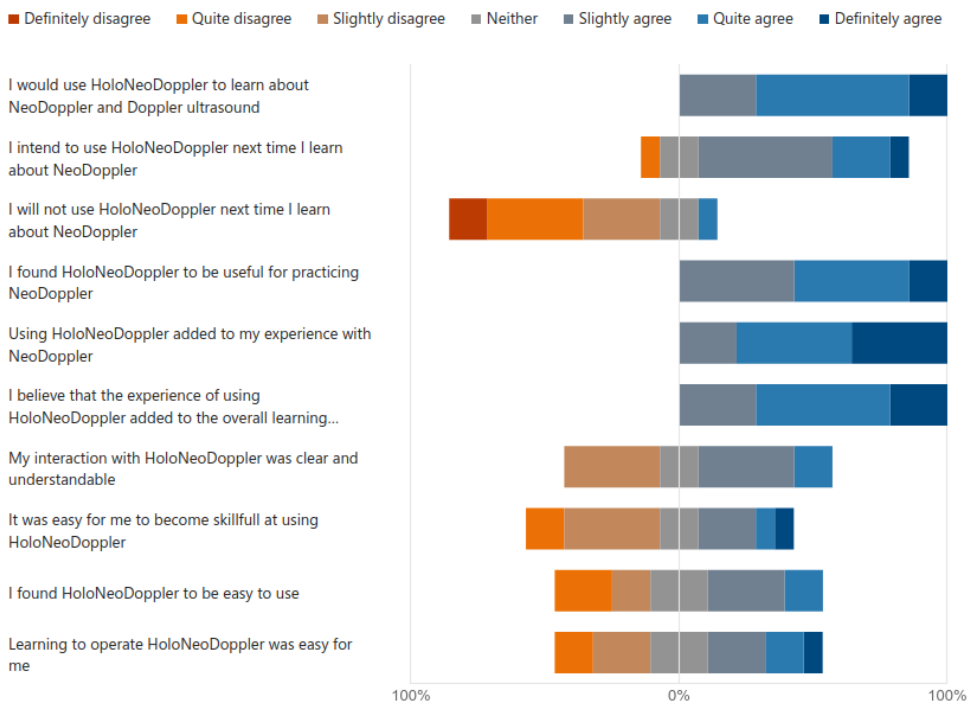

Figure 5.11: Technology Acceptance Model (TAM) results

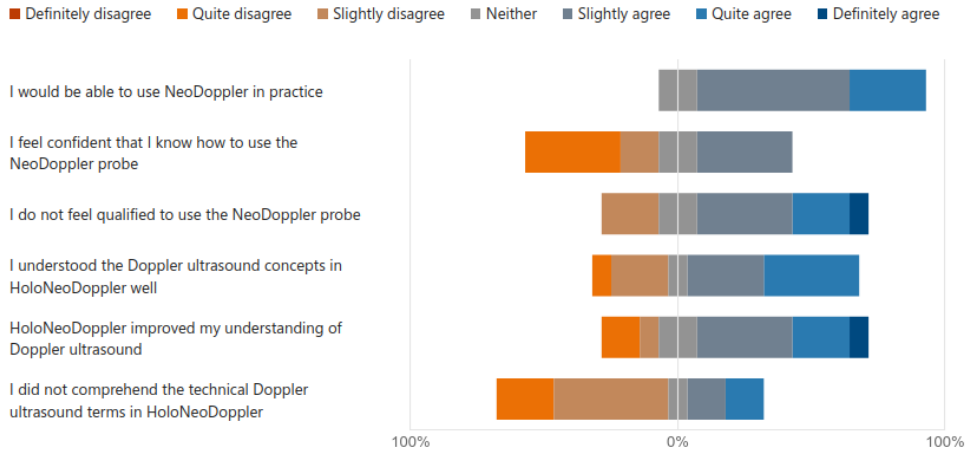

Figure 5.12: Perceived learning and technical understanding results

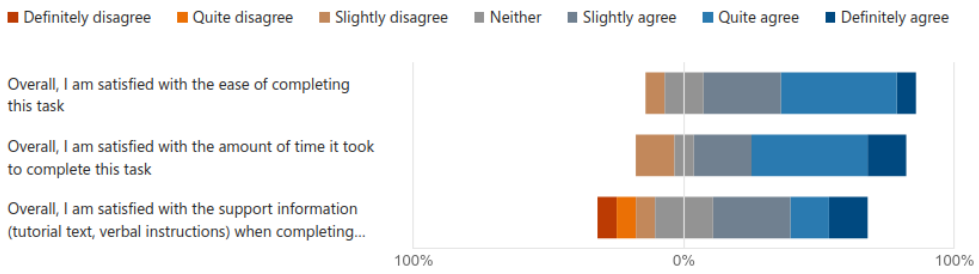

Figure 5.13: ASQ for finding a signal

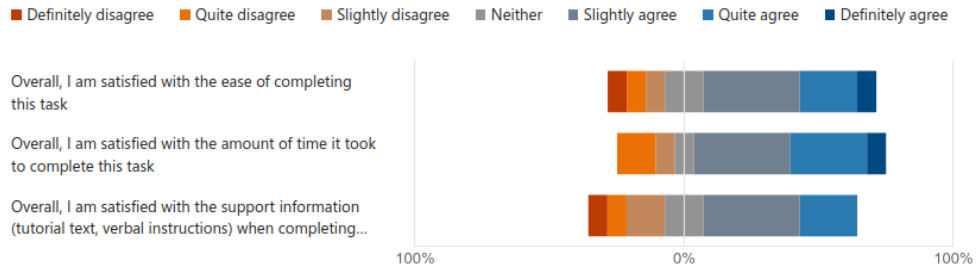

Figure 5.14: ASQ for getting a good angle

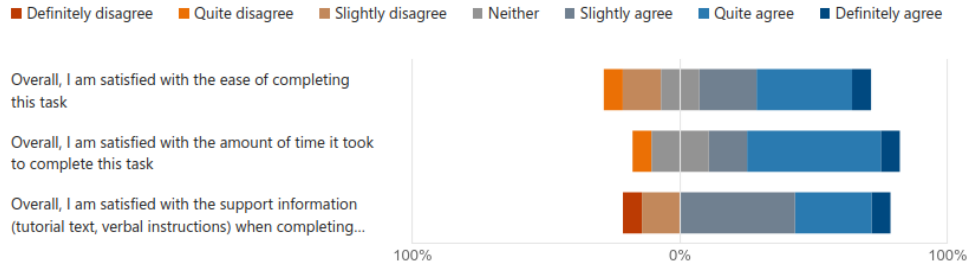

Figure 5.15: ASQ for adjusting PRF

The scores for each construct in the questionnaire was determined as the average of the answer to each question in the construct. Answers were encoded as numbers from 1 (definitely disagree) to 7 (definitely agree), and answers to negatively charged questions ("will not", "did not", "do not") were inverted. These scores are shown in Figure 5.16 and Table 5.4:

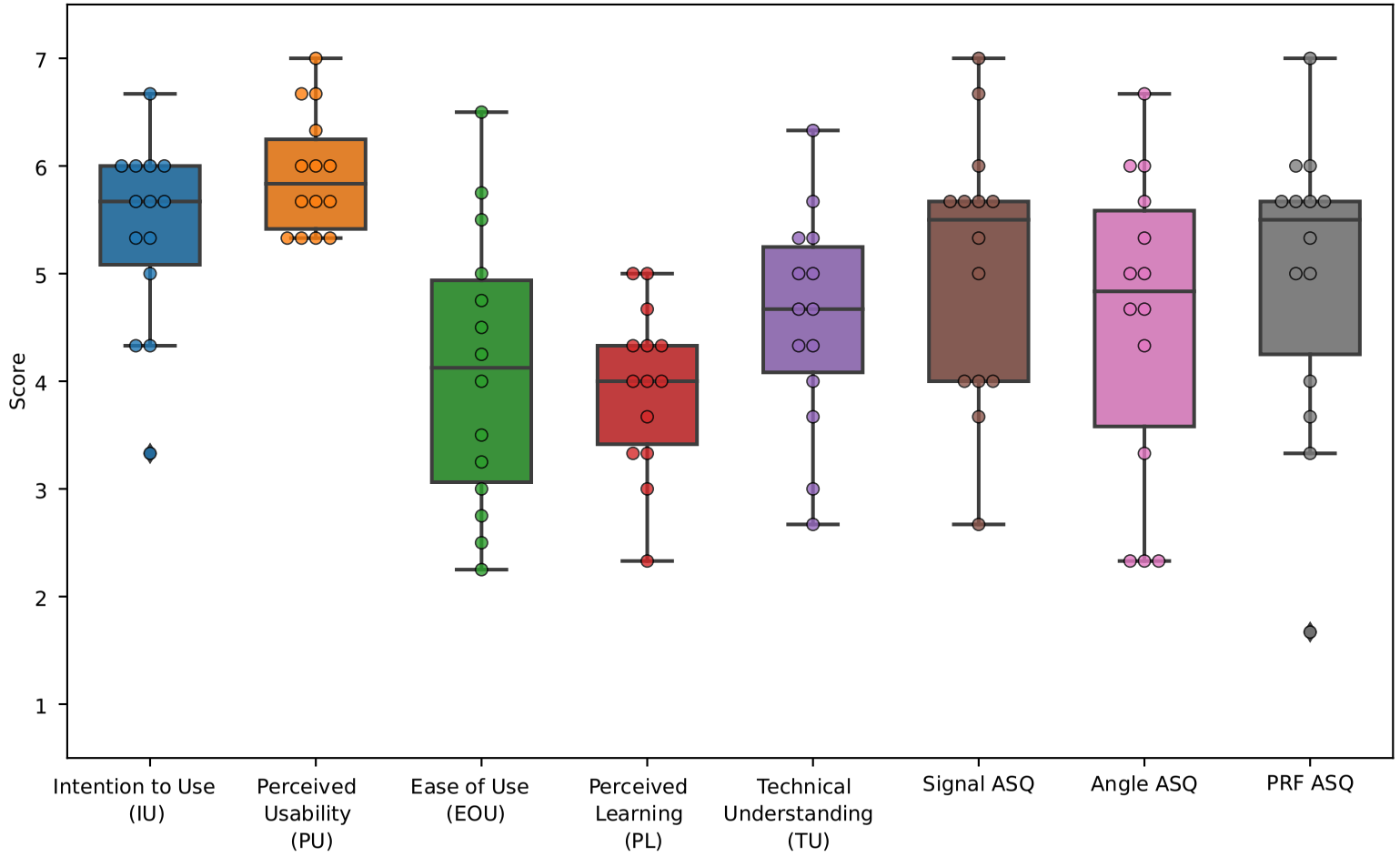

Figure 5.16: Box plot of construct scores

Construct	**Average ± deviation**	**Discretized**
Intention to Use	5.38 ± 1.13	Slightly agree
Perceived Usefulness	5.93 ± 0.75	Quite agree
Perceived Ease of Use	4.11 ± 1.37	Neither
Perceived Learning	3.95 ± 1.40	Neither
Technical Understanding	4.57 ± 1.40	Slightly agree
Signal ASQ	5.07 ± 1.40	Slightly agree
Angle ASQ	4.55 ± 1.55	Slightly agree
PRF ASQ	4.98 ± 1.42	Slightly agree

Table 5.4: Average construct scores with standard deviation

5.6 Qualitative Observations and Feedback

During the tests, we made several observations and received some feedback that did not fall neatly into the quantified data:

- One tester spent *more* time on their second attempt. We asked them why and discovered that this person had not understood that they were supposed to perform the tasks quickly.
- Another had trouble pressing buttons because their arms were so short that they had to stretch out to reach the UI.
- It seemed that most testers refrained from going back to check parts of the information base that they were uncertain about, except for at least one tester who did it of their own volition.
- Several testers commented that releasing their pinch was hard.
- Often, when testers struggled to pinch the probe, the back of their hand obscured the pinching gesture from the sensors on the HoloLens.
- In one case, a tester used the spectrogram screenshots that illustrated the impact of PRF adjustments (shown in Figure 4.20) as an ideal example that they should recreate. This screenshot was not intended as a demonstration of good practice, it was merely an illustration of the difference between low and high PRF.
- Some testers placed the measurement menu with sliders for the adjustable parameters down by the spectrogram, since they wanted to reach them easily, and complained about the default position of these settings. One tester suggested that the sliders could be placed somewhere around the baby model.
- One tester was confused by the angle displayed on the spectrogram being

yellow when it was less than 30°, and expected it to turn green in this case.
- One tester remarked that "This would have been easier if you were in a room [in VR] and didn't look through glasses."
- Some testers spent more time than strictly necessary on the reset button part of the tutorial, and did not seem to understand its purpose.
- One tester commented that when answering the question about confidence in using the NeoDoppler probe, the participants were likely to consider it in a clinical setting where there are a lot of different factors in addition to just placing and adjusting the probe.

A few testers found novel bugs:

- One tester experienced a bug where they did not reach the final menu and thus were unable to adjust the sampling depth for a while.
- Another tester saw that the probe's position was reset after they submitted their spectrogram, but the spectrogram still registered a signal from the probe, somehow.

5.7 Statistical Analysis

This section will briefly present the different statistical analyses that were conducted on the data presented in the preceding sections. The full analyses can be found in Appendix D. The unit of the timing variables was seconds, the angle variables were in degrees, and the other variables were nominal or on ordinal scales. We did not use the spectrogram scores for the analysis, since we received them quite late, and they were based on and highly correlated with the angles that the users achieved (see Table 5.1).

We only found one statistically significant result from applying t-tests with the timings and angles as dependents and each of the different demographics variables as groupings. For time on the first attempt split by prior experience with HoloLens, the difference in mean was statistically significant (p-value for non-equal variance was < 0.05), as shown in Figure 5.17.

Group Statistics

	HoloLens	N	Mean	Std. Deviation	Std. Error Mean
FirstTime	None	10	379.5000	119.61628	37.82599
	Beginner	4	245.0000	10.80123	5.40062

Independent Samples Test

		Levene's Test for Equality of Variances		t-test for Equality of Means						
									95% Confidence Interval of the Difference	
		F	Sig.	t	df	Sig. (2-tailed)	Mean Difference	Std. Error Difference	Lower	Upper
FirstTime	Equal variances assumed	8.833	.012	2.192	12	.049	134.50000	61.36834	.78988	268.21012
	Equal variances not assumed			3.520	9.359	.006	134.50000	38.20958	48.56670	220.43330

Figure 5.17: T-test for time on first attempt, grouped by HoloLens experience

After performing t-tests of each demographic factor on the construct scores, we found that the ASQ scores for the "find a good angle" task were significantly different for users with and without experience with mobile AR (see Figure 5.18) and HoloLens (see Figure 5.19).

Group Statistics

	Mobile_AR	N	Mean	Std. Deviation	Std. Error Mean
Angle_ASQ	None	9	3.9259	1.39222	.46407
	Beginner	5	5.6667	.70711	.31623

Independent Samples Test

		Levene's Test for Equality of Variances		t-test for Equality of Means						
									95% Confidence Interval of the Difference	
		F	Sig.	t	df	Sig. (2-tailed)	Mean Difference	Std. Error Difference	Lower	Upper
Angle_ASQ	Equal variances assumed	5.146	.043	-2.584	12	.024	-1.74074	.67369	-3.20859	-.27289
	Equal variances not assumed			-3.100	11.986	.009	-1.74074	.56157	-2.96446	-.51702

Independent Samples Effect Sizes

		Standardizer[a]	Point Estimate	95% Confidence Interval	
				Lower	Upper
Angle_ASQ	Cohen's d	1.20783	-1.441	-2.651	-.185
	Hedges' correction	1.29049	-1.349	-2.481	-.173
	Glass's delta	.70711	-2.462	-4.398	-.460

a. The denominator used in estimating the effect sizes.
Cohen's d uses the pooled standard deviation.
Hedges' correction uses the pooled standard deviation, plus a correction factor.
Glass's delta uses the sample standard deviation of the control group.

Figure 5.18: Effect of mobile AR experience on the ASQ score on the angle task

Group Statistics

	HoloLens	N	Mean	Std. Deviation	Std. Error Mean
Angle_ASQ	None	10	4.2000	1.57292	.49740
	Beginner	4	5.4167	.50000	.25000

Independent Samples Test

		Levene's Test for Equality of Variances		t-test for Equality of Means						
									95% Confidence Interval of the Difference	
		F	Sig.	t	df	Sig. (2-tailed)	Mean Difference	Std. Error Difference	Lower	Upper
Angle_ASQ	Equal variances assumed	4.709	.051	-1.485	12	.163	-1.21667	.81934	-3.00186	.56852
	Equal variances not assumed			-2.186	11.852	.050	-1.21667	.55669	-2.43127	-.00206

Independent Samples Effect Sizes

		Standardizer[a]	Point Estimate	95% Confidence Interval	
				Lower	Upper
Angle_ASQ	Cohen's d	1.38494	-.878	-2.072	.349
	Hedges' correction	1.47973	-.822	-1.940	.326
	Glass's delta	.50000	-2.433	-4.579	-.229

Figure 5.19: Effect of HoloLens experience on the ASQ score on the angle task

We performed linear regression for the angle on the second attempt, to check what could determine the quality of the second attempt. Only the angle on the first attempt was found to be a statistically significant determinant of the angle on the second attempt, as shown in Figure 5.20.

In addition to the second angle, we tested other possible dependent variables: time spent on the second attempt and time spent filling out the questionnaire. No interesting results were found.

Model Summary[b]

Model	R	R Square	Adjusted R Square	Std. Error of the Estimate
1	.945[a]	.892	.883	5.71840

a. Predictors: (Constant), FirstAngle

b. Dependent Variable: SecondAngle

ANOVA[a]

Model		Sum of Squares	df	Mean Square	F	Sig.
1	Regression	2985.636	1	2985.636	91.304	.000[b]
	Residual	359.701	11	32.700		
	Total	3345.337	12			

a. Dependent Variable: SecondAngle

b. Predictors: (Constant), FirstAngle

Coefficients[a]

Model		Unstandardized Coefficients		Standardized Coefficients		
		B	Std. Error	Beta	t	Sig.
1	(Constant)	2.200	4.800		.458	.656
	FirstAngle	1.022	.107	.945	9.555	.000

a. Dependent Variable: SecondAngle

Residuals Statistics[a]

	Minimum	Maximum	Mean	Std. Deviation	N
Predicted Value	24.1644	61.9640	45.4846	15.77349	13
Residual	-4.56395	15.98142	.00000	5.47495	13
Std. Predicted Value	-1.352	1.045	.000	1.000	13
Std. Residual	-.798	2.795	.000	.957	13

a. Dependent Variable: SecondAngle

Figure 5.20: Linear regression analysis where angle from first attempt determines angle from second attempt

Linear regression with the construct means revealed that only the ASQ score for the angle task was determined by the test results to a significant degree. As shown in Figure 5.21, time spent on the first attempt was statistically significant for this ASQ score, but the numerical impact was low.

Model Summary[b]

Model	R	R Square	Adjusted R Square	Std. Error of the Estimate
1	.668[a]	.447	.400	1.12097

a. Predictors: (Constant), FirstTime

b. Dependent Variable: Angle_ASQ

ANOVA[a]

Model		Sum of Squares	df	Mean Square	F	Sig.
1	Regression	12.167	1	12.167	9.683	.009[b]
	Residual	15.079	12	1.257		
	Total	27.246	13			

a. Dependent Variable: Angle_ASQ

b. Predictors: (Constant), FirstTime

Coefficients[a]

Model		Unstandardized Coefficients		Standardized Coefficients		
		B	Std. Error	Beta	t	Sig.
1	(Constant)	7.346	.948		7.751	.000
	FirstTime	-.008	.003	-.668	-3.112	.009

a. Dependent Variable: Angle_ASQ

Residuals Statistics[a]

	Minimum	Maximum	Mean	Std. Deviation	N
Predicted Value	2.5876	5.4588	4.5476	.96744	14
Residual	-2.22307	1.89477	.00000	1.07699	14
Std. Predicted Value	-2.026	.942	.000	1.000	14
Std. Residual	-1.983	1.690	.000	.961	14

a. Dependent Variable: Angle_ASQ

Figure 5.21: Linear regression analysis where time spent on first attempt determines angle ASQ score

Chapter 6

Discussion

In this chapter, we will discuss the implementation of our NeoDoppler simulation (Section 6.1) and the results of the user tests that were conducted to evaluate it (Section 6.2).

6.1 Implementation

6.1.1 Augmented Reality Scene

Like in HoloUmoja, a virtual model of the subject (here, a baby) was aligned with a physical manifestation (here, a baby doll) with Vuforia's image tracking. With the image marker placed on a 3D-printed stand together with the doll, the hologram was overlaid quite stably on the doll. A model of the cerebral arteries was placed inside the head to satisfy FRQ1.

However, in HoloNeoDoppler the probe was made virtual and the importance of the physical part of the simulation diminished. The only impact it could have was to provide a surface that users could move the probe along, but with the probe sticking to the head at all times, this seemed less important and could make the process more cumbersome, as some users experienced when the probe stuck inside the baby's head or appeared on the other side. In future versions of this project, it would be sensible to remove the physical baby and thus the image marker too. As one tester touched on, the simulation could just as well be ported to pure VR, since it no longer had any interaction with the physical world other than the user's fingers.

With this major departure from the intended physicality of the simulation, we can answer

RQ1: How can we merge a real-life model of the subjects with a digital model of cerebral arteries?

by stating that we ended up not having a real-world model of the subject in HoloNeoDoppler. It turned out to be a cumbersome obstruction, given that we abolished the physical probe in favor of more precise hand tracking.

Another element that users had some thoughts on, was that the measurement menu with sliders for various parameters ended up too far away from the probe and spectrogram. This made the users either move the menu or sometimes struggle to see what happened to the spectrogram or the depth window on the probe when they adjusted the sliders. One user suggested that the sliders could be placed by the baby by default, which would avoid the problem as long as the layout was sensible.

6.1.2 Artery Modeling

Modeling arteries with Bézier curves was our solution to FRQ2. This approach opened for more realistic Doppler ultrasound measurement, and was flexible enough that we could model the umbilical cord vein from HoloUmoja as well. However, creating curves that fit 3D models of arteries was a cumbersome process that took several hours, and might thus not be practical for cases with a larger variety of blood vessel networks. Determining the flow direction along an artery mesh, or automatically creating a parametric surface of arteries with embedded direction information, would have made the process faster. For a project of *this* scale, though, it was appropriate to use a solution involving some manual work.

With support for curved blood flow, an issue that some users experienced with the previous project was solved: They found it surprising that they were only able to hit *one* part of the vein [1]. Resolving this was listed as a future improvement there.

The rework of the blood flow modeling also made it possible to measure insonation angles in the full $[0°, 180°]$ range. This was not useful for NeoDoppler simulation per se, since it ended up being physically impossible to find an angle above 90° to the blood flow in the final version of HoloNeoDoppler. However, this was an important aspect of Doppler ultrasound that was plainly ignored in HoloUmoja, and with the Bézier-modeled umbilical cord, it would be possible to achieve angles over 90° given the less restrictive access users have to the abdomen since there's no skull with a fontanelle there.

6.1.3 Depth Window

The depth window provided an interesting obstacle for the users since we tuned the default window settings so that it was impossible to reach an insonation angle below 30° without first adjusting the window. It was implemented as a toggle between *inside* and *outside*, but with an averaged angle for the segments inside the window, making the depth window at the very least affect a range of artery segments. With these considerations, FRQ4 was well and truly complete.

6.1.4 Artery and Cranium Intersection

None of the participants had trouble seeing the fontanelle, at least not to such a degree that they would mention it, which indicated that the hole in the baby model was rendered suitably for this case. The baby model with a fontanelle hole blocked the virtual probe from interacting with the arteries, which satisfied FRQ3.

The revised procedure for determining artery intersection, shown in Algorithm 2, was a significant improvement in simplicity and functionality over HoloUmoja [1, p. 36], given that it avoided the complicated depth window calculations that did not work (see Code listing 4.1) in favor of simpler code that used raycasts to determine whether the depth window covered any arteries, and avoided edge cases where there was an artery hit before the ray reached the depth window, which would result in no hit with the old algorithm.

The arteries were placed inside the skull to the best of our ability, and the users did not comment on their positioning. Feedback from experts regarding the artery orientation was somewhat lacking, though the final two expert interviews (see Appendix B.3 and Appendix B.4) did lead to improvements. These interviews also lead to improvements in the fontanelle model. After all the adjustments that were made, users were able to quickly locate the fontanelle and get a signal from the cerebral arteries, indicating that FRQ6 was fulfilled.

6.1.5 Improved Spectrogram

The reworked spectrogram showed frequency values distorted by noise, to satisfy FRQ8, and looked much closer to a real spectrogram than the version in HoloUmoja (shown in Figure 2.13). It displayed a more complex wave than HoloUmoja, based on real data, which satisfied FRQ7. With improved temporal velocity variation in place, we could answer all of

RQ2: How can we simulate the directional and temporal pattern of arterial blood flow in a virtual environment?

By modeling cerebral arteries with Bézier curves, it was possible to use the first derivative of the curves as blood flow direction. The temporal pattern was quite simply the arterial velocity curve used as the basis for the improved Doppler spectrogram.

As shown in Figure 4.15, the resolution of the spectrogram would change when PRF changed, meaning FRQ9 was fulfilled. The spectrogram code ran well enough. It was optimized to the point where it did not impact frame rate at default PRF, but started affecting performance at higher PRFs. However, this did not pose an issue in the user tests, and the drop in frame rate did not hinder the users. This was the only part of the application that could majorly affect performance, other than the collider instantiation for the blood flow simulation. With the optimizations we made, NFRQ2 was clearly satisfied and we could answer

RQ3: How can we efficiently generate a realistic Doppler spectrogram based on artery interactions?

By generating random noise and overlaying a noisy version of an angle-modulated velocity curve on top of it, then running it through a Fourier transform to create a realistic spectrogram that varies based on PRF and insonation angle.

Regarding the information displayed above the spectrogram, one user interpreted the orange color of the angle text as an indication that the angle was *bad*, and expected it to turn green when they got an angle below 30°. The intention was to show negative and positive Doppler shifts in different colors, but this was irrelevant in HoloNeoDoppler since it was impossible to find an angle above 90°.

6.1.6 Probe Tracking

With the native HoloLens finger tracking, it was much easier to explain how to interact with the probe, to the point where several users naturally reached out to pinch the probe, even if they had tracked the baby before the instructions to do so had appeared. However, some users struggled with performing the pinching motion correctly, and it was noticeably hard to *release* the probe without nudging it in some unintended direction. The unintuitive limitations imposed by the sensors on the HoloLens meant users had to keep their gestures visible to the HoloLens. This was the assumption we made when users pinched straight forward and thus hid the gesture behind the back of their hands. Therefore, users *still* had to be careful about keeping some indication of what they did in view of the HoloLens,

though not for an external object. It might be possible that some users had an advantage on the pinching if they had used HoloLens before, since those *were* more likely to perform their task faster, according to an independent t-test of the test results (see Figure 5.17). This was expected since prior experience with a particular technology generally improves one's performance.

Regardless of the problems with performing the gesture correctly, users were eventually able to steer the probe to some adequate position and measure blood flow, which indicated that FRQ5 was satisfied.

Switching away from HoloUmoja's image and gyroscope tracking also meant that we avoided the issues present there, with two flipped axes on the gyroscope input, unreliable image tracking, and the need to explain how to hold the probe so that the image marker was visible at all times. However, this meant that we did not improve HoloUmoja's probe tracking. In HoloUmoja, it made sense to have a physical probe and it was thus necessary to track its position and orientation in some way. The solution used in HoloUmoja *was* inadequate, but since we went down a different path in our project, we made no contributions to the tracking in HoloUmoja.

6.1.7 Improved Tutorial

With the new pages in the menu, we showed information about Doppler ultrasound and made the menu less confusing (no BLE debug page interrupting the flow). Even with this new information, users were able to get through it relatively quickly, on average five and a half minutes (see Table 5.2). The new pages seemed to fulfill FRQ10. However, in our tests, the users were not intended to play around with the probe while the information was displayed. This was done to prevent users from performing their tasks before they were supposed to during the user tests. In a version that is meant for actual training, this should be handled differently. One user thought that the spectrogram on the PRF page, shown in Figure 4.20, was an ideal example. With its 45° insonation angle, that was *not* the case. It was unclear if other users shared this misunderstanding.

6.1.8 Evaluation Support

The submit button worked as expected, though the lack of feedback when pressing it confused the users slightly. We did not make its effect too clear, other than resetting the parameters and probe, since this was not supposed to be a feature in the final product. It was only added as a means of evaluation, resolving FRQ11.

While analyzing the results of the user tests, it would have been useful to know the depth window and PRF settings, as this could help explain why the submitted spectrograms ended up as they were. With the depth and window size stored, we could know whether improper depth window setting was a reason why the submitted spectrograms were captured with an average angle of 43°. The default depth was limited to force users to adjust the depth before they could get an angle below 30°. Knowing the PRF would help to evaluate submitted spectrograms where the velocity curve had a lower amplitude.

6.2 User Tests

6.2.1 Test Results

From looking at the test results in Table 5.2, it was evident that the testers were divided into six users who got a beam-flow angle below 30° and eight users who did not (and ended up around 50°). We know from the linear regression of angle in the first to the second attempt, shown in Figure 5.20, that the angles were very similar. In conclusion, the users did not improve their spectrograms that much, if at all. Their understanding of what was an optimal spectrogram did not seem to change from their first attempt, and their scores either stayed the same or (in two cases) decreased by one point.

One user, in particular, got a far worse angle on the second spectrogram — they went from 56.4° to 75.8°. This user might have cared more about getting *any* signal and submitting the result quickly in their second attempt, rather than achieving as good an angle as in their first attempt, and should be considered an outlier in this matter.

While the angle information in Figure 4.18 urged users to achieve an insonation angle less than 30°, angles below 60° were still *acceptable*, and most of the submitted spectrograms were at least *somewhat* readable, even the aforementioned 75.8°-spectrogram. Since ultrasound devices provide compensation options for bad insonation angles, angles up to 60° are still clinically relevant.

The tutorial page shown in Figure 4.20 used a 45°-spectrogram to illustrate PRF and might thus have misled users into thinking that it was an ideal spectrogram in other aspects than PRF.

Considering the differences on display here, we may answer

RQ4: How well do the intended users perform a clinically relevant Doppler examination with our application?

this way: All participants submitted at least one clinically relevant spectrogram. Almost half of them managed to find an insonation angle below 30°, while the remaining users submitted spectrograms with angles below 60° for the most part. The experiment was thus not a *perfect* success, but with some adjustments, users should be able to perform examinations with better scores. Since the participants had never used the actual NeoDoppler probe before, the fact that *all* users managed to produce at least one *acceptable* spectrogram seemed quite positive.

Only one user spent more time on their second attempt, as shown in the delta time column in Table 5.2, but this was due to them not understanding that they were timed. All other users reduced their time with 3 minutes and 46 seconds on average, though the reductions ranged from eight minutes to just above half a minute. With this one exception in mind, it seems apt to conclude that the users were more efficient when performing their tasks for the second time.

The users that performed their first attempt quickly, answered more positively on the ASQ questions for the task of finding a good angle, according to the regression analysis in Figure 5.21. This seems sensible, since one of the ASQ questions asked if they were satisfied with how quickly they were able to perform the task. Statistical analysis also found that users with experience using the HoloLens completed their first attempt slightly faster on average than the ones without, see Figure 5.17, which seems reasonable given how different the HoloLens is from other electronic devices that people interact with.

In some cases, users needed more specific instructions for how to press the buttons. Apart from a transparent hand showing the motion, there were no instructions for pressing buttons in our application. Adding some precise textual explanation of the gesture might help, though in one user's case the problem was that their arms were not long enough to reach the buttons naturally, so they had to stretch quite far out. Some users were having trouble pinching the probe, which also could be alleviated by displaying more specific instructions in the tutorial. The reset button page, which carried over unchanged from HoloUmoja, confused several users and could be removed from the tutorial without much issue. If the menu happened to fall out of view, we could have told the users how to bring it back, since it seemed likely to be a rare occasion.

6.2.2 Questionnaire Results

Regarding the questionnaire, both the Intention to Use and the Perceived Usability constructs were answered positively, indicating that the users found the applica-

tion useful and would likely use this simulation again or similar simulations for other cases later.

The Ease of Use score was spread more widely, according to Figure 5.16, likely due to different users having different degrees of familiarity with the modes of interaction featured in HoloNeoDoppler. This could indicate that some parts of the tutorial should be expanded to better serve inexperienced users.

Perceived Learning was more exclusively answered at *Neither* and below, though the "I would be able to use NeoDoppler in practice" question was answered more positively than the others for these constructs, as shown in Figure 5.12. We did receive a comment regarding these other questions, stating that the students could have answered negatively because they considered more than just using the probe. With this in mind, it seemed less certain that the negativity shown in the answers to the Perceived Learning questions was reliable.

With the results for the Technical Understanding construct, we may answer

RQ5: To what degree can users understand the technical details of Doppler ultrasound through our application?

like this: The Technical Understanding construct averaged at a score of *Slightly agree*, indicating that most participants did understand the Doppler ultrasound concepts featured in the simulation, or at least improved their understanding, see Figure 5.12. This should also serve as proof that NFRQ1 was fulfilled.

Answers to the ASQ for each task hovered around an average of *Slightly agree*, though users were less enthusiastic about their performance in the task of finding a good angle than the others. This task was also subject to a statistically significant difference shown in Figure 5.18 and Figure 5.19, where independent t-tests based on experience with the HoloLens or mobile AR revealed an impact on the angle ASQ specifically. While it seems rather odd that this would not affect the other tasks, it does seem reasonable that prior experience with mixed reality would impact the tests in some way. Along with this, there was a significant divide in how good an angle the users found. Those who got angles above 30° might have been aware of this and answered negatively on the ASQ.

6.3 Comparison to Related Work

Paper	**Hardware**	**Physical objects**	**Data**	**Tracking**
HoloUS, Nguyen *et al.* [35]	HoloLens 1	Probe, targeting model	Real	Image
Costa *et al.* [36]	HoloLens 2	Probe, metal ball	Simulated	Image
UltrARsound, von Haxthausen *et al.* [37]	HoloLens 2	Probe, subject	Simulated	Retroreflective spheres
HoloUmoja, Nylund [1]	HoloLens 2	Probe, abdomen	Simulated	Image, gyroscope
HoloNeoDoppler	HoloLens 2	Baby doll (optional)	Simulated	Image, hand

Table 6.1: Tabular comparison of different aspects of this and related projects

The simulation by Nguyen *et al.* required an actual ultrasound device to work, and was intended for ultrasound imaging instead of PW ultrasound. It used a real ultrasound probe with a marker on, whereas HoloNeoDoppler's probe was entirely virtual and did not require more expensive hardware than the HoloLens.

Costa *et al.* also used a tangible probe in their simulation, connected to an ultrasound *simulator*. This project used a black-and-white marker like in Nguyen *et al.*, and the focus seemed to be on tracking accuracy.

These two projects were dissimilar to HoloNeoDoppler in their hardware requirements, and their tracking approach was meant for large probes instead of the small NeoDoppler probe. Additionally, they did not provide their own ultrasound simulation, instead relying on existing tools.

The constellation of retroreflective spheres used in von Haxthausen *et al.* seemed unwieldy compared to simply grabbing a virtual probe, and this project also used an external ultrasound simulator [37].

As for HoloUmoja, it has been explored thoroughly in other parts of the text because HoloNeoDoppler was developed from it. HoloUmoja shares ultrasound mode and general approach with HoloNeoDoppler, but differs in tracking, the fidelity of the simulated spectrogram, and the detail of its simulated subject.

The other image tracking-based approaches before HoloUmoja had decent performance according to the papers, but used custom tracking code and either displayed information from the real ultrasound device they were connected to [35], or focused on tracking orientation and did not simulate ultrasound [36]. One thing that all the explored tracking approaches had in common, including hand tracking, was *blind spots* where the HoloLens would be unable to track the observed object. This was an issue even with retroreflective sphere tracking [37] and hand tracking.

6.4 Limitations

The education question in the demographics questionnaire seems less useful in this case, since all the participants were medical students. Most did not have a degree already, though there were a few with undergraduate degrees. Given their study program, it would have been interesting to ask for their year and specialization.

The issue with the perceived learning questions possibly being answered with more than just using the probe in mind could have been avoided by phrasing the question differently, to make it more targeted toward what HoloNeoDoppler actually teaches, and letting the respondents answer based on theoretically perfect behavior in other aspects of using NeoDoppler in practice.

Given the limited time for user tests, we were unable to do a dry run of the tests or an evaluation of the questions by a medical professional. Some of the aforementioned issues could have been avoided if we had the option to verify our tests like this. Another consequence of the tests being delayed until as late as the exam period was that it was difficult to recruit enough test subjects for the results to have substantial statistical significance.

Chapter 7

Conclusion

HoloUmoja was successfully turned into a training simulator for NeoDoppler and improved in several ways, fulfilling all functional and nonfunctional requirements.

RQ1 was handled like in HoloUmoja; a hologram of an infant with its cerebral arteries was laid on top of a physical baby doll, through image tracking of a marker fastened to a 3D-printed stand that held the marker in a fixed position relative to the doll. However, in HoloNeoDoppler the probe tracking was changed to involve pinching a virtual probe, which utilized the finger tracking built into the HoloLens and turned the physical baby doll into an obstruction if it happened to be moved slightly out of position.

RQ2 was solved by modeling the arteries with Bézier curves and casting rays from the probe onto these curves to determine the beam-flow angle. These rays were blocked by the skull and could only measure arterial blood flow through the fontanelle. The depth window feature that was imperfectly implemented in HoloUmoja was reworked.

A new spectrogram was made to answer RQ3, with background noise and a realistic velocity curve that responded to changes in insonation angle. The spectrogram was optimized to perform well on the HoloLens and avoid blocking the main thread with its expensive operations.

According to the test results, the answer to RQ4 was that *all* users were indeed able to perform a clinically relevant ultrasound examination, and almost half of them got a very good result.

As for RQ5: With the new pages of Doppler ultrasound information, users were able to learn the information required to understand the simulation.

In conclusion, the HoloNeoDoppler project accomplished its goals and was found to be both useful and fun to use, by experts and intended users alike.

7.1 Future Work

Based on the issues that were discussed in Chapter 6, we suggest these points as future work:

- The baby model should be placed on a surface without using an image marker, now that there is no need for a physical probe or baby anymore.
- Different variations of the arterial velocity curve could be added to train users for the unpredictable variety they are likely to face in real examinations.
- In the same vein, the cerebral arteries could be oriented and altered randomly each time the simulation loads.
- The interaction tutorial should be scrutinized to eliminate superfluous elements, like the reset button, as some parts of the tutorial could be needlessly confusing to users.
- To make the spectrogram interface more similar to NeoDoppler, a graph of the signals at different depths could be added, similar to Figure 2.10.
- The spectrogram screenshot on the PRF page (see Figure 4.20) should be replaced with one with angle $< 30°$ to avoid misleading users. There could be an additional page at the end that summarizes how to get a good spectrogram and shows another example.
- It should be considered to display the angle above the spectrogram in a different color since users were prone to thinking that orange/yellow meant failure.
- In a future test of HoloNeoDoppler or a similar application, the clinical situation that medical students are used to thinking about should be considered when formulating questions about perceived learning value.
- Since there no longer was a need for any physical components in the simulation, HoloNeoDoppler could be reimplemented as a pure VR application. However, if HoloNeoDoppler were to be enhanced with simulated ultrasound images of the heart, it would make sense to continue using AR as it would be possible to use a physical probe (with better tracking) for that additional mode.
- As one user suggested, the parameter controls should be placed together with the baby model and spectrogram, to provide easy access without requiring users to move the menu down to their working area themselves.

Bibliography

[1] M. E. Nylund, 'HoloUmoja - Augmented Reality training application for obstetric Doppler ultrasound,' *NTNU*, 2022.

[2] P. Holck, 'fontaneller,' *Store medisinske leksikon*, Jan. 2022. [Online]. Available: http://sml.snl.no/fontaneller (visited on 03/11/2022).

[3] R. Likert, 'A technique for the measurement of attitudes,' *Archives of Psychology*, vol. 22 140, pp. 55–55, 1932.

[4] R. Likert, S. Roslow and G. Murphy, 'A Simple and Reliable Method of Scoring the Thurstone Attitude Scales,' *The Journal of Social Psychology*, vol. 5, no. 2, pp. 228–238, May 1934, ISSN: 0022-4545. DOI: 10.1080/00224545.1934.9919450. [Online]. Available: https://doi.org/10.1080/00224545.1934.9919450 (visited on 04/05/2023).

[5] 'retrorefleksjon,' *Store norske leksikon*, Jun. 2020. [Online]. Available: http://snl.no/retrorefleksjon (visited on 01/12/2022).

[6] S. D. Vik, H. Torp, T. Follestad, R. Støen and S. A. Nyrnes, 'NeoDoppler: New ultrasound technology for continuous cerebral circulation monitoring in neonates,' *Pediatric Research*, vol. 87, no. 1, pp. 95–103, 2020, ISSN: 0031-3998. DOI: 10.1038/s41390-019-0535-0. [Online]. Available: https://www.ncbi.nlm.nih.gov/pmc/articles/PMC6960092/ (visited on 14/11/2022).

[7] A. M. C. Watkins, C. R. West and R. W. I. Cooke, 'Blood pressure and cerebral haemorrhage and ischaemia in very low birthweight infants,' *Early Human Development*, vol. 19, no. 2, pp. 103–110, May 1989, ISSN: 0378-3782. DOI: 10.1016/0378-3782(89)90120-5. [Online]. Available: https://www.sciencedirect.com/science/article/pii/0378378289901205 (visited on 14/11/2022).

[8] J. J. Volpe, 'Brain injury in the premature infant – from pathogenesis to prevention,' *Brain and Development*, vol. 19, no. 8, pp. 519–534, Dec. 1997, ISSN: 0387-7604. DOI: 10.1016/S0387-7604(97)00078-8. [Online]. Available: https://www.sciencedirect.com/science/article/pii/S0387760497000788 (visited on 14/11/2022).

[9] C. Gutvik, *NeoDoppler*, 2020. [Online]. Available: https://cimonmedical.com/neodoppler/ (visited on 03/11/2022).

[10] J. M. Rubin, O. D. Kripfgans, J. B. Fowlkes, G. M. Weiner, M. C. Treadwell and S. Z. Pinter, 'Bedside Cerebral Blood Flow Quantification in Neonates,' *Ultrasound in Medicine & Biology*, vol. 48, no. 12, pp. 2468–2475, Dec. 2022, ISSN: 0301-5629. DOI: 10.1016/j.ultrasmedbio.2022.07.010. [Online]. Available: https://www.sciencedirect.com/science/article/pii/S0301562922005014 (visited on 15/11/2022).

[11] S. Ehehalt, M. Kehrer, R. Goelz, C. Poets and M. Schöning, 'Cerebral blood flow volume measurements with ultrasound: Interobserver reproducibility in preterm and term neonates,' *Ultrasound in Medicine & Biology*, vol. 31, no. 2, pp. 191–196, Feb. 2005, ISSN: 0301-5629. DOI: 10.1016/j.ultrasmedbio.2004.10.002. [Online]. Available: https://www.sciencedirect.com/science/article/pii/S0301562904002972 (visited on 15/11/2022).

[12] S. Barteit, L. Lanfermann, T. Bärnighausen, F. Neuhann and C. Beiersmann, 'Augmented, Mixed, and Virtual Reality-Based Head-Mounted Devices for Medical Education: Systematic Review,' *JMIR Serious Games*, vol. 9, no. 3, e29080, Jul. 2021. DOI: 10.2196/29080. [Online]. Available: https://games.jmir.org/2021/3/e29080 (visited on 09/09/2022).

[13] L. Chen, T. W. Day, W. Tang and N. W. John, 'Recent Developments and Future Challenges in Medical Mixed Reality,' in *2017 IEEE International Symposium on Mixed and Augmented Reality (ISMAR)*, Oct. 2017, pp. 123–135. DOI: 10.1109/ISMAR.2017.29.

[14] P. Milgram, H. Takemura, A. Utsumi and F. Kishino, 'Augmented reality: A class of displays on the reality-virtuality continuum,' in *Telemanipulator and Telepresence Technologies*, vol. 2351, SPIE, Dec. 1995, pp. 282–292. DOI: 10.1117/12.197321. [Online]. Available: https://www.spiedigitallibrary.org/conference-proceedings-of-

spie/2351/0000/Augmented-reality--a-class-of-displays-on-the-reality/10.1117/12.197321.full (visited on 09/09/2022).

[15] D. Weinstein, *What Is Extended Reality?* May 2022. [Online]. Available: https://blogs.nvidia.com/blog/2022/05/20/what-is-extended-reality/ (visited on 30/11/2022).

[16] D. M. Markowitz and J. N. Bailenson, 'Virtual reality and the psychology of climate change,' *Current Opinion in Psychology*, Psychology of Climate Change (2021), vol. 42, pp. 60–65, Dec. 2021, ISSN: 2352-250X. DOI: 10.1016/j.copsyc.2021.03.009. [Online]. Available: https://www.sciencedirect.com/science/article/pii/S2352250X2100035X (visited on 13/09/2022).

[17] M. H. Abidi, A. Al-Ahmari, A. Ahmad, W. Ameen and H. Alkhalefah, 'Assessment of virtual reality-based manufacturing assembly training system,' *The International Journal of Advanced Manufacturing Technology*, vol. 105, no. 9, pp. 3743–3759, Dec. 2019, ISSN: 1433-3015. DOI: 10.1007/s00170-019-03801-3. [Online]. Available: https://doi.org/10.1007/s00170-019-03801-3 (visited on 06/12/2022).

[18] B. L. Luk, M.-L. Lam, T.-H. Chen, J. Zhao, S. M. Tsui and C.-C. Chieng, '3D Immersive Display Application for Nuclear Education and Public Acceptance,' in *Volume 8: Computational Fluid Dynamics (CFD); Nuclear Education and Public Acceptance*, London, England: American Society of Mechanical Engineers, Jul. 2018, V008T12A005, ISBN: 978-0-7918-5152-4. DOI: 10.1115/ICONE26-81161. [Online]. Available: https://asmedigitalcollection.asme.org/ICONE/proceedings/ICONE26/51524/London,%20England/275993 (visited on 13/09/2022).

[19] R. Ryan, G. Ryan and M. F. Higgins, *Exploring virtual and augmented reality simulation in obstetrics and gynaecology training; a qualitative study*, Dec. 2020. DOI: 10.1101/2020.12.13.20248133. [Online]. Available: https://www.medrxiv.org/content/10.1101/2020.12.13.20248133v1 (visited on 22/09/2022).

[20] P. Holck, 'arteria cerebri anterior,' *Store norske leksikon*, Nov. 2022. [Online]. Available: http://snl.no/arteria_cerebri_anterior (visited on 17/11/2022).

[21] J. K. S. Jansen, 'Willis' pulsårering,' *Store medisinske leksikon*, Oct. 2022. [Online]. Available: http://sml.snl.no/Willis'_puls%C3%A5rering (visited on 17/11/2022).

[22] Rhcastilhos, *Schematic representation of the circle of Willis, arteries of the brain and brain stem.* Jan. 2007. [Online]. Available: https://commons.wikimedia.org/wiki/File:Circle_of_Willis_en.svg (visited on 17/11/2022).

[23] Z. A. Vesoulis, A. A. Flower, S. Zanelli, A. Rambhia, M. Abubakar, H. V. Whitehead, K. D. Fairchild and A. M. Mathur, 'Blood Pressure Extremes and Severe IVH In Preterm Infants,' *Pediatric research*, vol. 87, no. 1, pp. 69–73, Jan. 2020, ISSN: 0031-3998. DOI: 10.1038/s41390-019-0585-3. [Online]. Available: https://www.ncbi.nlm.nih.gov/pmc/articles/PMC6962547/ (visited on 18/11/2022).

[24] R. E. Berg, 'Sound | Properties, Types, & Facts,' *Encyclopedia Britannica*, Sep. 2022. [Online]. Available: https://www.britannica.com/science/sound-physics (visited on 02/12/2022).

[25] T. Gjestland, 'lyd,' *Store norske leksikon*, Oct. 2019. [Online]. Available: http://snl.no/lyd (visited on 02/12/2022).

[26] H. Ormestad, 'ultralyd,' *Store norske leksikon*, Oct. 2021. [Online]. Available: http://snl.no/ultralyd (visited on 02/12/2022).

[27] H. Shankar, P. S. Pagel and D. S. Warner, 'Potential Adverse Ultrasound-related Biological Effects: A Critical Review,' *Anesthesiology*, vol. 115, no. 5, pp. 1109–1124, Nov. 2011, ISSN: 0003-3022. DOI: 10.1097/ALN.0b013e31822fd1f1. [Online]. Available: https://doi.org/10.1097/ALN.0b013e31822fd1f1 (visited on 02/12/2022).

[28] A. Støylen, *Basic ultrasound, echocardiography and Doppler ultrasound*. [Online]. Available: https://folk.ntnu.no/stoylen/strainrate/Basic_Doppler_ultrasound (visited on 13/10/2022).

[29] EGG &ECHO, *Continuous Wave Doppler (CW Doppler)*. [Online]. Available: https://ecgwaves.com/topic/continuous-wave-doppler-cw-doppler/ (visited on 15/06/2023).

[30] EGG &ECHO, *Pulsed Wave Doppler*. [Online]. Available: https://ecgwaves.com/topic/pulsed-wave-doppler/ (visited on 24/11/2022).

[31] BAYOOCARE GmbH, *NeoDoppler User Manual*, 2022.

[32] C. Shannon, 'Communication in the Presence of Noise,' *Proceedings of the IRE*, vol. 37, no. 1, pp. 10–21, Jan. 1949, ISSN: 2162-6634. DOI: 10.1109/JRPROC.1949.232969.

[33] G. Kiss, *Private correspondence with Gabriel Kiss*, 2022.

[34] GE HealthCare, *Venue™ Family R3 Tutorial - Pulse Wave Doppler*, Mar. 2021. [Online]. Available: https://www.youtube.com/watch?v=LqMAxGHXKMw (visited on 31/05/2023).

[35] T. Nguyen, W. Plishker, A. Matisoff, K. Sharma and R. Shekhar, 'HoloUS: Augmented reality visualization of live ultrasound images using HoloLens for ultrasound-guided procedures,' *International Journal of Computer Assisted Radiology and Surgery*, vol. 17, no. 2, pp. 385–391, Feb. 2022, ISSN: 1861-6429. DOI: 10.1007/s11548-021-02526-7. [Online]. Available: https://doi.org/10.1007/s11548-021-02526-7 (visited on 24/10/2022).

[36] J. N. Costa, J. Gomes-Fonseca, S. Valente, L. Ferreira, B. Oliveira, H. R. Torres, P. Morais, V. Alves and J. L. Vilaça, 'Ultrasound training simulator using augmented reality glasses: An accuracy and precision assessment study,' in *2022 44th Annual International Conference of the IEEE Engineering in Medicine & Biology Society (EMBC)*, Jul. 2022, pp. 4461–4464. DOI: 10.1109/EMBC48229.2022.9871406.

[37] F. von Haxthausen, R. Moreta-Martinez, A. Pose Díez de la Lastra, J. Pascau and F. Ernst, 'UltrARsound: In situ visualization of live ultrasound images using HoloLens 2,' *International Journal of Computer Assisted Radiology and Surgery*, vol. 17, no. 11, pp. 2081–2091, Nov. 2022, ISSN: 1861-6429. DOI: 10.1007/s11548-022-02695-z. [Online]. Available: https://doi.org/10.1007/s11548-022-02695-z (visited on 01/12/2022).

[38] C. L. Byrne, *Signal Processing: A Mathematical Approach, Second Edition*, Second. CRC Press, 2015, ISBN: 978-1-4822-4184-6. (visited on 23/05/2023).

[39] E. Hughes, *Windowing Functions in Radar Technology*. [Online]. Available: https://www.skyradar.com/blog/windowing-functions-in-radar-technology (visited on 30/05/2023).

[40] Q. Kong, *Qingkai's Blog: Signal Processing: Why do we need taper in FFT*, Oct. 2016. [Online]. Available: https://qingkaikong.blogspot.com/2016/10/signal-processing-why-do-we-need-taper.html (visited on 30/05/2023).

[41] T. Theoharis, G. Papaioannu, N. Platis and N. M. Patrikalakis, *Graphics & Visualization: Principles & Algorithms*. Wellesley, Mass: A.K. Peters, 2008, ISBN: 978-1-56881-274-8.

[42] M. Hazewinkel, *Encyclopaedia of Mathematics: Supplement*. Springer Science & Business Media, Aug. 1997, ISBN: 978-0-7923-4709-5.

[43] M. Melo, *Understanding Bézier Curves*, Aug. 2021. [Online]. Available: https://mmrndev.medium.com/understanding-b%C3%A9zier-curves-f6eaa0fa6c7d (visited on 15/11/2022).

[44] Unity Technologies, *Important Classes - GameObject*, 2021. [Online]. Available: https://docs.unity3d.com/Manual/class-GameObject.html (visited on 08/11/2022).

[45] Unity Technologies, *Transforms*, 2021. [Online]. Available: https://docs.unity3d.com/Manual/class-Transform.html (visited on 08/11/2022).

[46] Unity Technologies, *Unity - Scripting API: Transform*, 2021. [Online]. Available: https://docs.unity3d.com/ScriptReference/Transform.html (visited on 15/11/2022).

[47] Unity Technologies, *Introduction to components*, 2021. [Online]. Available: https://docs.unity3d.com/Manual/Components.html (visited on 15/11/2022).

[48] Unity Technologies, *Important Classes - MonoBehaviour*, 2021. [Online]. Available: https://docs.unity3d.com/Manual/class-MonoBehaviour.html (visited on 08/11/2022).

[49] Unity Technologies, *Unity - Manual: Introduction to collision*, 2021. [Online]. Available: https://docs.unity3d.com/Manual/CollidersOverview.html (visited on 19/06/2023).

[50] Unity Technologies, *Unity - Scripting API: Physics.Raycast*, 2021. [Online]. Available: https://docs.unity3d.com/ScriptReference/Physics.Raycast.html (visited on 19/06/2023).

[51] cjdgit, M. Patel, T. P. Milligan, v-chmccl and V. Tieto, *App quality criteria - Mixed Reality*, Aug. 2022. [Online]. Available: https://learn.microsoft.com/en-us/windows/mixed-reality/develop/advanced-concepts/app-quality-criteria-overview (visited on 09/06/2023).

[52] PTC Inc., *Vuforia Engine Overview | VuforiaLibrary*. [Online]. Available: https://library.vuforia.com/getting-started/vuforia-features (visited on 24/11/2022).

[53] *What is the Mixed Reality Toolkit*, Microsoft, Nov. 2022. [Online]. Available: https://github.com/microsoft/MixedRealityToolkit-Unity (visited on 29/11/2022).

[54] S. Cooley, Q. Wen, B. Hanson, J. Mathew and S. Paniagua, *HoloLens 2 hardware*, Oct. 2022. [Online]. Available: https://learn.microsoft.com/en-us/hololens/hololens2-hardware (visited on 25/11/2022).

[55] F. D. Davis, 'A technology acceptance model for empirically testing new end-user information systems : Theory and results,' Thesis, Massachusetts Institute of Technology, 1985. [Online]. Available: https://dspace.mit.edu/handle/1721.1/15192 (visited on 28/04/2023).

[56] V. Venkatesh, J. A. Aloysius, H. Hoehle and S. Burton, 'Design and Evaluation of Auto-Id Enabled Shopping Assistance Artifacts in Customers' Mobile Phones: Two Retail Store Laboratory Experiments,' *MIS Quarterly*, vol. 41, no. 1, pp. 83–114, 2017, ISSN: 0276-7783. JSTOR: 26629638. [Online]. Available: https://www.jstor.org/stable/26629638 (visited on 28/04/2023).

[57] IBM, *SPSS Statistics - Overview*, May 2023. [Online]. Available: https://www.ibm.com/products/spss-statistics (visited on 13/06/2023).

[58] R. Butterworth, *Optimize your 3D models to use with Dynamics 365 Guides and Power Apps - Dynamics 365 Mixed Reality*, Feb. 2023. [Online]. Available: https://learn.microsoft.com/en-us/dynamics365/mixed-reality/guides/3d-content-guidelines/optimize-models (visited on 13/06/2023).

[59] J. R. Lewis, 'IBM computer usability satisfaction questionnaires: Psychometric evaluation and instructions for use,' *International Journal of Human-Computer Interaction*, Sep. 2009. DOI: 10.1080/10447319509526110. [Online]. Available: https://www.tandfonline.com/doi/abs/10.1080/10447319509526110 (visited on 04/05/2023).

[60] J. Lewis, 'Psychometric evaluation of an after-scenario questionnaire for computer usability studies: The ASQ,' *SIGCHI Bull.*, vol. 23, pp. 78–81, Jan. 1991. DOI: 10.1145/122672.122692.

Appendix A

Progress

A.1 Pre-Project Task Board

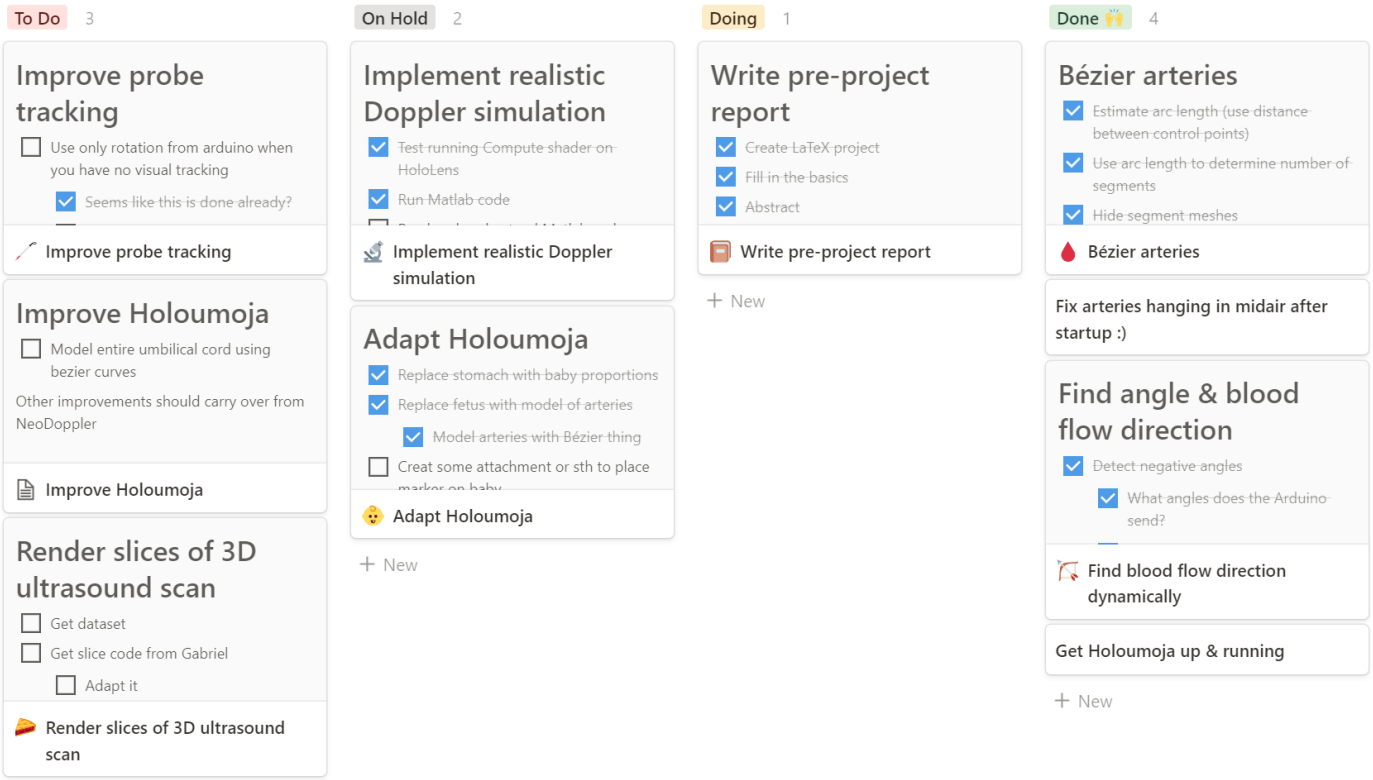

Figure A.1: Project task board after completion of preparatory project. Note that there are several subtasks inside the larger tasks.

A.2 Master Thesis Task Board

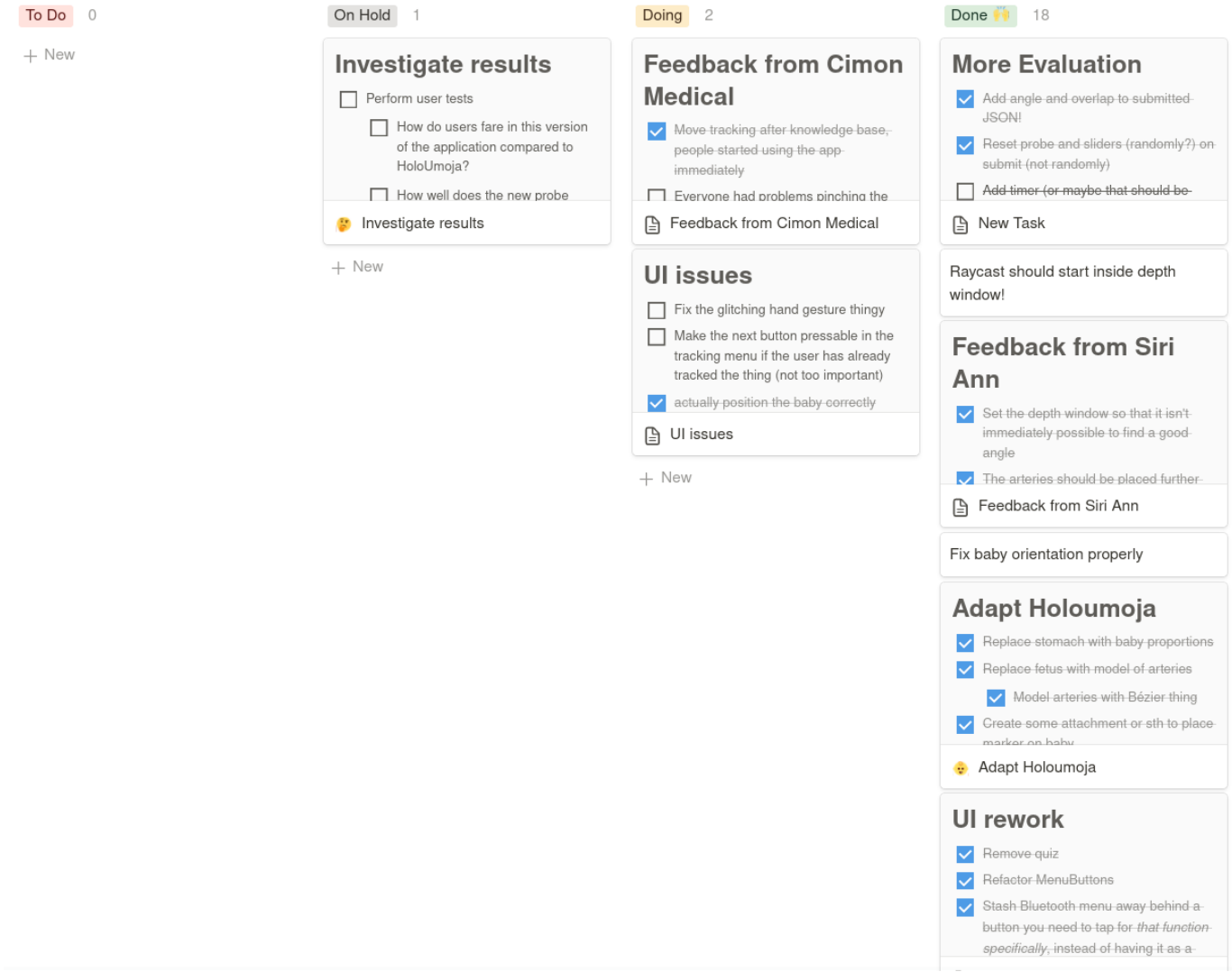

Figure A.2: Project task board near completion of master thesis. Note that there are several subtasks inside the larger tasks.

Appendix B

Expert Interviews

B.1 Expert Interview 1

Date September 21, 2022

Participants Siri Ann Nyrnes, Hans Torp and Gabriel Kiss

From the preparatory project. Demo of HoloUmoja and discussion of HoloNeoDoppler. Hans Torp demonstrated the Matlab test interface for NeoDoppler. At this point the interface in Figure 2.10 was not ready yet.

Notes from this interview were lost.

B.2 Expert Interview 2

Date February 28, 2023

Participants Siri Ann Nyrnes, Hans Torp and Gabriel Kiss

- Probe beam should be 1 cm in diameter.
- Move the spectrogram closer to the head.
- Currently it is hard to hit the arteries.
    - Use cylinder cast?
    - Make the fontanelle bigger or remove it altogether.
- Spectrogram is very on/off.
    - Make the angle change gradual.
    - Use the distance to the middle of the probe beam as a diminishing factor.

- The simulation should be simpler, since using the real thing is very simple.
  - Make the probe sit on the head, let users move it.
  - Probe follows head normal (roughly), base direction on that.
- The current probe tracking is very cumbersome.
  - Use finger tracking somehow?

B.3 Expert Interview 3

Date May 5, 2023

Participants Hans Torp and 3 employees of Cimon Medical

- Issue: HoloLens overheated due to air temperature and charging, we assume. It was almost out of battery.
- Feedback from Hans:
  - Arteries might be in wrong position
  - Hard to find the arteries within the fontanelle
- Feedback from employee 1:
  - Spectrogram too far in, had to look up from the baby
  - Tricky to pick up the probe
  - Lost the probe sometimes, which made him lose signal as well
  - Easy to see that you get a signal
  - In reality you want to get as deep as possible, to the central arteries, to get your signal (2.5-3 cm in)
- Feedback from employee 2:
  - Spectrogram was too far down
  - Noticed that he grabbed the probe at an offset, as it seemed
  - Better with fixed rotation
  - Should adjust arteries so that it is easy to hit the large ones
  - Use color M mode (used for setting depth window on the actual device)
  - Adjust arteries based on anatomy, the carotid arteries should face down the neck!
  - Perhaps expand the fontanelle
- Feedback from employee 3:

    - The fontanelle looked like someone had beaten the head with a hammer
    - Restricted rotation
    - Fontanelle is larger, actually
    - Probe should lie on the skin all the time
- Main takeaways:
    - Fontanelle should be larger, see images for realism
    - Artery model should be rotated so the carotid arteries point into the neck
    - Baby model should be adjusted, was a little too low
    - Spectrogram was placed weirdly sometimes, it was stuck down too low at one point and too far back at another, making it difficult to see the spectrogram while they were controlling the probe
    - The probe should always follow the surface of the head, since there is not way of adjusting it in the current production model! (Gabriel talked about an old version)
    - Everyone had problems pinching the probe; we should make the instructions for pinching clearer
    - None of the employees got to the measure menu by themselves, perhaps we should delay the tracking menu until after the knowledge base?

B.4 Expert Interview 4

Date May 9, 2023

Participants Siri Ann Nyrnes and Gabriel Kiss

- Observation: Menu reset may not be necessary to use, but it should be fine to tell them about it
- Had problems pinching the probe sometimes
- Found good angle very quickly, without adjusting the depth window
- The probe sometimes disappeared (unclear how)
- Much improved from last time, very pedagogical
- The spectrogram looked a little rough on some beats (known issue)
- The anterior cerebral artery should be perpendicular to the fontanelle
- Main takeaways:

- Should set the depth window so that it isn't immediately possible to get below 30° angle
- The arteries should be placed further back into the skull so that the ACA points up to the middle of the fontanelle

Appendix C

Questionnaires

C.1 Consent Form

This consent form was adapted from the consent form for the feedback survey for the *Digital Technologies Workshop* at *URSA MAJOR Autumn School*.

Norwegian University of Science and Technology, HoloNeoDoppler - Request for participation/Informed Consent

C.1.1 Background and Purpose

HoloNeoDoppler is an augmented reality training application for the NeoDoppler probe, which monitors cerebral blood flow in neonates (babies born too early).

The aim of this study is to obtain your feedback on the current version of HoloNeoDoppler, and measure your performance on the tasks that it is meant to train you on. Your inputs will provide us insights on how we could improve the application.

The data collected will be used for research purposes only. No personal data will be collected.

C.1.2 What does participation in the project imply?

The participation includes responding to this questionnaire, which includes demographic information and your feedback on the use of the technologies.

C.1.3 What will happen to the information about you?

No personal data will be collected, and your identity will not be recognizable from the data that is collected. The data that is gathered will be stored on cloud services that are accessible only by the author. The participants will not be recognizable in any of the publications that report the results from this study. The data will be deleted by the completion of the HoloNeoDoppler project in June 2023.

C.1.4 Voluntary Participation

It is voluntary to participate in this study. If you have any questions concerning the project, please contact:

(contact information omitted)

Date: 10 May 2023

C.1.5 Consent for Participation in the Study

I have received and understood information about the HoloNeoDoppler project and this study.

□ I accept

C.2 Demographics Questionnaire

Question	Alternatives
General demographics	
What is your age?	(text input)
What is your gender?	Man Woman Non-binary Prefer not to say
What is the highest level of education you have obtained?	High School Undergraduate Degree Master's Degree Doctoral Degree
Experience with Extended Reality	
How would you rate your level of experience with mobile AR applications? (e.g. Pokemon Go, Ikea Place)	None Beginner Intermediate Expert
How would you rate your level of experience with Head Mounted Displays? (VR/AR headsets like Oculus and HoloLens)	None Beginner Intermediate Expert
How would you rate your level of experience with the HoloLens 1/2?	None Beginner Intermediate Expert

Table C.1: Demographics questionnaire

C.3 Main Questionnaire

The questionnaire consisted of a set of statements that users ranked their agreement with on a Likert scale.

Constructs	**Statements**
Technology Acceptance Model adapted from Venkatesh *et al.* [56]	
Intention to Use	I would use HoloNeoDoppler to learn about NeoDoppler and Doppler ultrasound I intend to use HoloNeoDoppler next time I learn about NeoDoppler I will not use HoloNeoDoppler next time I learn about NeoDoppler
Perceived Usefulness	I found HoloNeoDoppler to be useful for practicing NeoDoppler Using HoloNeoDoppler added to my experience with NeoDoppler I believe that the experience of using HoloNeoDoppler added to the overall learning process
Perceived Ease of Use	My interaction with HoloNeoDoppler was clear and understandable It was easy for me to become skillful at using HoloNeoDoppler I found HoloNeoDoppler to be easy to use Learning to operate HoloNeoDoppler was easy for me
Case-specific questions, formulated by the author	
Perceived Learning	I would be able to use NeoDoppler in practice I feel confident that I know how to use the NeoDoppler probe I do not feel qualified to use the NeoDoppler probe
Technical Understanding	I understood the Doppler ultrasound concepts in HoloNeoDoppler well HoloNeoDoppler improved my understanding of Doppler ultrasound I did not comprehend the technical Doppler ultrasound terms in HoloNeoDoppler
After-Scenario Questionnaire, repeated for each task [59, 60]	
User satisfaction	Overall, I am satisfied with the ease of completing this task Overall, I am satisfied with the amount of time it took to complete this task Overall, I am satisfied with the support information (tutorial text, verbal instructions) when completing this task

Table C.2: Post-simulation questionnaire

Appendix D

Statistics

D.1 T-tests

The following pages contain all independent t-test analyses that were performed to find the results highlighted in Chapter 5.

T-Test: Effect of age (split at 25) on test results

Group Statistics

	Age	N	Mean	Std. Deviation	Std. Error Mean
FirstAngle	>= 25.00	10	40.9600	15.88152	5.02218
	< 25.00	4	40.5000	18.45770	9.22885
SecondAngle	>= 25.00	9	47.6556	16.89431	5.63144
	< 25.00	4	40.6000	17.55126	8.77563
TutorialTime	>= 25.00	9	314.22	130.945	43.648
	< 25.00	3	373.33	110.151	63.596
FirstTime	>= 25.00	10	329.0000	123.23870	38.97150
	< 25.00	4	371.2500	114.04495	57.02247
SecondTime	>= 25.00	10	145.5000	118.47292	37.46443
	< 25.00	4	110.0000	56.71567	28.35783
QuestionnaireTime	>= 25.00	8	281.2500	55.14591	19.49702
	< 25.00	4	287.5000	68.98067	34.49034

Independent Samples Test

		Levene's Test for Equality of Variances		t-test for Equality of Means						
									95% Confidence Interval of the Difference	
		F	Sig.	t	df	Sig. (2-tailed)	Mean Difference	Std. Error Difference	Lower	Upper
FirstAngle	Equal variances assumed	.393	.543	.047	12	.963	.46000	9.79890	-20.88998	21.80998
	Equal variances not assumed			.044	4.897	.967	.46000	10.50685	-26.72091	27.64091
SecondAngle	Equal variances assumed	.091	.768	.688	11	.506	7.05556	10.26139	-15.52961	29.64072
	Equal variances not assumed			.677	5.622	.525	7.05556	10.42712	-18.88035	32.99146
TutorialTime	Equal variances assumed	.049	.829	-.698	10	.501	-59.111	84.706	-247.848	129.626
	Equal variances not assumed			-.766	4.101	.485	-59.111	77.134	-271.213	152.991
FirstTime	Equal variances assumed	.158	.698	-.590	12	.566	-42.25000	71.58798	-198.22680	113.72680
	Equal variances not assumed			-.612	6.019	.563	-42.25000	69.06765	-211.12105	126.62105
SecondTime	Equal variances assumed	.609	.450	.564	12	.583	35.50000	62.97511	-101.71098	172.71098
	Equal variances not assumed			.756	11.219	.465	35.50000	46.98670	-67.67125	138.67125
QuestionnaireTime	Equal variances assumed	.163	.695	-.171	10	.868	-6.25000	36.51840	-87.61807	75.11807
	Equal variances not assumed			-.158	5.005	.881	-6.25000	39.61966	-108.06720	95.56720

Independent Samples Effect Sizes

		Standardizer[a]	Point Estimate	95% Confidence Interval	
				Lower	Upper
FirstAngle	Cohen's d	16.56317	.028	-1.132	1.187
	Hedges' correction	17.69680	.026	-1.060	1.111
	Glass's delta	18.45770	.025	-1.137	1.183
SecondAngle	Cohen's d	17.07599	.413	-.786	1.594
	Hedges' correction	18.36207	.384	-.731	1.483
	Glass's delta	17.55126	.402	-.844	1.590
TutorialTime	Cohen's d	127.059	-.465	-1.776	.868
	Hedges' correction	137.697	-.429	-1.639	.801
	Glass's delta	110.151	-.537	-1.879	.910
FirstTime	Cohen's d	121.00577	-.349	-1.510	.826
	Hedges' correction	129.28770	-.327	-1.413	.773
	Glass's delta	114.04495	-.370	-1.537	.850
SecondTime	Cohen's d	106.44737	.333	-.840	1.494
	Hedges' correction	113.73289	.312	-.786	1.398
	Glass's delta	56.71567	.626	-.669	1.839
QuestionnaireTime	Cohen's d	59.63430	-.105	-1.303	1.099
	Hedges' correction	64.62702	-.097	-1.203	1.014
	Glass's delta	68.98067	-.091	-1.286	1.119

a. The denominator used in estimating the effect sizes.
Cohen's d uses the pooled standard deviation.
Hedges' correction uses the pooled standard deviation, plus a correction factor.
Glass's delta uses the sample standard deviation of the control group.

T-Test: Effect of gender on test results

Group Statistics

	Gender	N	Mean	Std. Deviation	Std. Error Mean
FirstAngle	Woman	10	39.4600	16.19171	5.12027
	Man	4	44.2500	17.00559	8.50279
SecondAngle	Woman	9	42.8111	15.26634	5.08878
	Man	4	51.5000	20.58948	10.29474
TutorialTime	Woman	8	345.00	151.846	53.686
	Man	4	297.00	24.207	12.104
FirstTime	Woman	10	358.5000	131.84692	41.69366
	Man	4	297.5000	67.63875	33.81937
SecondTime	Woman	10	112.0000	49.17090	15.54921
	Man	4	193.7500	181.40080	90.70040
QuestionnaireTime	Woman	8	285.0000	52.37229	18.51640
	Man	4	280.0000	73.93691	36.96846

Independent Samples Test

		Levene's Test for Equality of Variances		t-test for Equality of Means						
									95% Confidence Interval of the Difference	
		F	Sig.	t	df	Sig. (2-tailed)	Mean Difference	Std. Error Difference	Lower	Upper
FirstAngle	Equal variances assumed	.514	.487	-.494	12	.630	-4.79000	9.70176	-25.92832	16.34832
	Equal variances not assumed			-.483	5.336	.649	-4.79000	9.92545	-29.82799	20.24799
SecondAngle	Equal variances assumed	.069	.797	-.856	11	.410	-8.68889	10.14684	-31.02193	13.64415
	Equal variances not assumed			-.757	4.543	.487	-8.68889	11.48379	-39.12385	21.74607
TutorialTime	Equal variances assumed	8.406	.016	.614	10	.553	48.000	78.220	-126.286	222.286
	Equal variances not assumed			.872	7.683	.410	48.000	55.033	-79.823	175.823

Independent Samples Test

		Levene's Test for Equality of Variances		t-test for Equality of Means						
									95% Confidence Interval of the Difference	
		F	Sig.	t	df	Sig. (2-tailed)	Mean Difference	Std. Error Difference	Lower	Upper
FirstTime	Equal variances assumed	2.711	.126	.866	12	.404	61.00000	70.45219	-92.50213	214.50213
	Equal variances not assumed			1.136	10.762	.281	61.00000	53.68530	-57.47974	179.47974
SecondTime	Equal variances assumed	10.023	.008	-1.379	12	.193	-81.75000	59.27869	-210.90718	47.40718
	Equal variances not assumed			-.888	3.178	.436	-81.75000	92.02359	-365.54498	202.04498
QuestionnaireTime	Equal variances assumed	.510	.492	.137	10	.894	5.00000	36.53765	-76.41096	86.41096
	Equal variances not assumed			.121	4.571	.909	5.00000	41.34639	-104.35779	114.35779

Independent Samples Effect Sizes

		Standardizer[a]	Point Estimate	95% Confidence Interval	
				Lower	Upper
FirstAngle	Cohen's d	16.39897	-.292	-1.451	.879
	Hedges' correction	17.52135	-.273	-1.358	.823
	Glass's delta	17.00559	-.282	-1.440	.919
SecondAngle	Cohen's d	16.88536	-.515	-1.700	.693
	Hedges' correction	18.15708	-.479	-1.581	.645
	Glass's delta	20.58948	-.422	-1.612	.829
TutorialTime	Cohen's d	127.733	.376	-.844	1.578
	Hedges' correction	138.427	.347	-.779	1.456
	Glass's delta	24.207	1.983	.015	3.863
FirstTime	Cohen's d	119.08593	.512	-.675	1.679
	Hedges' correction	127.23646	.479	-.632	1.572
	Glass's delta	67.63875	.902	-.496	2.200
SecondTime	Cohen's d	100.19928	-.816	-2.004	.403
	Hedges' correction	107.05717	-.764	-1.876	.378
	Glass's delta	181.40080	-.451	-1.628	.791
QuestionnaireTime	Cohen's d	59.66574	.084	-1.119	1.283
	Hedges' correction	64.66109	.077	-1.033	1.183
	Glass's delta	73.93691	.068	-1.139	1.264

a. The denominator used in estimating the effect sizes.
Cohen's d uses the pooled standard deviation.
Hedges' correction uses the pooled standard deviation, plus a correction factor.
Glass's delta uses the sample standard deviation of the control group.

T-Test: Effect of HoloLens experience on test results

Group Statistics

	HoloLens	N	Mean	Std. Deviation	Std. Error Mean
FirstAngle	None	10	39.6600	16.63452	5.26030
	Beginner	4	43.7500	15.85886	7.92943
SecondAngle	None	9	42.9444	15.40350	5.13450
	Beginner	4	51.2000	20.48137	10.24069
TutorialTime	None	9	355.89	125.328	41.776
	Beginner	3	248.33	93.853	54.186
FirstTime	None	10	379.5000	119.61628	37.82599
	Beginner	4	245.0000	10.80123	5.40062
SecondTime	None	10	136.5000	121.24470	38.34094
	Beginner	4	132.5000	49.07477	24.53739
QuestionnaireTime	None	9	277.7778	63.20162	21.06721
	Beginner	3	300.0000	36.05551	20.81666

Independent Samples Test

		Levene's Test for Equality of Variances		t-test for Equality of Means						
									95% Confidence Interval of the Difference	
		F	Sig.	t	df	Sig. (2-tailed)	Mean Difference	Std. Error Difference	Lower	Upper
FirstAngle	Equal variances assumed	1.407	.259	-.420	12	.682	-4.09000	9.72842	-25.28641	17.10641
	Equal variances not assumed			-.430	5.844	.683	-4.09000	9.51559	-27.52508	19.34508
SecondAngle	Equal variances assumed	.021	.888	-.811	11	.435	-8.25556	10.17968	-30.66087	14.14976
	Equal variances not assumed			-.721	4.589	.506	-8.25556	11.45577	-38.51450	22.00339
TutorialTime	Equal variances assumed	.548	.476	1.348	10	.207	107.556	79.798	-70.245	285.356
	Equal variances not assumed			1.572	4.672	.181	107.556	68.420	-72.109	287.220

Independent Samples Test

		Levene's Test for Equality of Variances		t-test for Equality of Means						
									95% Confidence Interval of the Difference	
		F	Sig.	t	df	Sig. (2-tailed)	Mean Difference	Std. Error Difference	Lower	Upper
FirstTime	Equal variances assumed	8.833	.012	2.192	12	.049	134.50000	61.36834	.78988	268.21012
	Equal variances not assumed			3.520	9.359	.006	134.50000	38.20958	48.56670	220.43330
SecondTime	Equal variances assumed	.728	.410	.063	12	.951	4.00000	63.79304	-134.99310	142.99310
	Equal variances not assumed			.088	11.896	.931	4.00000	45.52045	-95.27716	103.27716
QuestionnaireTime	Equal variances assumed	.976	.346	-.567	10	.583	-22.22222	39.18932	-109.54146	65.09701
	Equal variances not assumed			-.750	6.492	.479	-22.22222	29.61690	-93.38076	48.93632

Independent Samples Effect Sizes

		Standardizer[a]	Point Estimate	95% Confidence Interval	
				Lower	Upper
FirstAngle	Cohen's d	16.44403	-.249	-1.407	.920
	Hedges' correction	17.56950	-.233	-1.317	.861
	Glass's delta	15.85886	-.258	-1.414	.938
SecondAngle	Cohen's d	16.94001	-.487	-1.672	.718
	Hedges' correction	18.21585	-.453	-1.554	.668
	Glass's delta	20.48137	-.403	-1.591	.844
TutorialTime	Cohen's d	119.697	.899	-.485	2.241
	Hedges' correction	129.718	.829	-.448	2.068
	Glass's delta	93.853	1.146	-.591	2.749
FirstTime	Cohen's d	103.73142	1.297	.006	2.542
	Hedges' correction	110.83106	1.214	.006	2.379
	Glass's delta	10.80123	12.452	3.246	22.040
SecondTime	Cohen's d	107.82992	.037	-1.123	1.196
	Hedges' correction	115.21007	.035	-1.051	1.119
	Glass's delta	49.07477	.082	-1.086	1.236
QuestionnaireTime	Cohen's d	58.78397	-.378	-1.686	.948
	Hedges' correction	63.70550	-.349	-1.555	.875
	Glass's delta	36.05551	-.616	-1.981	.862

a. The denominator used in estimating the effect sizes.
Cohen's d uses the pooled standard deviation.
Hedges' correction uses the pooled standard deviation, plus a correction factor.
Glass's delta uses the sample standard deviation of the control group.

T-Test: Effect of HMD experience on test results

Group Statistics

	HMD	N	Mean	Std. Deviation	Std. Error Mean
FirstAngle	None	9	41.3222	16.93729	5.64576
	Beginner	5	39.9400	15.74446	7.04114
SecondAngle	None	8	45.1125	15.56346	5.50251
	Beginner	5	46.0800	20.29106	9.07444
TutorialTime	None	9	342.56	142.070	47.357
	Beginner	3	288.33	24.664	14.240
FirstTime	None	9	358.8889	116.31793	38.77264
	Beginner	5	309.0000	127.05314	56.81989
SecondTime	None	9	153.8889	127.37194	42.45731
	Beginner	5	102.0000	16.80774	7.51665
QuestionnaireTime	None	8	263.7500	50.40904	17.82229
	Beginner	4	322.5000	53.77422	26.88711

Independent Samples Test

		Levene's Test for Equality of Variances		t-test for Equality of Means						
									95% Confidence Interval of the Difference	
		F	Sig.	t	df	Sig. (2-tailed)	Mean Difference	Std. Error Difference	Lower	Upper
FirstAngle	Equal variances assumed	.949	.349	.150	12	.883	1.38222	9.23072	-18.72980	21.49424
	Equal variances not assumed			.153	8.948	.882	1.38222	9.02509	-19.05221	21.81665
SecondAngle	Equal variances assumed	.055	.818	-.097	11	.924	-.96750	9.93753	-22.83985	20.90485
	Equal variances not assumed			-.091	6.946	.930	-.96750	10.61240	-26.10165	24.16665
TutorialTime	Equal variances assumed	4.347	.064	.638	10	.538	54.222	85.033	-135.242	243.686
	Equal variances not assumed			1.096	9.211	.301	54.222	49.451	-57.255	165.699

Independent Samples Test

		Levene's Test for Equality of Variances		t-test for Equality of Means						
									95% Confidence Interval of the Difference	
		F	Sig.	t	df	Sig. (2-tailed)	Mean Difference	Std. Error Difference	Lower	Upper
FirstTime	Equal variances assumed	.002	.963	.745	12	.470	49.88889	66.93452	-95.94891	195.72669
	Equal variances not assumed			.725	7.752	.490	49.88889	68.78821	-109.62468	209.40245
SecondTime	Equal variances assumed	3.821	.074	.891	12	.391	51.88889	58.25971	-75.04811	178.82589
	Equal variances not assumed			1.203	8.493	.261	51.88889	43.11755	-46.54527	150.32305
QuestionnaireTime	Equal variances assumed	.000	.987	-1.865	10	.092	-58.75000	31.50149	-128.93969	11.43969
	Equal variances not assumed			-1.821	5.740	.121	-58.75000	32.25757	-138.55454	21.05454

Independent Samples Effect Sizes

		Standardizer[a]	Point Estimate	95% Confidence Interval	
				Lower	Upper
FirstAngle	Cohen's d	16.54924	.084	-1.012	1.176
	Hedges' correction	17.68191	.078	-.947	1.100
	Glass's delta	15.74446	.088	-1.012	1.177
SecondAngle	Cohen's d	17.43157	-.056	-1.172	1.063
	Hedges' correction	18.74444	-.052	-1.090	.989
	Glass's delta	20.29106	-.048	-1.163	1.073
TutorialTime	Cohen's d	127.549	.425	-.905	1.734
	Hedges' correction	138.227	.392	-.835	1.600
	Glass's delta	24.664	2.198	-.198	4.541
FirstTime	Cohen's d	120.00309	.416	-.698	1.513
	Hedges' correction	128.21639	.389	-.653	1.416
	Glass's delta	127.05314	.393	-.754	1.495
SecondTime	Cohen's d	104.45050	.497	-.624	1.598
	Hedges' correction	111.59935	.465	-.584	1.495
	Glass's delta	16.80774	3.087	.742	5.389
QuestionnaireTime	Cohen's d	51.44171	-1.142	-2.416	.180
	Hedges' correction	55.74853	-1.054	-2.229	.166
	Glass's delta	53.77422	-1.093	-2.499	.422

a. The denominator used in estimating the effect sizes.
Cohen's d uses the pooled standard deviation.
Hedges' correction uses the pooled standard deviation, plus a correction factor.
Glass's delta uses the sample standard deviation of the control group.

T-Test: Effect of mobile AR experience on test results

Group Statistics

	Mobile_AR	N	Mean	Std. Deviation	Std. Error Mean
FirstAngle	None	9	41.7778	16.38359	5.46120
	Beginner	5	39.1200	16.75252	7.49196
SecondAngle	None	8	45.2750	15.34906	5.42671
	Beginner	5	45.8200	20.58682	9.20670
TutorialTime	None	9	335.89	144.645	48.215
	Beginner	3	308.33	10.408	6.009
FirstTime	None	9	374.4444	130.27482	43.42494
	Beginner	5	281.0000	65.13448	29.12902
SecondTime	None	9	114.4444	51.13979	17.04660
	Beginner	5	173.0000	164.03506	73.35871
QuestionnaireTime	None	8	275.0000	33.80617	11.95229
	Beginner	4	300.0000	93.09493	46.54747

Independent Samples Test

		Levene's Test for Equality of Variances		t-test for Equality of Means						
									95% Confidence Interval of the Difference	
		F	Sig.	t	df	Sig. (2-tailed)	Mean Difference	Std. Error Difference	Lower	Upper
FirstAngle	Equal variances assumed	.206	.658	.289	12	.778	2.65778	9.20743	-17.40350	22.71905
	Equal variances not assumed			.287	8.220	.781	2.65778	9.27114	-18.62240	23.93796
SecondAngle	Equal variances assumed	.119	.737	-.055	11	.957	-.54500	9.94045	-22.42378	21.33378
	Equal variances not assumed			-.051	6.794	.961	-.54500	10.68703	-25.97224	24.88224
TutorialTime	Equal variances assumed	7.071	.024	.319	10	.756	27.556	86.305	-164.745	219.856
	Equal variances not assumed			.567	8.243	.586	27.556	48.588	-83.917	139.028

Independent Samples Test

		Levene's Test for Equality of Variances		t-test for Equality of Means						
									95% Confidence Interval of the Difference	
		F	Sig.	t	df	Sig. (2-tailed)	Mean Difference	Std. Error Difference	Lower	Upper
FirstTime	Equal variances assumed	4.478	.056	1.485	12	.163	93.44444	62.92840	-43.66476	230.55365
	Equal variances not assumed			1.787	11.971	.099	93.44444	52.28982	-20.51539	207.40428
SecondTime	Equal variances assumed	5.051	.044	-1.014	12	.330	-58.55556	57.73071	-184.33998	67.22887
	Equal variances not assumed			-.777	4.437	.476	-58.55556	75.31326	-259.77900	142.66789
QuestionnaireTime	Equal variances assumed	3.341	.098	-.700	10	.500	-25.00000	35.70714	-104.56047	54.56047
	Equal variances not assumed			-.520	3.402	.635	-25.00000	48.05751	-168.20165	118.20165

Independent Samples Effect Sizes

		Standardizer[a]	Point Estimate	95% Confidence Interval	
				Lower	Upper
FirstAngle	Cohen's d	16.50748	.161	-.937	1.253
	Hedges' correction	17.63729	.151	-.877	1.173
	Glass's delta	16.75252	.159	-.949	1.248
SecondAngle	Cohen's d	17.43670	-.031	-1.148	1.087
	Hedges' correction	18.74995	-.029	-1.068	1.011
	Glass's delta	20.58682	-.026	-1.142	1.093
TutorialTime	Cohen's d	129.458	.213	-1.102	1.518
	Hedges' correction	140.296	.196	-1.017	1.400
	Glass's delta	10.408	2.647	-.062	5.354
FirstTime	Cohen's d	112.82074	.828	-.329	1.954
	Hedges' correction	120.54247	.775	-.308	1.829
	Glass's delta	65.13448	1.435	-.063	2.844
SecondTime	Cohen's d	103.50210	-.566	-1.670	.561
	Hedges' correction	110.58604	-.530	-1.563	.525
	Glass's delta	164.03506	-.357	-1.456	.782
QuestionnaireTime	Cohen's d	58.30952	-.429	-1.633	.796
	Hedges' correction	63.19133	-.396	-1.507	.735
	Glass's delta	93.09493	-.269	-1.466	.969

a. The denominator used in estimating the effect sizes.
Cohen's d uses the pooled standard deviation.
Hedges' correction uses the pooled standard deviation, plus a correction factor.
Glass's delta uses the sample standard deviation of the control group.

T-Test: Effect of HoloLens experience on time spent in first attempt

Group Statistics

	HoloLens	N	Mean	Std. Deviation	Std. Error Mean
FirstTime	None	10	379.5000	119.61628	37.82599
	Beginner	4	245.0000	10.80123	5.40062

Independent Samples Test

		Levene's Test for Equality of Variances		t-test for Equality of Means						
									95% Confidence Interval of the Difference	
		F	Sig.	t	df	Sig. (2-tailed)	Mean Difference	Std. Error Difference	Lower	Upper
FirstTime	Equal variances assumed	8.833	.012	2.192	12	.049	134.50000	61.36834	.78988	268.21012
	Equal variances not assumed			3.520	9.359	.006	134.50000	38.20958	48.56670	220.43330

Independent Samples Effect Sizes

		Standardizer[a]	Point Estimate	95% Confidence Interval	
				Lower	Upper
FirstTime	Cohen's d	103.73142	1.297	.006	2.542
	Hedges' correction	110.83106	1.214	.006	2.379
	Glass's delta	10.80123	12.452	3.246	22.040

a. The denominator used in estimating the effect sizes.
Cohen's d uses the pooled standard deviation.
Hedges' correction uses the pooled standard deviation, plus a correction factor.
Glass's delta uses the sample standard deviation of the control group.

T-Test: Effect of gender on questionnaire results

Group Statistics

	Gender	N	Mean	Std. Deviation	Std. Error Mean
IU	Woman	10	5.3000	.88122	.27867
	Man	4	5.5833	.95743	.47871
PU	Woman	10	5.9333	.58373	.18459
	Man	4	5.9167	.56928	.28464
EOU	Woman	10	4.0000	1.45297	.45947
	Man	4	4.3750	.92421	.46211
PL	Woman	10	3.7333	.78253	.24746
	Man	4	4.5000	.33333	.16667
TU	Woman	10	4.4000	1.15256	.36447
	Man	4	5.0000	.27217	.13608
Signal_ASQ	Woman	10	4.8667	1.40721	.44500
	Man	4	5.5833	.41944	.20972
Angle_ASQ	Woman	10	4.2333	1.58737	.50197
	Man	4	5.3333	.60858	.30429
PRF_ASQ	Woman	10	5.0333	1.50267	.47519
	Man	4	4.8333	1.17063	.58531

Independent Samples Test

		Levene's Test for Equality of Variances		t-test for Equality of Means						
									95% Confidence Interval of the Difference	
		F	Sig.	t	df	Sig. (2-tailed)	Mean Difference	Std. Error Difference	Lower	Upper
IU	Equal variances assumed	.004	.950	-.532	12	.605	-.28333	.53296	-1.44456	.87790
	Equal variances not assumed			-.512	5.179	.630	-.28333	.55391	-1.69251	1.12584
PU	Equal variances assumed	.073	.791	.049	12	.962	.01667	.34322	-.73115	.76448
	Equal variances not assumed			.049	5.717	.962	.01667	.33925	-.82352	.85685
EOU	Equal variances assumed	2.024	.180	-.473	12	.645	-.37500	.79304	-2.10288	1.35288
	Equal variances not assumed			-.575	8.948	.579	-.37500	.65165	-1.85044	1.10044
PL	Equal variances assumed	2.106	.172	-1.857	12	.088	-.76667	.41287	-1.66624	.13290
	Equal variances not assumed			-2.570	11.758	.025	-.76667	.29835	-1.41820	-.11513
TU	Equal variances assumed	4.036	.068	-1.007	12	.334	-.60000	.59597	-1.89852	.69852
	Equal variances not assumed			-1.542	11.041	.151	-.60000	.38905	-1.45590	.25590
Signal_ASQ	Equal variances assumed	7.837	.016	-.980	12	.347	-.71667	.73158	-2.31064	.87731
	Equal variances not assumed			-1.457	11.709	.171	-.71667	.49194	-1.79148	.35814
Angle_ASQ	Equal variances assumed	4.297	.060	-1.321	12	.211	-1.10000	.83297	-2.91489	.71489
	Equal variances not assumed			-1.874	11.978	.086	-1.10000	.58700	-2.37923	.17923

Independent Samples Test

		Levene's Test for Equality of Variances		t-test for Equality of Means						
									95% Confidence Interval of the Difference	
		F	Sig.	t	df	Sig. (2-tailed)	Mean Difference	Std. Error Difference	Lower	Upper
PRF_ASQ	Equal variances assumed	.002	.961	.237	12	.817	.20000	.84418	-1.63931	2.03931
	Equal variances not assumed			.265	7.213	.798	.20000	.75392	-1.57211	1.97211

Independent Samples Effect Sizes

				95% Confidence Interval	
		Standardizer[a]	Point Estimate	Lower	Upper
IU	Cohen's d	.90087	-.315	-1.474	.858
	Hedges' correction	.96253	-.294	-1.380	.803
	Glass's delta	.95743	-.296	-1.455	.908
PU	Cohen's d	.58015	.029	-1.131	1.188
	Hedges' correction	.61986	.027	-1.059	1.112
	Glass's delta	.56928	.029	-1.133	1.187
EOU	Cohen's d	1.34048	-.280	-1.439	.891
	Hedges' correction	1.43222	-.262	-1.347	.834
	Glass's delta	.92421	-.406	-1.576	.824
PL	Cohen's d	.69788	-1.099	-2.317	.160
	Hedges' correction	.74565	-1.028	-2.169	.149
	Glass's delta	.33333	-2.300	-4.359	-.176
TU	Cohen's d	1.00738	-.596	-1.767	.599
	Hedges' correction	1.07633	-.557	-1.654	.561
	Glass's delta	.27217	-2.205	-4.202	-.137
Signal_ASQ	Cohen's d	1.23659	-.580	-1.750	.614
	Hedges' correction	1.32123	-.542	-1.638	.575
	Glass's delta	.41944	-1.709	-3.402	.078

Independent Samples Effect Sizes

		Standardizer[a]	Point Estimate	95% Confidence Interval	
				Lower	Upper
Angle_ASQ	Cohen's d	1.40798	-.781	-1.966	.434
	Hedges' correction	1.50435	-.731	-1.840	.406
	Glass's delta	.60858	-1.807	-3.559	.033
PRF_ASQ	Cohen's d	1.42692	.140	-1.024	1.298
	Hedges' correction	1.52459	.131	-.958	1.215
	Glass's delta	1.17063	.171	-1.009	1.324

a. The denominator used in estimating the effect sizes.
Cohen's d uses the pooled standard deviation.
Hedges' correction uses the pooled standard deviation, plus a correction factor.
Glass's delta uses the sample standard deviation of the control group.

T-Test: Effect of Mobile AR experience on questionnaire results

Group Statistics

	Mobile_AR	N	Mean	Std. Deviation	Std. Error Mean
IU	None	9	5.3333	.66667	.22222
	Beginner	5	5.4667	1.26051	.56372
PU	None	9	5.9259	.61864	.20621
	Beginner	5	5.9333	.49441	.22111
EOU	None	9	3.5556	1.17112	.39037
	Beginner	5	5.1000	.91173	.40774
PL	None	9	3.8519	.83518	.27839
	Beginner	5	4.1333	.64979	.29059
TU	None	9	4.5926	1.22222	.40741
	Beginner	5	4.5333	.55777	.24944
Signal_ASQ	None	9	4.6667	1.29099	.43033
	Beginner	5	5.8000	.76739	.34319
Angle_ASQ	None	9	3.9259	1.39222	.46407
	Beginner	5	5.6667	.70711	.31623
PRF_ASQ	None	9	4.7778	1.60728	.53576
	Beginner	5	5.3333	.84984	.38006

Independent Samples Test

		Levene's Test for Equality of Variances		t-test for Equality of Means						
									95% Confidence Interval of the Difference	
		F	Sig.	t	df	Sig. (2-tailed)	Mean Difference	Std. Error Difference	Lower	Upper
IU	Equal variances assumed	1.123	.310	-.263	12	.797	-.13333	.50691	-1.23779	.97112
	Equal variances not assumed			-.220	5.276	.834	-.13333	.60594	-1.66675	1.40008
PU	Equal variances assumed	.943	.351	-.023	12	.982	-.00741	.32362	-.71251	.69769
	Equal variances not assumed			-.024	10.146	.981	-.00741	.30235	-.67976	.66494
EOU	Equal variances assumed	.315	.585	-2.537	12	.026	-1.54444	.60883	-2.87096	-.21793
	Equal variances not assumed			-2.736	10.347	.020	-1.54444	.56448	-2.79650	-.29239
PL	Equal variances assumed	.310	.588	-.648	12	.529	-.28148	.43412	-1.22734	.66438
	Equal variances not assumed			-.699	10.352	.500	-.28148	.40243	-1.17403	.61107
TU	Equal variances assumed	3.013	.108	.101	12	.921	.05926	.58489	-1.21510	1.33362
	Equal variances not assumed			.124	11.804	.903	.05926	.47771	-.98349	1.10201
Signal_ASQ	Equal variances assumed	3.892	.072	-1.777	12	.101	-1.13333	.63777	-2.52291	.25625
	Equal variances not assumed			-2.059	11.836	.062	-1.13333	.55042	-2.33444	.06777
Angle_ASQ	Equal variances assumed	5.146	.043	-2.584	12	.024	-1.74074	.67369	-3.20859	-.27289
	Equal variances not assumed			-3.100	11.986	.009	-1.74074	.56157	-2.96446	-.51702

Independent Samples Test

		Levene's Test for Equality of Variances		t-test for Equality of Means						
									95% Confidence Interval of the Difference	
		F	Sig.	t	df	Sig. (2-tailed)	Mean Difference	Std. Error Difference	Lower	Upper
PRF_ASQ	Equal variances assumed	1.918	.191	-.711	12	.491	-.55556	.78147	-2.25824	1.14713
	Equal variances not assumed			-.846	12.000	.414	-.55556	.65687	-1.98676	.87565

Independent Samples Effect Sizes

				95% Confidence Interval	
		Standardizer[a]	Point Estimate	Lower	Upper
IU	Cohen's d	.90880	-.147	-1.238	.951
	Hedges' correction	.97101	-.137	-1.159	.890
	Glass's delta	1.26051	-.106	-1.195	.996
PU	Cohen's d	.58019	-.013	-1.106	1.081
	Hedges' correction	.61990	-.012	-1.035	1.011
	Glass's delta	.49441	-.015	-1.107	1.079
EOU	Cohen's d	1.09153	-1.415	-2.620	-.164
	Hedges' correction	1.16624	-1.324	-2.452	-.153
	Glass's delta	.91173	-1.694	-3.223	-.079
PL	Cohen's d	.77831	-.362	-1.457	.748
	Hedges' correction	.83158	-.338	-1.364	.700
	Glass's delta	.64979	-.433	-1.540	.722
TU	Cohen's d	1.04861	.057	-1.038	1.149
	Hedges' correction	1.12038	.053	-.972	1.075
	Glass's delta	.55777	.106	-.996	1.195
Signal_ASQ	Cohen's d	1.14342	-.991	-2.135	.188
	Hedges' correction	1.22168	-.928	-1.998	.176
	Glass's delta	.76739	-1.477	-2.905	.040

Independent Samples Effect Sizes

		Standardizer[a]	Point Estimate	95% Confidence Interval	
				Lower	Upper
Angle_ASQ	Cohen's d	1.20783	-1.441	-2.651	-.185
	Hedges' correction	1.29049	-1.349	-2.481	-.173
	Glass's delta	.70711	-2.462	-4.398	-.460
PRF_ASQ	Cohen's d	1.40106	-.397	-1.493	.716
	Hedges' correction	1.49695	-.371	-1.397	.670
	Glass's delta	.84984	-.654	-1.798	.557

a. The denominator used in estimating the effect sizes.
Cohen's d uses the pooled standard deviation.
Hedges' correction uses the pooled standard deviation, plus a correction factor.
Glass's delta uses the sample standard deviation of the control group.

T-Test: Effect of HMD experience on questionnaire results

Group Statistics

	HMD	N	Mean	Std. Deviation	Std. Error Mean
IU	None	9	5.4815	.80123	.26708
	Beginner	5	5.2000	1.06979	.47842
PU	None	9	6.0741	.61864	.20621
	Beginner	5	5.6667	.33333	.14907
EOU	None	9	3.8889	1.25693	.41898
	Beginner	5	4.5000	1.42522	.63738
PL	None	9	3.8519	.83518	.27839
	Beginner	5	4.1333	.64979	.29059
TU	None	9	4.8519	.98758	.32919
	Beginner	5	4.0667	.92496	.41366
Signal_ASQ	None	9	5.0370	1.11111	.37037
	Beginner	5	5.1333	1.57410	.70396
Angle_ASQ	None	9	4.3333	1.40436	.46812
	Beginner	5	4.9333	1.60555	.71802
PRF_ASQ	None	9	5.2593	1.13990	.37997
	Beginner	5	4.4667	1.74165	.77889

Independent Samples Test

		Levene's Test for Equality of Variances		t-test for Equality of Means						
									95% Confidence Interval of the Difference	
		F	Sig.	t	df	Sig. (2-tailed)	Mean Difference	Std. Error Difference	Lower	Upper
IU	Equal variances assumed	.115	.740	.561	12	.585	.28148	.50183	-.81191	1.37488
	Equal variances not assumed			.514	6.563	.624	.28148	.54792	-1.03185	1.59481
PU	Equal variances assumed	3.993	.069	1.351	12	.202	.40741	.30150	-.24950	1.06431
	Equal variances not assumed			1.601	11.995	.135	.40741	.25445	-.14702	.96184
EOU	Equal variances assumed	.114	.741	-.833	12	.421	-.61111	.73371	-2.20972	.98749
	Equal variances not assumed			-.801	7.503	.448	-.61111	.76275	-2.39050	1.16828
PL	Equal variances assumed	.310	.588	-.648	12	.529	-.28148	.43412	-1.22734	.66438
	Equal variances not assumed			-.699	10.352	.500	-.28148	.40243	-1.17403	.61107
TU	Equal variances assumed	.015	.903	1.456	12	.171	.78519	.53945	-.39018	1.96055
	Equal variances not assumed			1.485	8.888	.172	.78519	.52866	-.41301	1.98338
Signal_ASQ	Equal variances assumed	.014	.909	-.134	12	.895	-.09630	.71625	-1.65687	1.46428
	Equal variances not assumed			-.121	6.280	.907	-.09630	.79544	-2.02181	1.82921
Angle_ASQ	Equal variances assumed	.020	.889	-.730	12	.480	-.60000	.82242	-2.39190	1.19190
	Equal variances not assumed			-.700	7.450	.505	-.60000	.85714	-2.60226	1.40226

Independent Samples Test

		Levene's Test for Equality of Variances		t-test for Equality of Means						
									95% Confidence Interval of the Difference	
		F	Sig.	t	df	Sig. (2-tailed)	Mean Difference	Std. Error Difference	Lower	Upper
PRF_ASQ	Equal variances assumed	1.101	.315	1.037	12	.320	.79259	.76424	-.87255	2.45774
	Equal variances not assumed			.915	5.962	.396	.79259	.86663	-1.33128	2.91647

Independent Samples Effect Sizes

				95% Confidence Interval	
		Standardizer[a]	Point Estimate	Lower	Upper
IU	Cohen's d	.89970	.313	-.794	1.407
	Hedges' correction	.96128	.293	-.743	1.317
	Glass's delta	1.06979	.263	-.860	1.355
PU	Cohen's d	.54054	.754	-.394	1.872
	Hedges' correction	.57753	.705	-.369	1.752
	Glass's delta	.33333	1.222	-.187	2.543
EOU	Cohen's d	1.31542	-.465	-1.564	.653
	Hedges' correction	1.40545	-.435	-1.464	.611
	Glass's delta	1.42522	-.429	-1.535	.725
PL	Cohen's d	.77831	-.362	-1.457	.748
	Hedges' correction	.83158	-.338	-1.364	.700
	Glass's delta	.64979	-.433	-1.540	.722
TU	Cohen's d	.96716	.812	-.343	1.936
	Hedges' correction	1.03335	.760	-.321	1.812
	Glass's delta	.92496	.849	-.422	2.042
Signal_ASQ	Cohen's d	1.28412	-.075	-1.167	1.020
	Hedges' correction	1.37201	-.070	-1.092	.955
	Glass's delta	1.57410	-.061	-1.151	1.036

Independent Samples Effect Sizes

		Standardizer[a]	Point Estimate	95% Confidence Interval	
				Lower	Upper
Angle_ASQ	Cohen's d	1.47447	-.407	-1.504	.706
	Hedges' correction	1.57539	-.381	-1.407	.661
	Glass's delta	1.60555	-.374	-1.474	.769
PRF_ASQ	Cohen's d	1.37017	.578	-.550	1.684
	Hedges' correction	1.46395	.541	-.515	1.576
	Glass's delta	1.74165	.455	-.705	1.565

a. The denominator used in estimating the effect sizes.
Cohen's d uses the pooled standard deviation.
Hedges' correction uses the pooled standard deviation, plus a correction factor.
Glass's delta uses the sample standard deviation of the control group.

T-Test: Effect of HoloLens experience on questionnaire results

Group Statistics

	HoloLens	N	Mean	Std. Deviation	Std. Error Mean
IU	None	10	5.5000	.77380	.24470
	Beginner	4	5.0833	1.16667	.58333
PU	None	10	6.0333	.61764	.19532
	Beginner	4	5.6667	.27217	.13608
EOU	None	10	3.8250	1.40954	.44574
	Beginner	4	4.8125	.65749	.32874
PL	None	10	4.0667	.69921	.22111
	Beginner	4	3.6667	.94281	.47140
TU	None	10	4.4667	1.16746	.36918
	Beginner	4	4.8333	.43033	.21517
Signal_ASQ	None	10	4.9333	1.44701	.45758
	Beginner	4	5.4167	.31914	.15957
Angle_ASQ	None	10	4.2000	1.57292	.49740
	Beginner	4	5.4167	.50000	.25000
PRF_ASQ	None	10	4.9333	1.58543	.50136
	Beginner	4	5.0833	.78764	.39382

Independent Samples Test

		Levene's Test for Equality of Variances		t-test for Equality of Means						
									95% Confidence Interval of the Difference	
		F	Sig.	t	df	Sig. (2-tailed)	Mean Difference	Std. Error Difference	Lower	Upper
IU	Equal variances assumed	.835	.379	.793	12	.443	.41667	.52562	-.72855	1.56189
	Equal variances not assumed			.659	4.106	.545	.41667	.63258	-1.32187	2.15520
PU	Equal variances assumed	4.055	.067	1.123	12	.283	.36667	.32653	-.34478	1.07811
	Equal variances not assumed			1.540	11.634	.150	.36667	.23805	-.15381	.88714
EOU	Equal variances assumed	2.913	.114	-1.320	12	.211	-.98750	.74791	-2.61705	.64205
	Equal variances not assumed			-1.783	11.365	.101	-.98750	.55385	-2.20176	.22676
PL	Equal variances assumed	.215	.651	.881	12	.396	.40000	.45399	-.58917	1.38917
	Equal variances not assumed			.768	4.394	.482	.40000	.52068	-.99590	1.79590
TU	Equal variances assumed	3.366	.091	-.600	12	.560	-.36667	.61154	-1.69910	.96577
	Equal variances not assumed			-.858	11.999	.408	-.36667	.42731	-1.29770	.56437
Signal_ASQ	Equal variances assumed	12.410	.004	-.647	12	.530	-.48333	.74736	-2.11168	1.14502
	Equal variances not assumed			-.997	10.841	.340	-.48333	.48461	-1.55186	.58519
Angle_ASQ	Equal variances assumed	4.709	.051	-1.485	12	.163	-1.21667	.81934	-3.00186	.56852
	Equal variances not assumed			-2.186	11.852	.050	-1.21667	.55669	-2.43127	-.00206

Independent Samples Test

		Levene's Test for Equality of Variances		t-test for Equality of Means						
									95% Confidence Interval of the Difference	
		F	Sig.	t	df	Sig. (2-tailed)	Mean Difference	Std. Error Difference	Lower	Upper
PRF_ASQ	Equal variances assumed	1.757	.210	-.178	12	.862	-.15000	.84504	-1.99119	1.69119
	Equal variances not assumed			-.235	10.986	.818	-.15000	.63753	-1.55343	1.25343

Independent Samples Effect Sizes

				95% Confidence Interval	
		Standardizer[a]	Point Estimate	Lower	Upper
IU	Cohen's d	.88845	.469	-.715	1.634
	Hedges' correction	.94926	.439	-.669	1.529
	Glass's delta	1.16667	.357	-.860	1.522
PU	Cohen's d	.55193	.664	-.538	1.840
	Hedges' correction	.58971	.622	-.503	1.722
	Glass's delta	.27217	1.347	-.252	2.843
EOU	Cohen's d	1.26419	-.781	-1.966	.434
	Hedges' correction	1.35071	-.731	-1.840	.406
	Glass's delta	.65749	-1.502	-3.079	.176
PL	Cohen's d	.76739	.521	-.667	1.689
	Hedges' correction	.81991	.488	-.624	1.580
	Glass's delta	.94281	.424	-.810	1.597
TU	Cohen's d	1.03369	-.355	-1.516	.820
	Hedges' correction	1.10444	-.332	-1.418	.768
	Glass's delta	.43033	-.852	-2.132	.526
Signal_ASQ	Cohen's d	1.26326	-.383	-1.544	.795
	Hedges' correction	1.34972	-.358	-1.445	.744
	Glass's delta	.31914	-1.514	-3.098	.170

Independent Samples Effect Sizes

		Standardizer[a]	Point Estimate	95% Confidence Interval	
				Lower	Upper
Angle_ASQ	Cohen's d	1.38494	-.878	-2.072	.349
	Hedges' correction	1.47973	-.822	-1.940	.326
	Glass's delta	.50000	-2.433	-4.579	-.229
PRF_ASQ	Cohen's d	1.42838	-.105	-1.263	1.057
	Hedges' correction	1.52614	-.098	-1.182	.990
	Glass's delta	.78764	-.190	-1.344	.993

a. The denominator used in estimating the effect sizes.
Cohen's d uses the pooled standard deviation.
Hedges' correction uses the pooled standard deviation, plus a correction factor.
Glass's delta uses the sample standard deviation of the control group.

T-Test: Effect of age on questionnaire

Group Statistics

	Age	N	Mean	Std. Deviation	Std. Error Mean
IU	>= 25.00	10	5.3667	.94868	.30000
	< 25.00	4	5.4167	.78764	.39382
PU	>= 25.00	10	5.9333	.58373	.18459
	< 25.00	4	5.9167	.56928	.28464
EOU	>= 25.00	10	4.2750	1.07011	.33840
	< 25.00	4	3.6875	1.88608	.94304
PL	>= 25.00	10	4.0667	.71665	.22662
	< 25.00	4	3.6667	.90267	.45134
TU	>= 25.00	10	4.7667	.88958	.28131
	< 25.00	4	4.0833	1.25831	.62915
Signal_ASQ	>= 25.00	10	5.3667	.83813	.26504
	< 25.00	4	4.3333	1.86587	.93294
Angle_ASQ	>= 25.00	10	4.7667	1.17641	.37201
	< 25.00	4	4.0000	2.09054	1.04527
PRF_ASQ	>= 25.00	10	5.1000	1.14450	.36192
	< 25.00	4	4.6667	2.01843	1.00922

Independent Samples Test

		Levene's Test for Equality of Variances		t-test for Equality of Means						
									95% Confidence Interval of the Difference	
		F	Sig.	t	df	Sig. (2-tailed)	Mean Difference	Std. Error Difference	Lower	Upper
IU	Equal variances assumed	.109	.747	-.093	12	.928	-.05000	.53901	-1.22440	1.12440
	Equal variances not assumed			-.101	6.736	.922	-.05000	.49507	-1.23002	1.13002
PU	Equal variances assumed	.073	.791	.049	12	.962	.01667	.34322	-.73115	.76448
	Equal variances not assumed			.049	5.717	.962	.01667	.33925	-.82352	.85685
EOU	Equal variances assumed	1.850	.199	.751	12	.467	.58750	.78222	-1.11680	2.29180
	Equal variances not assumed			.586	3.801	.591	.58750	1.00192	-2.25255	3.42755
PL	Equal variances assumed	.441	.519	.881	12	.396	.40000	.45399	-.58917	1.38917
	Equal variances not assumed			.792	4.606	.467	.40000	.50504	-.93238	1.73238
TU	Equal variances assumed	.612	.449	1.161	12	.268	.68333	.58845	-.59879	1.96546
	Equal variances not assumed			.992	4.263	.374	.68333	.68918	-1.18452	2.55119
Signal_ASQ	Equal variances assumed	2.989	.109	1.478	12	.165	1.03333	.69931	-.49032	2.55699
	Equal variances not assumed			1.065	3.496	.355	1.03333	.96985	-1.81957	3.88623
Angle_ASQ	Equal variances assumed	3.161	.101	.888	12	.392	.76667	.86354	-1.11482	2.64815
	Equal variances not assumed			.691	3.788	.530	.76667	1.10950	-2.38304	3.91637

Independent Samples Test

		Levene's Test for Equality of Variances		t-test for Equality of Means						
									95% Confidence Interval of the Difference	
		F	Sig.	t	df	Sig. (2-tailed)	Mean Difference	Std. Error Difference	Lower	Upper
PRF_ASQ	Equal variances assumed	1.786	.206	.518	12	.614	.43333	.83685	-1.39001	2.25668
	Equal variances not assumed			.404	3.800	.708	.43333	1.07215	-2.60615	3.47282

Independent Samples Effect Sizes

				95% Confidence Interval	
		Standardizer[a]	Point Estimate	Lower	Upper
IU	Cohen's d	.91109	-.055	-1.213	1.106
	Hedges' correction	.97345	-.051	-1.136	1.035
	Glass's delta	.78764	-.063	-1.219	1.102
PU	Cohen's d	.58015	.029	-1.131	1.188
	Hedges' correction	.61986	.027	-1.059	1.112
	Glass's delta	.56928	.029	-1.133	1.187
EOU	Cohen's d	1.32219	.444	-.737	1.608
	Hedges' correction	1.41268	.416	-.690	1.505
	Glass's delta	1.88608	.311	-.895	1.472
PL	Cohen's d	.76739	.521	-.667	1.689
	Hedges' correction	.81991	.488	-.624	1.580
	Glass's delta	.90267	.443	-.796	1.619
TU	Cohen's d	.99466	.687	-.517	1.865
	Hedges' correction	1.06274	.643	-.484	1.745
	Glass's delta	1.25831	.543	-.725	1.737
Signal_ASQ	Cohen's d	1.18204	.874	-.352	2.068
	Hedges' correction	1.26294	.818	-.330	1.935
	Glass's delta	1.86587	.554	-.718	1.750

Independent Samples Effect Sizes

		Standardizer[a]	Point Estimate	95% Confidence Interval	
				Lower	Upper
Angle_ASQ	Cohen's d	1.45964	.525	-.663	1.693
	Hedges' correction	1.55954	.492	-.621	1.584
	Glass's delta	2.09054	.367	-.853	1.532
PRF_ASQ	Cohen's d	1.41454	.306	-.866	1.466
	Hedges' correction	1.51136	.287	-.810	1.372
	Glass's delta	2.01843	.215	-.973	1.369

a. The denominator used in estimating the effect sizes.
Cohen's d uses the pooled standard deviation.
Hedges' correction uses the pooled standard deviation, plus a correction factor.
Glass's delta uses the sample standard deviation of the control group.

T-Test: Effect of mobile AR experience on angle ASQ score

Group Statistics

	Mobile_AR	N	Mean	Std. Deviation	Std. Error Mean
Angle_ASQ	None	9	3.9259	1.39222	.46407
	Beginner	5	5.6667	.70711	.31623

Independent Samples Test

		Levene's Test for Equality of Variances		t-test for Equality of Means						
									95% Confidence Interval of the Difference	
		F	Sig.	t	df	Sig. (2-tailed)	Mean Difference	Std. Error Difference	Lower	Upper
Angle_ASQ	Equal variances assumed	5.146	.043	-2.584	12	.024	-1.74074	.67369	-3.20859	-.27289
	Equal variances not assumed			-3.100	11.986	.009	-1.74074	.56157	-2.96446	-.51702

Independent Samples Effect Sizes

		Standardizer[a]	Point Estimate	95% Confidence Interval	
				Lower	Upper
Angle_ASQ	Cohen's d	1.20783	-1.441	-2.651	-.185
	Hedges' correction	1.29049	-1.349	-2.481	-.173
	Glass's delta	.70711	-2.462	-4.398	-.460

a. The denominator used in estimating the effect sizes.
Cohen's d uses the pooled standard deviation.
Hedges' correction uses the pooled standard deviation, plus a correction factor.
Glass's delta uses the sample standard deviation of the control group.

T-Test: Effect of HoloLens experience on angle ASQ score

Group Statistics

	HoloLens	N	Mean	Std. Deviation	Std. Error Mean
Angle_ASQ	None	10	4.2000	1.57292	.49740
	Beginner	4	5.4167	.50000	.25000

Independent Samples Test

		Levene's Test for Equality of Variances		t-test for Equality of Means						
									95% Confidence Interval of the Difference	
		F	Sig.	t	df	Sig. (2-tailed)	Mean Difference	Std. Error Difference	Lower	Upper
Angle_ASQ	Equal variances assumed	4.709	.051	-1.485	12	.163	-1.21667	.81934	-3.00186	.56852
	Equal variances not assumed			-2.186	11.852	.050	-1.21667	.55669	-2.43127	-.00206

Independent Samples Effect Sizes

		Standardizer[a]	Point Estimate	95% Confidence Interval	
				Lower	Upper
Angle_ASQ	Cohen's d	1.38494	-.878	-2.072	.349
	Hedges' correction	1.47973	-.822	-1.940	.326
	Glass's delta	.50000	-2.433	-4.579	-.229

a. The denominator used in estimating the effect sizes.
Cohen's d uses the pooled standard deviation.
Hedges' correction uses the pooled standard deviation, plus a correction factor.
Glass's delta uses the sample standard deviation of the control group.

D.2 Linear Regressions

The following pages contain all linear regression analyses that were performed to find the results highlighted in Chapter 5.

Regression: Various factors determine second angle

Variables Entered/Removed[a]

Model	Variables Entered	Variables Removed	Method
1	QuestionnaireTime, FirstTime, TutorialTime, FirstAngle, SecondTime[b]	.	Enter

a. Dependent Variable: SecondAngle

b. All requested variables entered.

Model Summary[b]

Model	R	R Square	Adjusted R Square	Std. Error of the Estimate
1	.958[a]	.919	.837	6.88521

a. Predictors: (Constant), QuestionnaireTime, FirstTime, TutorialTime, FirstAngle, SecondTime

b. Dependent Variable: SecondAngle

ANOVA[a]

Model		Sum of Squares	df	Mean Square	F	Sig.
1	Regression	2674.851	5	534.970	11.285	.009[b]
	Residual	237.030	5	47.406		
	Total	2911.882	10			

a. Dependent Variable: SecondAngle

b. Predictors: (Constant), QuestionnaireTime, FirstTime, TutorialTime, FirstAngle, SecondTime

Coefficients[a]

Model		Unstandardized Coefficients		Standardized Coefficients		
		B	Std. Error	Beta	t	Sig.
1	(Constant)	-49.438	43.451		-1.138	.307
	TutorialTime	.029	.030	.159	.971	.376
	FirstAngle	1.061	.193	.946	5.497	.003
	FirstTime	-.001	.023	-.009	-.056	.957
	SecondTime	.050	.039	.334	1.278	.257
	QuestionnaireTime	.126	.094	.357	1.339	.238

a. Dependent Variable: SecondAngle

Residuals Statistics[a]

	Minimum	Maximum	Mean	Std. Deviation	N
Predicted Value	22.8194	65.6286	46.4273	16.35497	11
Residual	-5.45838	10.17138	.00000	4.86858	11
Std. Predicted Value	-1.443	1.174	.000	1.000	11
Std. Residual	-.793	1.477	.000	.707	11

a. Dependent Variable: SecondAngle

Charts

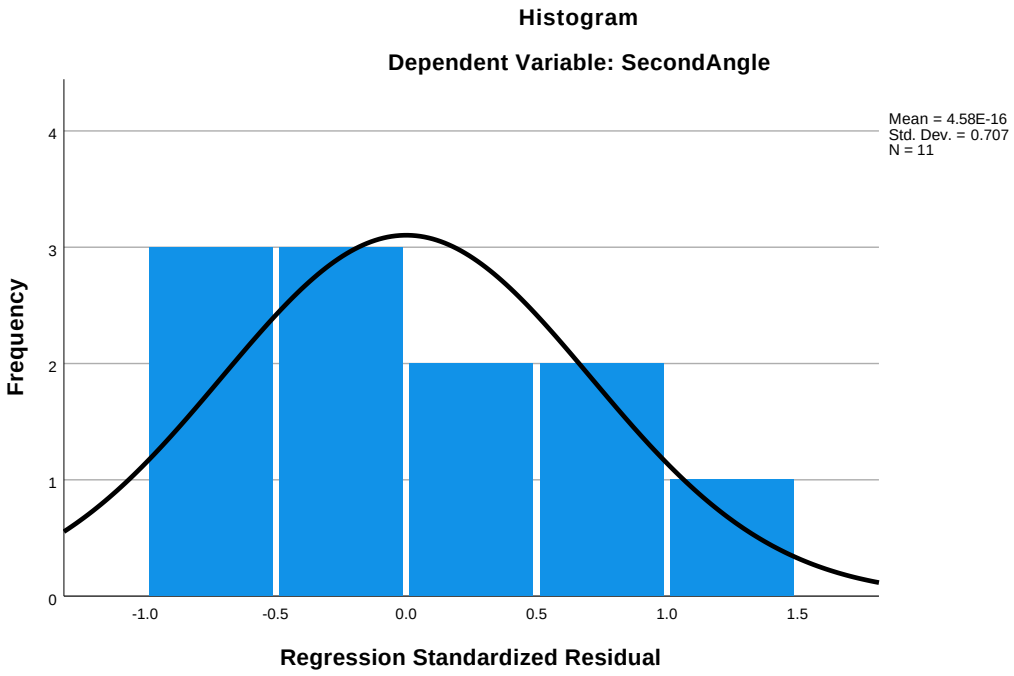

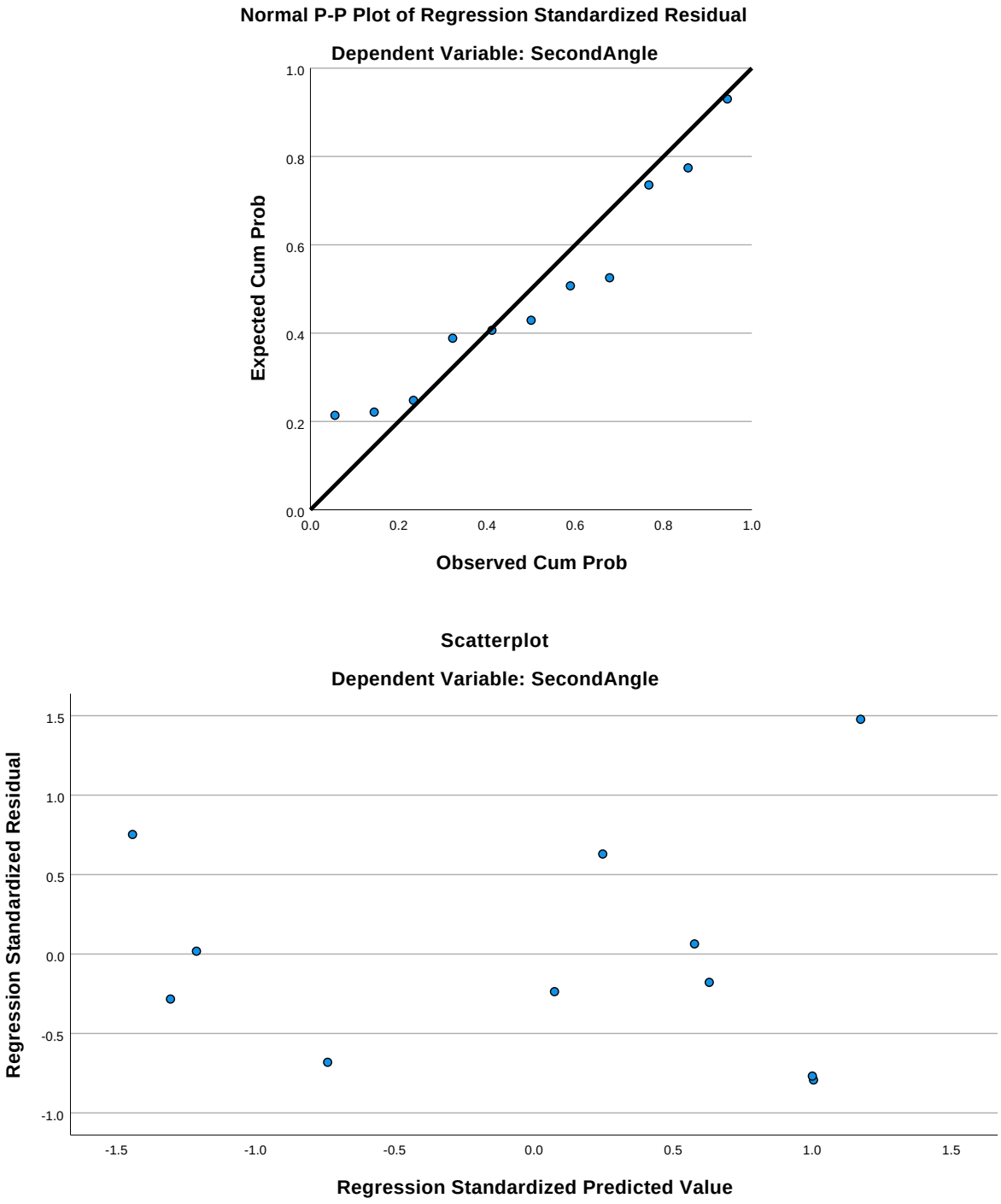

Regression: First angle determines second angle

Variables Entered/Removed[a]

Model	Variables Entered	Variables Removed	Method
1	FirstAngle[b]	.	Enter

a. Dependent Variable: SecondAngle

b. All requested variables entered.

Model Summary[b]

Model	R	R Square	Adjusted R Square	Std. Error of the Estimate
1	.945[a]	.892	.883	5.71840

a. Predictors: (Constant), FirstAngle

b. Dependent Variable: SecondAngle

ANOVA[a]

Model		Sum of Squares	df	Mean Square	F	Sig.
1	Regression	2985.636	1	2985.636	91.304	.000[b]
	Residual	359.701	11	32.700		
	Total	3345.337	12			

a. Dependent Variable: SecondAngle

b. Predictors: (Constant), FirstAngle

Coefficients[a]

Model		Unstandardized Coefficients		Standardized Coefficients		
		B	Std. Error	Beta	t	Sig.
1	(Constant)	2.200	4.800		.458	.656
	FirstAngle	1.022	.107	.945	9.555	.000

a. Dependent Variable: SecondAngle

Residuals Statistics[a]

	Minimum	Maximum	Mean	Std. Deviation	N
Predicted Value	24.1644	61.9640	45.4846	15.77349	13
Residual	-4.56395	15.98142	.00000	5.47495	13
Std. Predicted Value	-1.352	1.045	.000	1.000	13
Std. Residual	-.798	2.795	.000	.957	13

a. Dependent Variable: SecondAngle

Charts

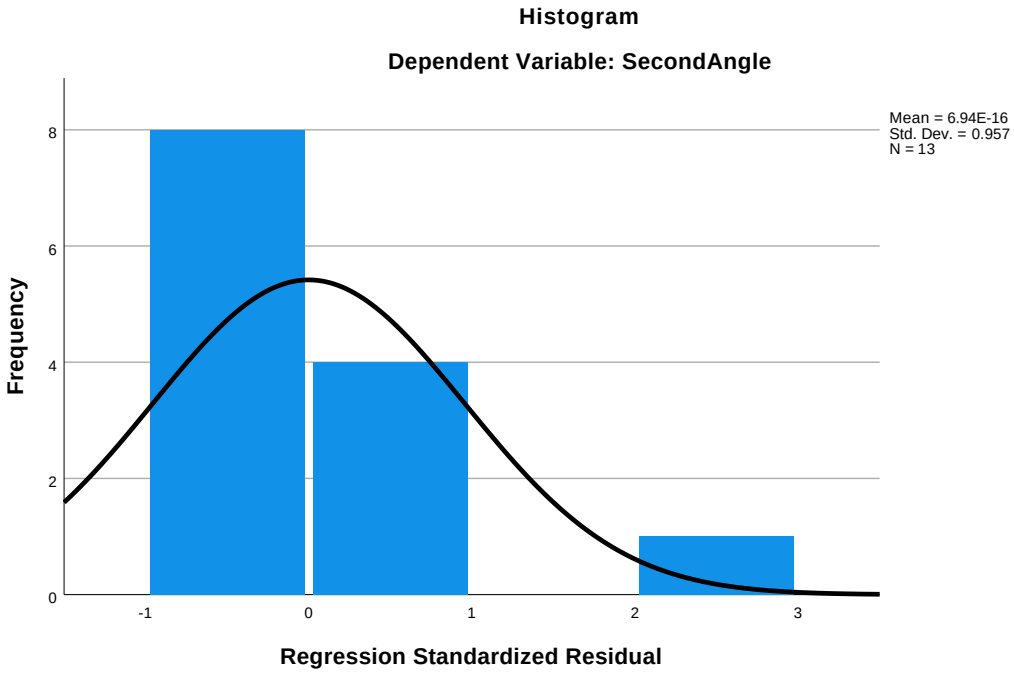

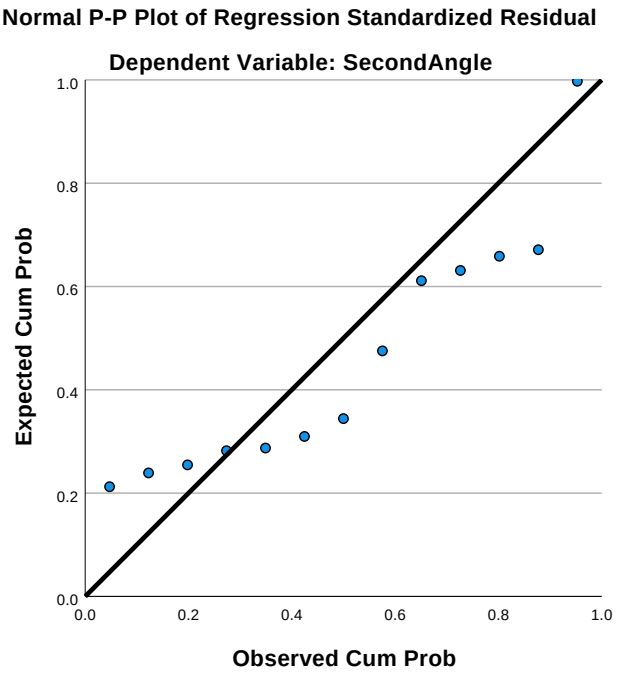

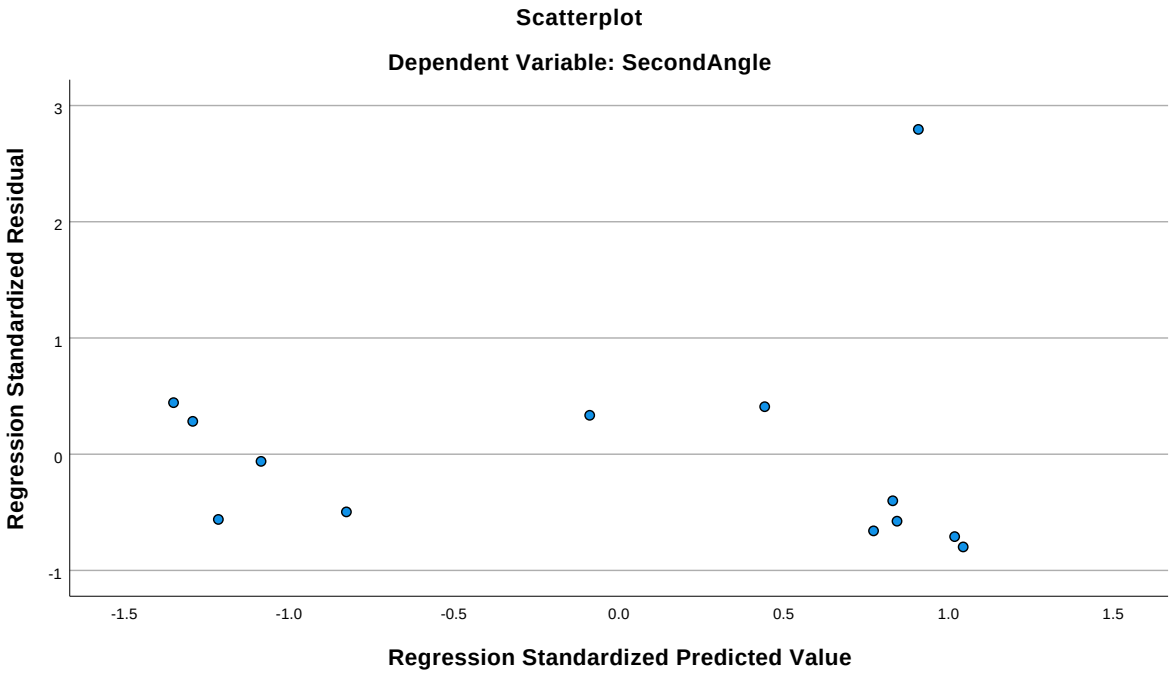

Regression: Intention to Use

Variables Entered/Removed[a]

Model	Variables Entered	Variables Removed	Method
1	QuestionnaireTime, FirstTime, TutorialTime, FirstAngle, SecondTime, SecondAngle[b]	.	Enter

a. Dependent Variable: IU

b. All requested variables entered.

Model Summary[b]

Model	R	R Square	Adjusted R Square	Std. Error of the Estimate
1	.882[a]	.778	.446	.52372

a. Predictors: (Constant), QuestionnaireTime, FirstTime, TutorialTime, FirstAngle, SecondTime, SecondAngle

b. Dependent Variable: IU

ANOVA[a]

Model		Sum of Squares	df	Mean Square	F	Sig.
1	Regression	3.852	6	.642	2.341	.215[b]
	Residual	1.097	4	.274		
	Total	4.949	10			

a. Dependent Variable: IU

b. Predictors: (Constant), QuestionnaireTime, FirstTime, TutorialTime, FirstAngle, SecondTime, SecondAngle

Coefficients[a]

Model		Unstandardized Coefficients		Standardized Coefficients		
		B	Std. Error	Beta	t	Sig.
1	(Constant)	7.180	3.708		1.936	.125
	TutorialTime	-.001	.002	-.136	-.411	.702
	FirstTime	-.001	.002	-.171	-.565	.602
	FirstAngle	-.082	.039	-1.766	-2.096	.104
	SecondTime	.001	.003	.236	.425	.693
	SecondAngle	.042	.034	1.012	1.226	.287
	QuestionnaireTime	.001	.008	.081	.140	.895

a. Dependent Variable: IU

Residuals Statistics[a]

	Minimum	Maximum	Mean	Std. Deviation	N
Predicted Value	4.6283	6.6893	5.4545	.62067	11
Residual	-.58917	.42687	.00000	.33123	11
Std. Predicted Value	-1.331	1.989	.000	1.000	11
Std. Residual	-1.125	.815	.000	.632	11

a. Dependent Variable: IU

Charts

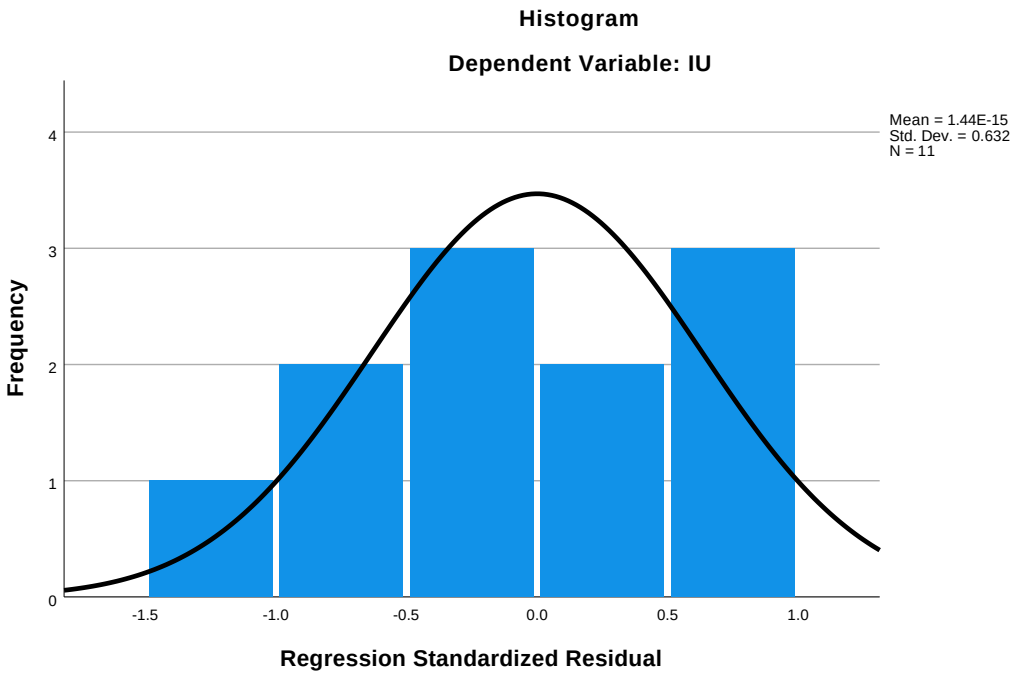

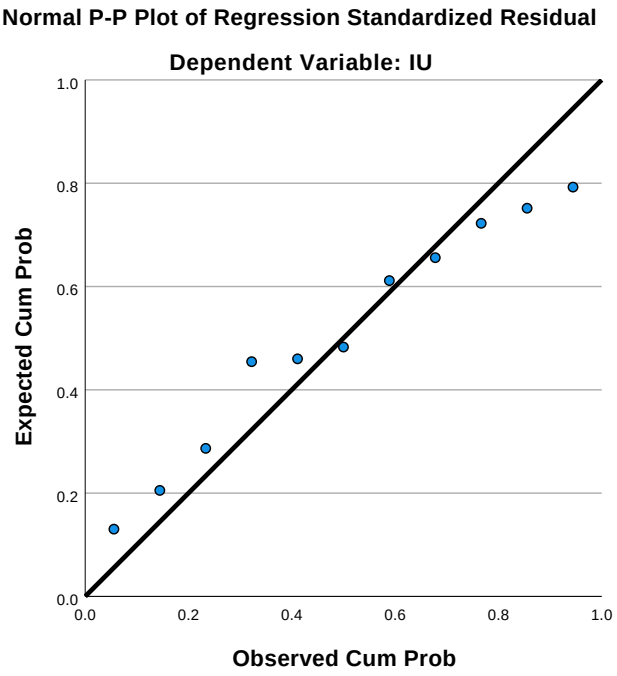

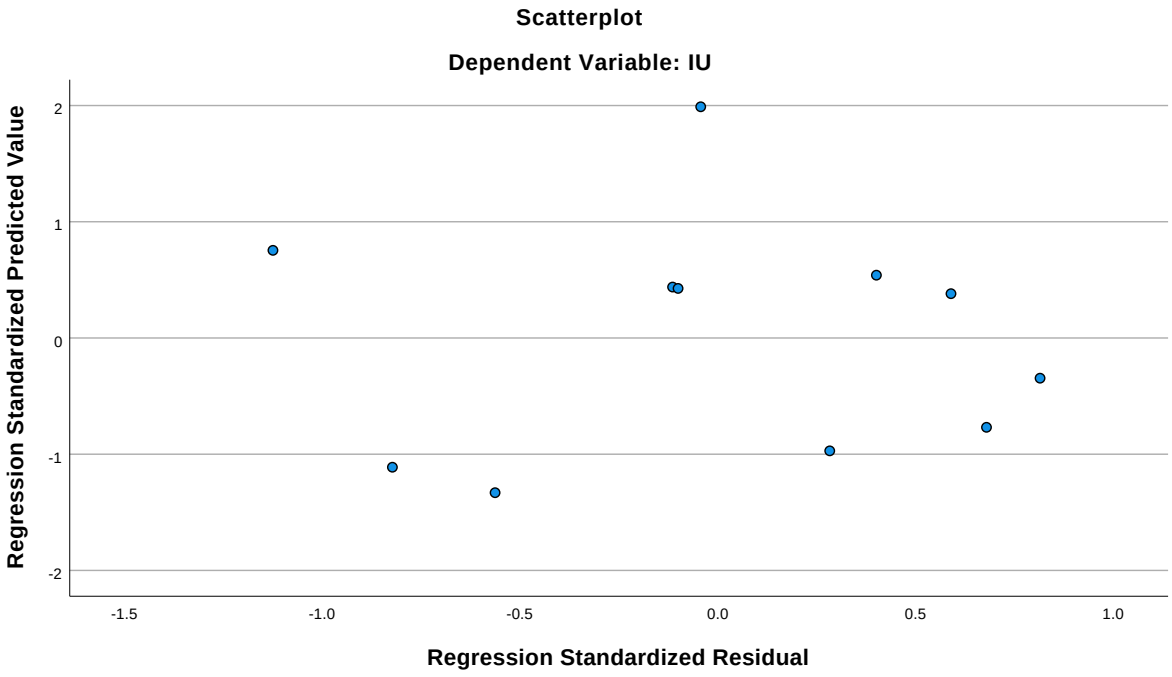

Regression: Perceived Usefulness

Variables Entered/Removed[a]

Model	Variables Entered	Variables Removed	Method
1	QuestionnaireTime, FirstTime, TutorialTime, FirstAngle, SecondTime, SecondAngle[b]	.	Enter

a. Dependent Variable: PU

b. All requested variables entered.

Model Summary[b]

Model	R	R Square	Adjusted R Square	Std. Error of the Estimate
1	.845[a]	.713	.283	.42379

a. Predictors: (Constant), QuestionnaireTime, FirstTime, TutorialTime, FirstAngle, SecondTime, SecondAngle

b. Dependent Variable: PU

ANOVA[a]

Model		Sum of Squares	df	Mean Square	F	Sig.
1	Regression	1.787	6	.298	1.658	.325[b]
	Residual	.718	4	.180		
	Total	2.505	10			

a. Dependent Variable: PU

b. Predictors: (Constant), QuestionnaireTime, FirstTime, TutorialTime, FirstAngle, SecondTime, SecondAngle

Coefficients[a]

Model		Unstandardized Coefficients		Standardized Coefficients		
		B	Std. Error	Beta	t	Sig.
1	(Constant)	3.873	3.001		1.291	.266
	TutorialTime	.002	.002	.444	1.184	.302
	FirstTime	-.002	.001	-.375	-1.088	.338
	FirstAngle	.007	.032	.209	.218	.838
	SecondTime	.004	.003	.863	1.367	.243
	SecondAngle	-.031	.028	-1.052	-1.121	.325
	QuestionnaireTime	.009	.007	.862	1.321	.257

a. Dependent Variable: PU

Residuals Statistics[a]

	Minimum	Maximum	Mean	Std. Deviation	N
Predicted Value	5.3252	6.5996	5.8788	.42269	11
Residual	-.42353	.47650	.00000	.26803	11
Std. Predicted Value	-1.310	1.705	.000	1.000	11
Std. Residual	-.999	1.124	.000	.632	11

a. Dependent Variable: PU

Charts

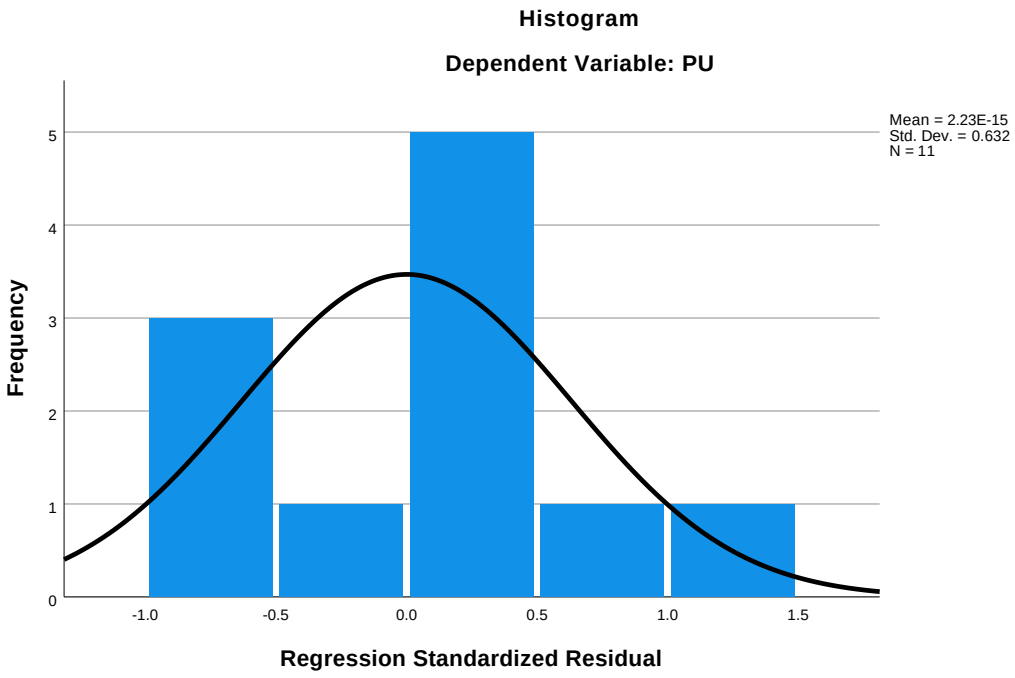

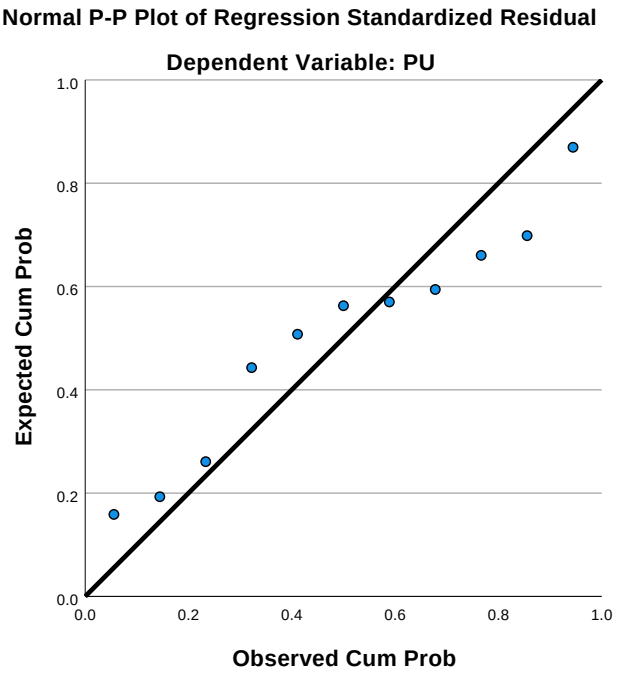

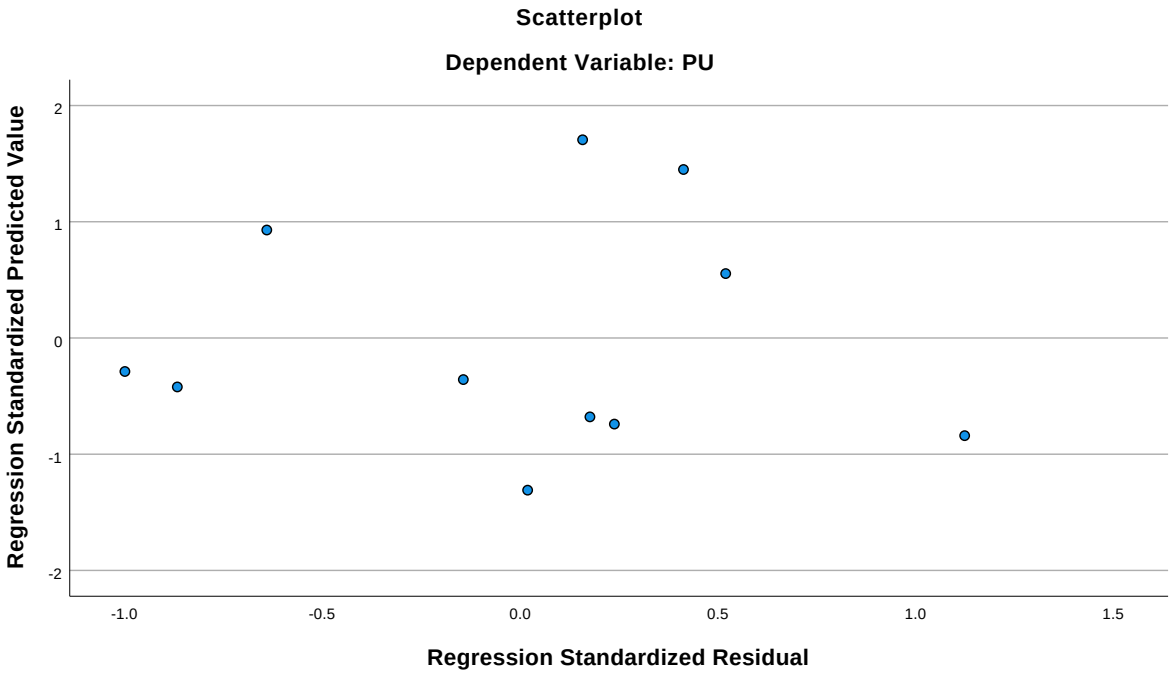

Regression: Perceived Ease of Use

Variables Entered/Removed[a]

Model	Variables Entered	Variables Removed	Method
1	QuestionnaireTime, FirstTime, TutorialTime, FirstAngle, SecondTime, SecondAngle[b]	.	Enter

a. Dependent Variable: EOU

b. All requested variables entered.

Model Summary[b]

Model	R	R Square	Adjusted R Square	Std. Error of the Estimate
1	.902[a]	.814	.535	.83272

a. Predictors: (Constant), QuestionnaireTime, FirstTime, TutorialTime, FirstAngle, SecondTime, SecondAngle

b. Dependent Variable: EOU

ANOVA[a]

Model		Sum of Squares	df	Mean Square	F	Sig.
1	Regression	12.147	6	2.024	2.920	.160[b]
	Residual	2.774	4	.693		
	Total	14.920	10			

a. Dependent Variable: EOU

b. Predictors: (Constant), QuestionnaireTime, FirstTime, TutorialTime, FirstAngle, SecondTime, SecondAngle

Coefficients[a]

Model		Unstandardized Coefficients		Standardized Coefficients		
		B	Std. Error	Beta	t	Sig.
1	(Constant)	.696	5.896		.118	.912
	TutorialTime	-.005	.004	-.354	-1.174	.306
	FirstTime	-.003	.003	-.300	-1.079	.341
	FirstAngle	-.007	.062	-.089	-.115	.914
	SecondTime	.010	.005	.982	1.932	.126
	SecondAngle	-.020	.054	-.273	-.361	.736
	QuestionnaireTime	.020	.013	.777	1.478	.213

a. Dependent Variable: EOU

Residuals Statistics[a]

	Minimum	Maximum	Mean	Std. Deviation	N
Predicted Value	1.8038	5.5477	3.8864	1.10212	11
Residual	-.91134	.66397	.00000	.52666	11
Std. Predicted Value	-1.890	1.507	.000	1.000	11
Std. Residual	-1.094	.797	.000	.632	11

a. Dependent Variable: EOU

Charts

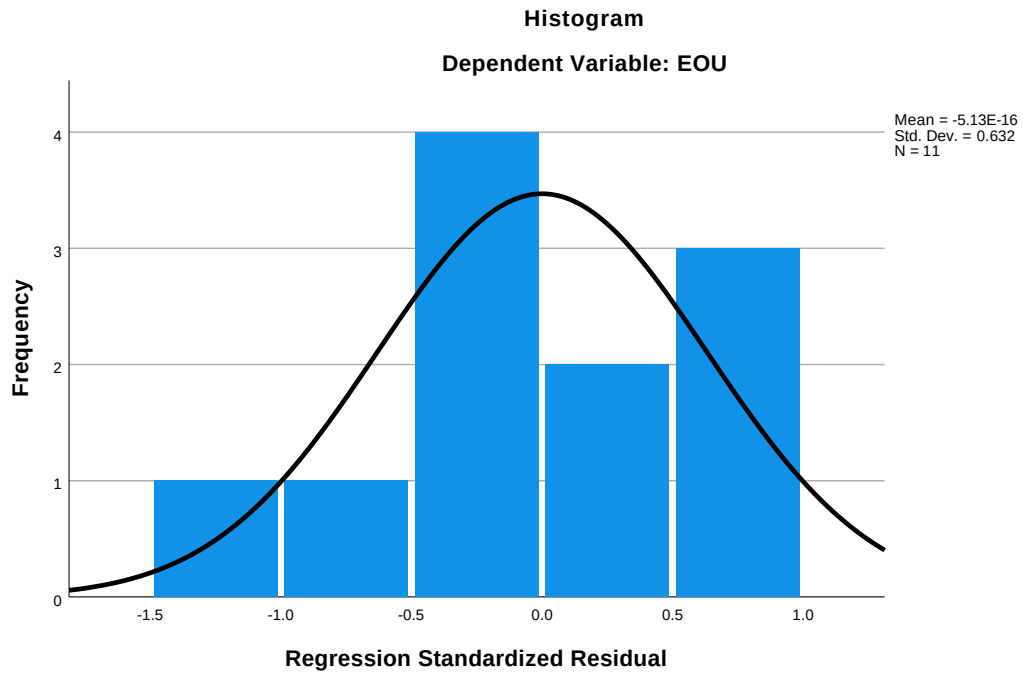

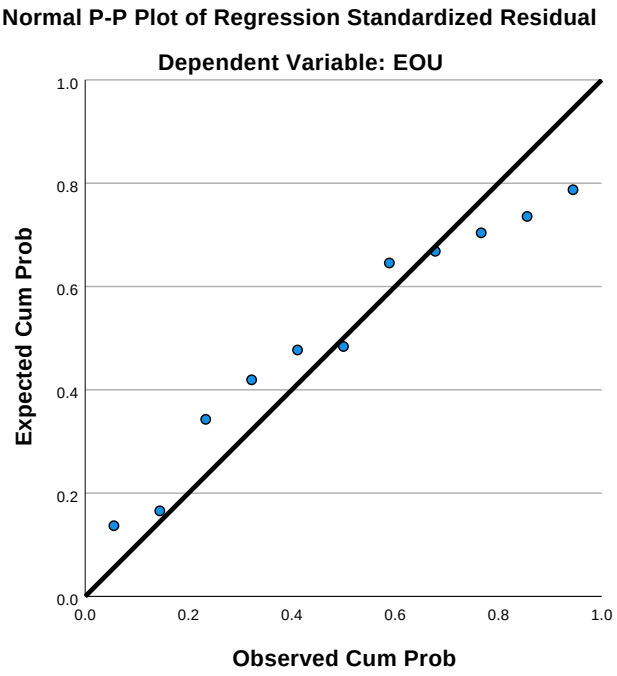

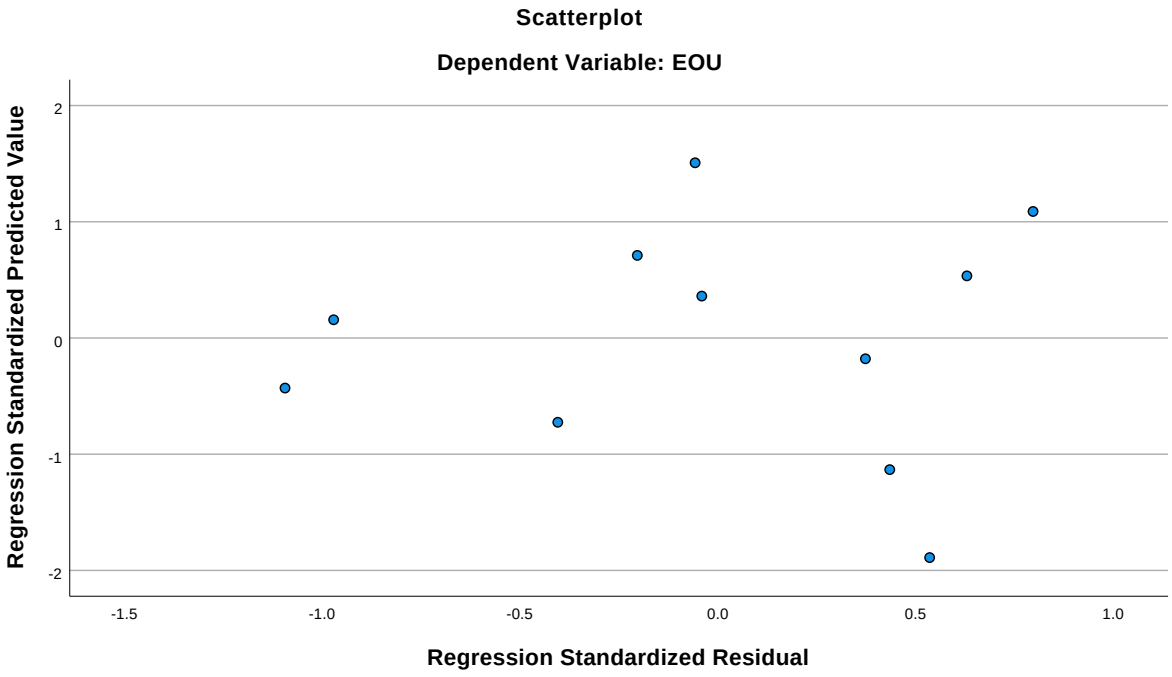

Regression: Perceived Learning

Variables Entered/Removed[a]

Model	Variables Entered	Variables Removed	Method
1	QuestionnaireTime, FirstTime, TutorialTime, FirstAngle, SecondTime, SecondAngle[b]	.	Enter

a. Dependent Variable: PL

b. All requested variables entered.

Model Summary[b]

Model	R	R Square	Adjusted R Square	Std. Error of the Estimate
1	.761[a]	.580	-.050	.85690

a. Predictors: (Constant), QuestionnaireTime, FirstTime, TutorialTime, FirstAngle, SecondTime, SecondAngle

b. Dependent Variable: PL

ANOVA[a]

Model		Sum of Squares	df	Mean Square	F	Sig.
1	Regression	4.053	6	.675	.920	.559[b]
	Residual	2.937	4	.734		
	Total	6.990	10			

a. Dependent Variable: PL

b. Predictors: (Constant), QuestionnaireTime, FirstTime, TutorialTime, FirstAngle, SecondTime, SecondAngle

Coefficients[a]

Model		Unstandardized Coefficients		Standardized Coefficients		
		B	Std. Error	Beta	t	Sig.
1	(Constant)	-.470	6.067		-.077	.942
	TutorialTime	.001	.004	.071	.157	.883
	FirstTime	.003	.003	.486	1.163	.310
	FirstAngle	-.057	.064	-1.028	-.887	.425
	SecondTime	.004	.006	.532	.697	.524
	SecondAngle	.039	.056	.800	.704	.520
	QuestionnaireTime	.011	.014	.657	.831	.453

a. Dependent Variable: PL

Residuals Statistics[a]

	Minimum	Maximum	Mean	Std. Deviation	N
Predicted Value	3.2702	5.2337	4.0303	.63662	11
Residual	-.93686	.82870	.00000	.54195	11
Std. Predicted Value	-1.194	1.890	.000	1.000	11
Std. Residual	-1.093	.967	.000	.632	11

a. Dependent Variable: PL

Charts

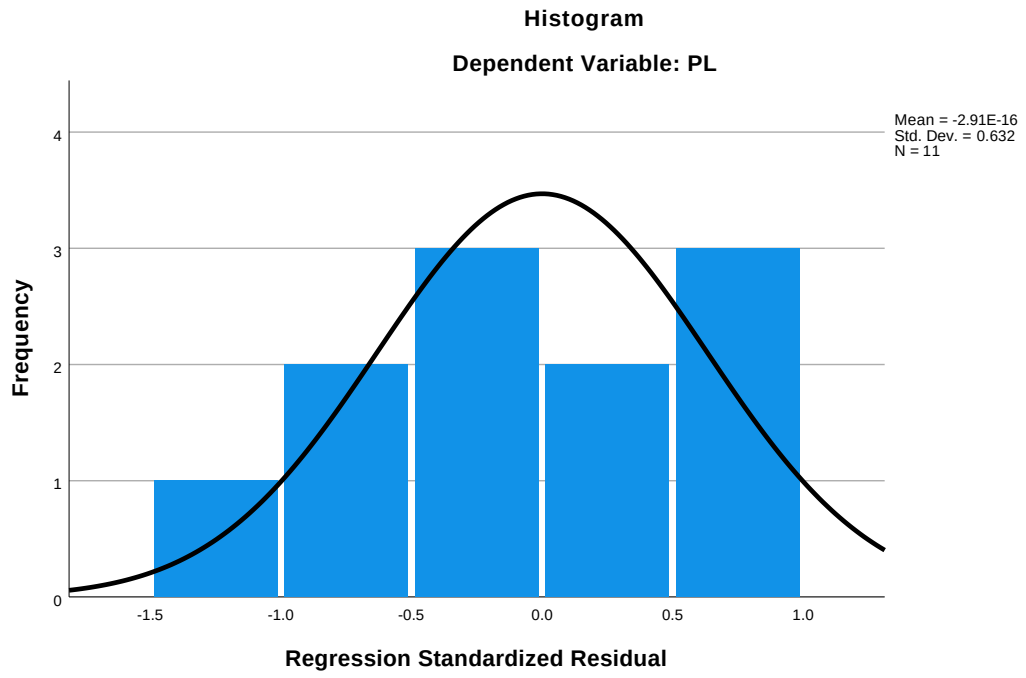

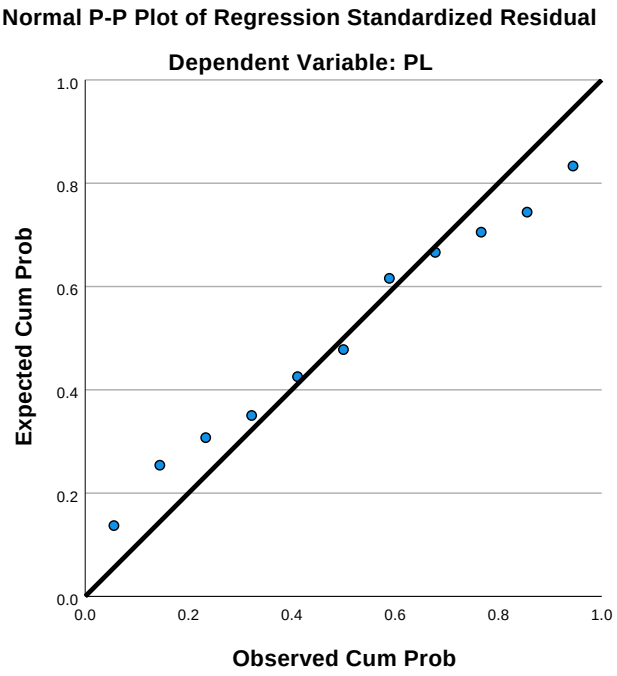

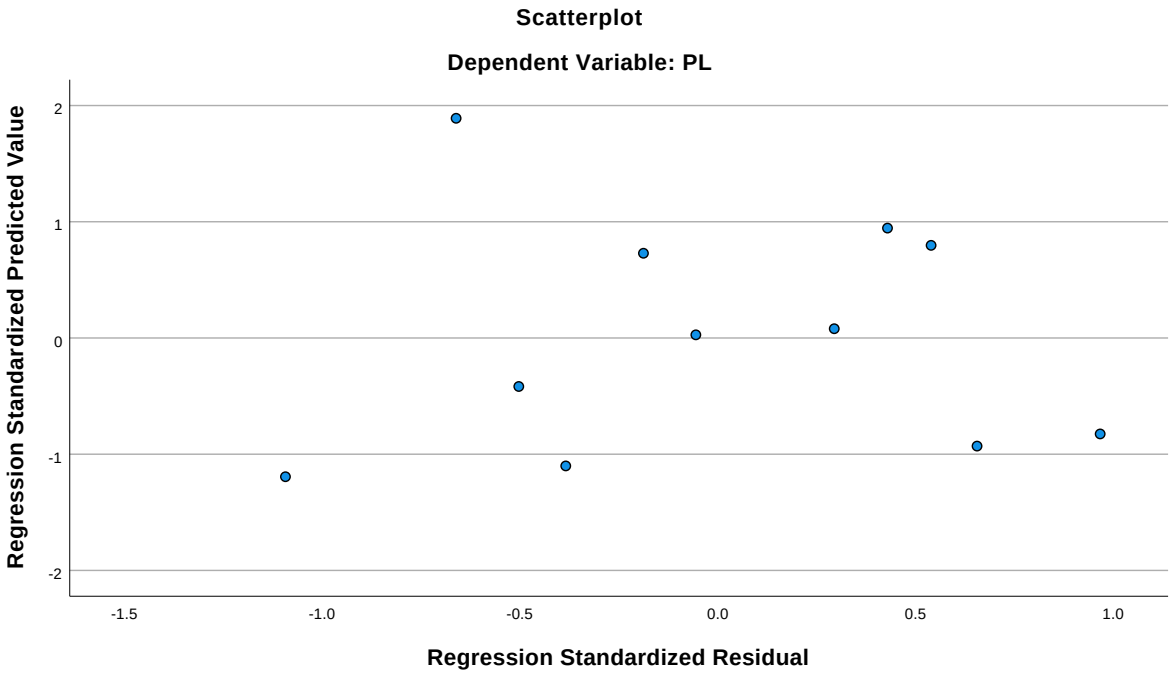

Regression: Technical Understanding

Variables Entered/Removed[a]

Model	Variables Entered	Variables Removed	Method
1	QuestionnaireTime, FirstTime, TutorialTime, FirstAngle, SecondTime, SecondAngle[b]	.	Enter

a. Dependent Variable: TU

b. All requested variables entered.

Model Summary[b]

Model	R	R Square	Adjusted R Square	Std. Error of the Estimate
1	.807[a]	.651	.128	1.03224

a. Predictors: (Constant), QuestionnaireTime, FirstTime, TutorialTime, FirstAngle, SecondTime, SecondAngle

b. Dependent Variable: TU

ANOVA[a]

Model		Sum of Squares	df	Mean Square	F	Sig.
1	Regression	7.960	6	1.327	1.245	.435[b]
	Residual	4.262	4	1.066		
	Total	12.222	10			

a. Dependent Variable: TU

b. Predictors: (Constant), QuestionnaireTime, FirstTime, TutorialTime, FirstAngle, SecondTime, SecondAngle

Coefficients[a]

Model		Unstandardized Coefficients		Standardized Coefficients		
		B	Std. Error	Beta	t	Sig.
1	(Constant)	-6.618	7.309		-.905	.416
	TutorialTime	.005	.005	.434	1.050	.353
	FirstTime	-.003	.003	-.323	-.848	.444
	FirstAngle	.083	.077	1.147	1.086	.339
	SecondTime	.013	.007	1.319	1.895	.131
	SecondAngle	-.103	.067	-1.597	-1.543	.198
	QuestionnaireTime	.037	.017	1.622	2.253	.087

a. Dependent Variable: TU

Residuals Statistics[a]

	Minimum	Maximum	Mean	Std. Deviation	N
Predicted Value	2.9124	5.8694	4.6667	.89220	11
Residual	-1.20278	.90623	.00000	.65284	11
Std. Predicted Value	-1.966	1.348	.000	1.000	11
Std. Residual	-1.165	.878	.000	.632	11

a. Dependent Variable: TU

Charts

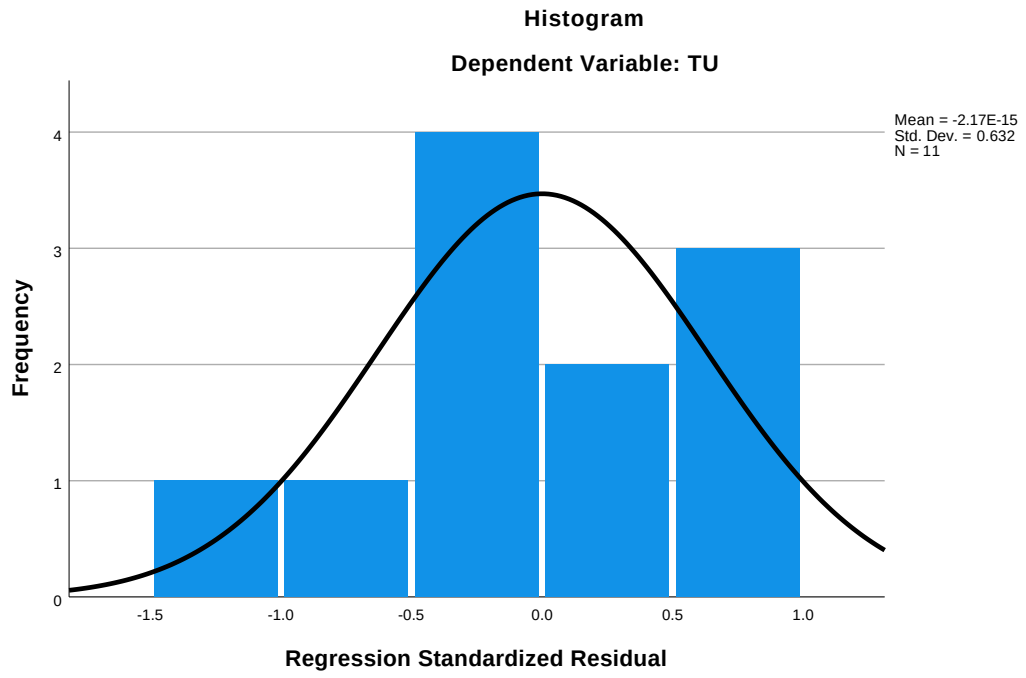

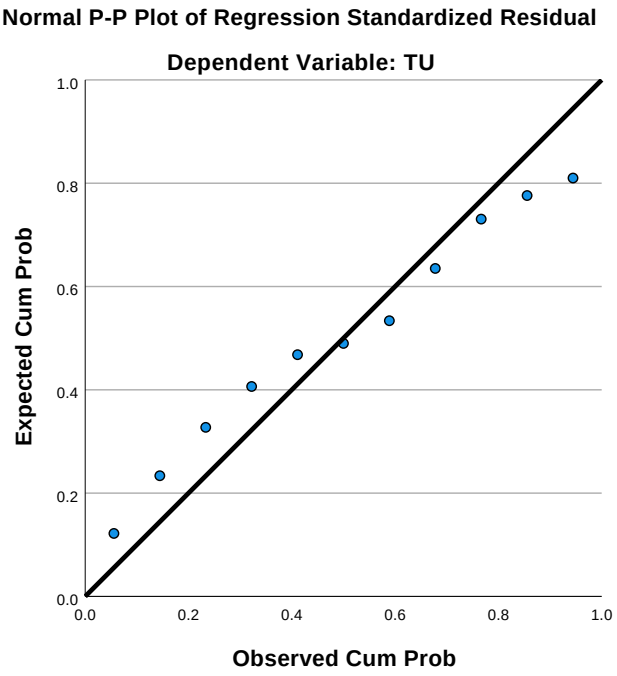

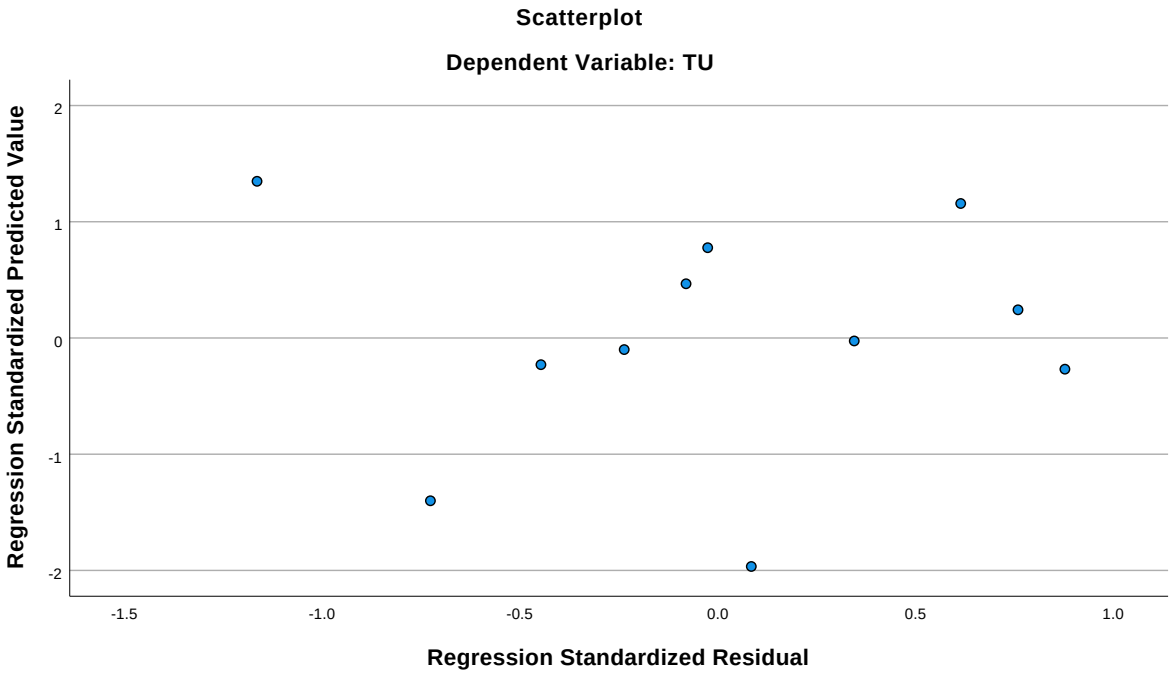

Regression: Signal ASQ

Variables Entered/Removed[a]

Model	Variables Entered	Variables Removed	Method
1	QuestionnaireTime, FirstTime, TutorialTime, FirstAngle, SecondTime, SecondAngle[b]	.	Enter

a. Dependent Variable: Signal_ASQ

b. All requested variables entered.

Model Summary[b]

Model	R	R Square	Adjusted R Square	Std. Error of the Estimate
1	.816[a]	.665	.163	1.11199

a. Predictors: (Constant), QuestionnaireTime, FirstTime, TutorialTime, FirstAngle, SecondTime, SecondAngle

b. Dependent Variable: Signal_ASQ

ANOVA[a]

Model		Sum of Squares	df	Mean Square	F	Sig.
1	Regression	9.822	6	1.637	1.324	.410[b]
	Residual	4.946	4	1.237		
	Total	14.768	10			

a. Dependent Variable: Signal_ASQ

b. Predictors: (Constant), QuestionnaireTime, FirstTime, TutorialTime, FirstAngle, SecondTime, SecondAngle

Coefficients[a]

Model		Unstandardized Coefficients		Standardized Coefficients		
		B	Std. Error	Beta	t	Sig.
1	(Constant)	-7.626	7.874		-.969	.388
	TutorialTime	.001	.005	.072	.177	.868
	FirstTime	.000	.004	.010	.028	.979
	FirstAngle	.058	.083	.722	.697	.524
	SecondTime	.015	.007	1.389	2.036	.111
	SecondAngle	-.051	.072	-.720	-.710	.517
	QuestionnaireTime	.037	.018	1.453	2.059	.109

a. Dependent Variable: Signal_ASQ

Residuals Statistics[a]

	Minimum	Maximum	Mean	Std. Deviation	N
Predicted Value	3.3875	6.2471	4.9697	.99104	11
Residual	-1.17619	.82624	.00000	.70328	11
Std. Predicted Value	-1.597	1.289	.000	1.000	11
Std. Residual	-1.058	.743	.000	.632	11

a. Dependent Variable: Signal_ASQ

Charts

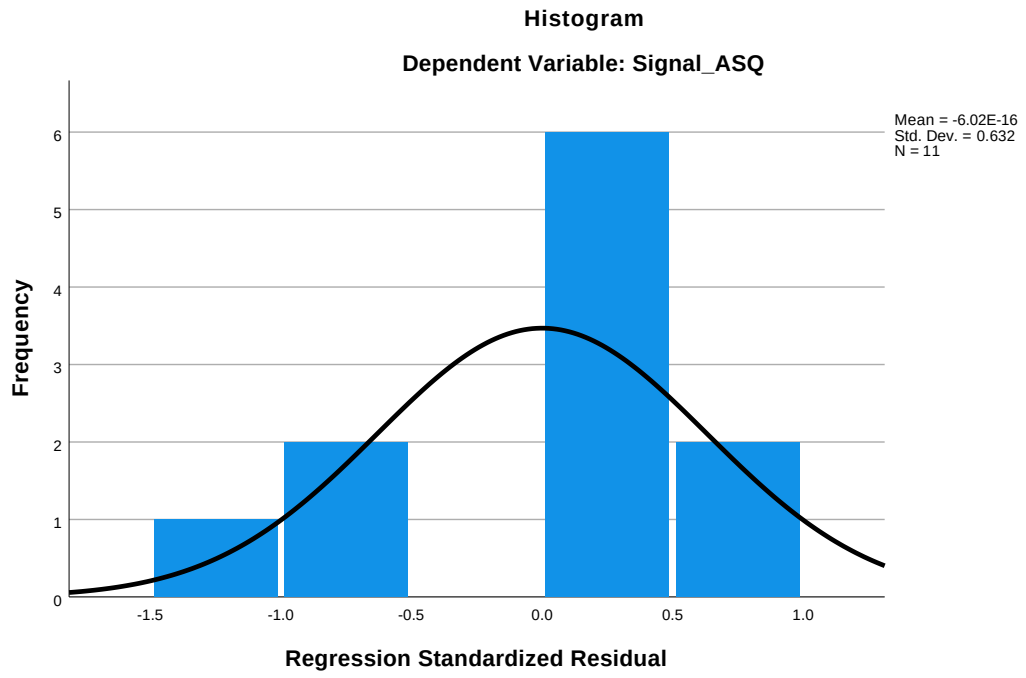

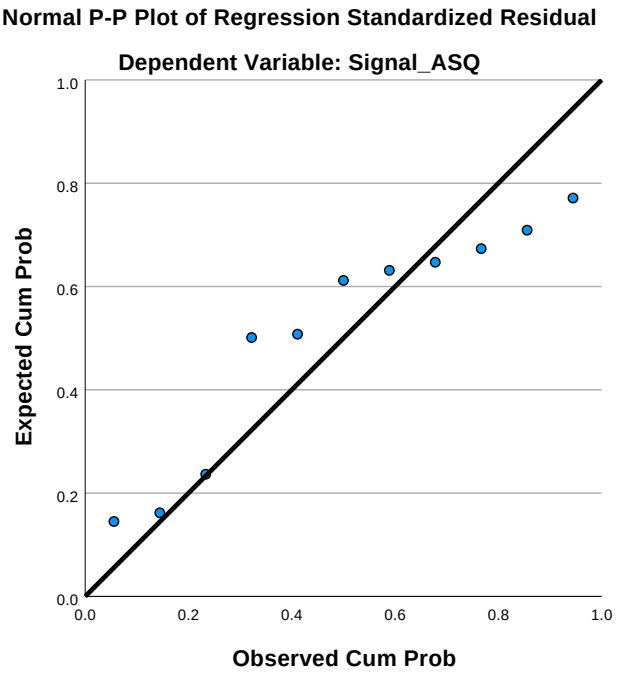

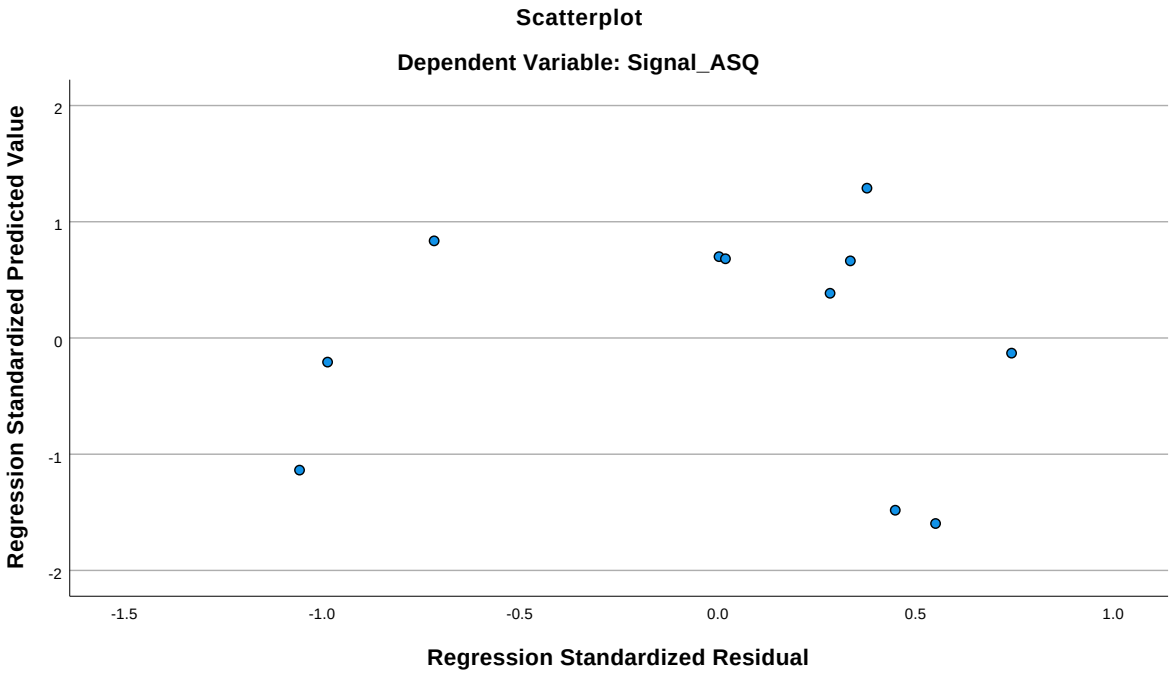

Regression: Angle ASQ

Variables Entered/Removed[a]

Model	Variables Entered	Variables Removed	Method
1	QuestionnaireTime, FirstTime, TutorialTime, FirstAngle, SecondTime, SecondAngle[b]	.	Enter

a. Dependent Variable: Angle_ASQ

b. All requested variables entered.

Model Summary[b]

Model	R	R Square	Adjusted R Square	Std. Error of the Estimate
1	.897[a]	.805	.513	1.03486

a. Predictors: (Constant), QuestionnaireTime, FirstTime, TutorialTime, FirstAngle, SecondTime, SecondAngle

b. Dependent Variable: Angle_ASQ

ANOVA[a]

Model		Sum of Squares	df	Mean Square	F	Sig.
1	Regression	17.716	6	2.953	2.757	.173[b]
	Residual	4.284	4	1.071		
	Total	22.000	10			

a. Dependent Variable: Angle_ASQ

b. Predictors: (Constant), QuestionnaireTime, FirstTime, TutorialTime, FirstAngle, SecondTime, SecondAngle

Coefficients[a]

Model		Unstandardized Coefficients		Standardized Coefficients		
		B	Std. Error	Beta	t	Sig.
1	(Constant)	9.376	7.328		1.280	.270
	TutorialTime	-.005	.005	-.289	-.937	.402
	FirstTime	-.011	.004	-.871	-3.062	.038
	FirstAngle	-.075	.077	-.766	-.971	.387
	SecondTime	.004	.007	.284	.546	.614
	SecondAngle	.027	.067	.308	.398	.711
	QuestionnaireTime	.006	.017	.205	.381	.723

a. Dependent Variable: Angle_ASQ

Residuals Statistics[a]

	Minimum	Maximum	Mean	Std. Deviation	N
Predicted Value	1.8407	5.9342	4.3333	1.33103	11
Residual	-1.03820	.97450	.00000	.65450	11
Std. Predicted Value	-1.873	1.203	.000	1.000	11
Std. Residual	-1.003	.942	.000	.632	11

a. Dependent Variable: Angle_ASQ

Charts

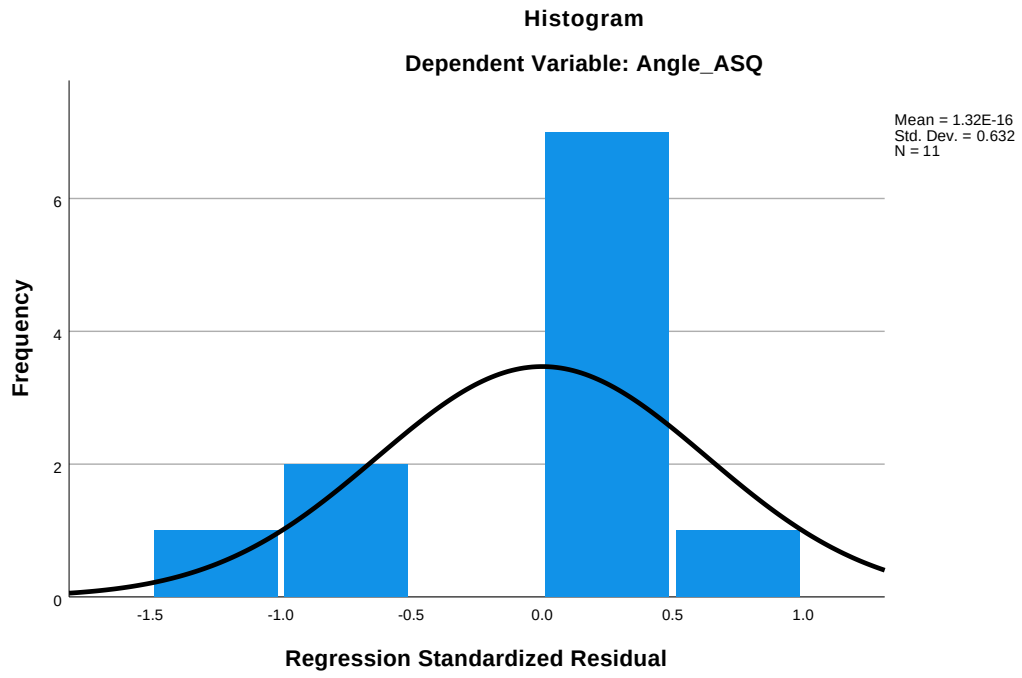

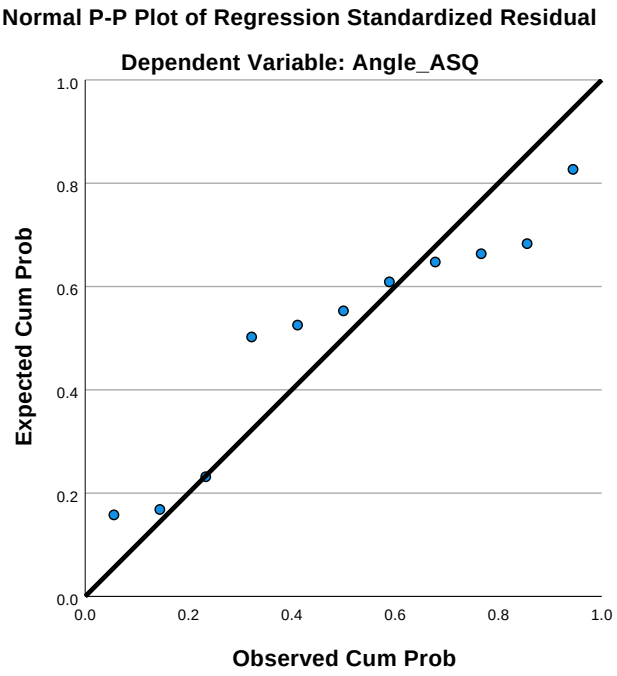

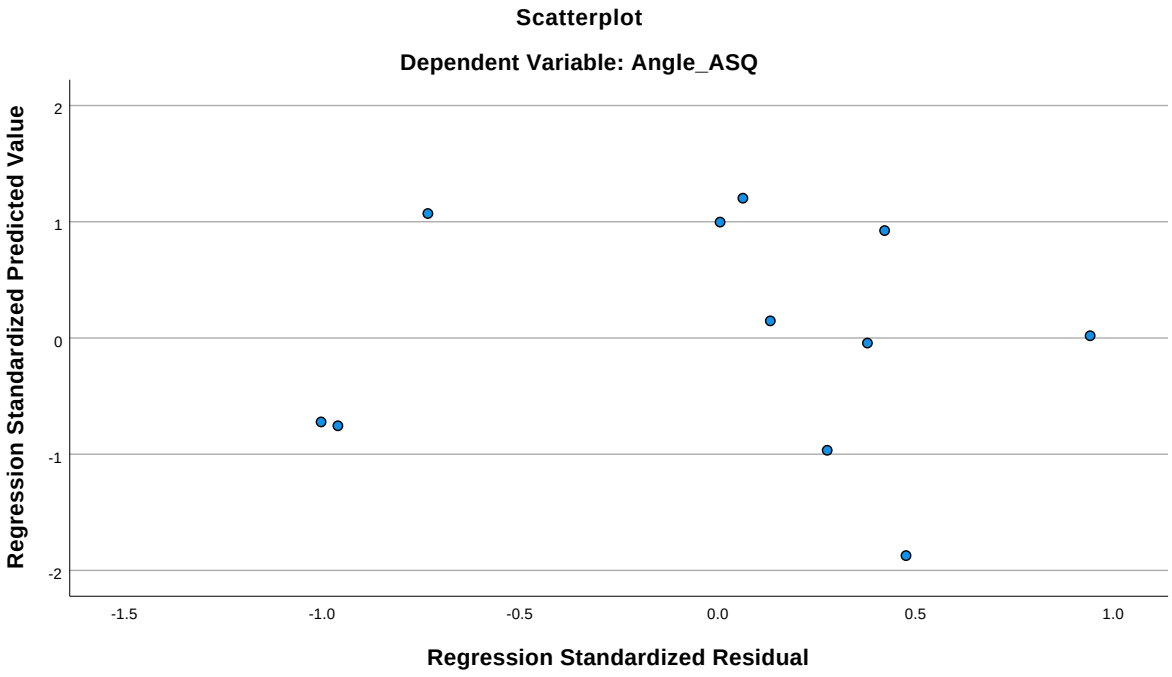

Regression: PRF ASQ

Variables Entered/Removed[a]

Model	Variables Entered	Variables Removed	Method
1	QuestionnaireTime, FirstTime, TutorialTime, FirstAngle, SecondTime, SecondAngle[b]	.	Enter

a. Dependent Variable: PRF_ASQ

b. All requested variables entered.

Model Summary[b]

Model	R	R Square	Adjusted R Square	Std. Error of the Estimate
1	.641[a]	.410	-.474	1.85696

a. Predictors: (Constant), QuestionnaireTime, FirstTime, TutorialTime, FirstAngle, SecondTime, SecondAngle

b. Dependent Variable: PRF_ASQ

ANOVA[a]

Model		Sum of Squares	df	Mean Square	F	Sig.
1	Regression	9.601	6	1.600	.464	.809[b]
	Residual	13.793	4	3.448		
	Total	23.394	10			

a. Dependent Variable: PRF_ASQ

b. Predictors: (Constant), QuestionnaireTime, FirstTime, TutorialTime, FirstAngle, SecondTime, SecondAngle

Coefficients[a]

Model		Unstandardized Coefficients		Standardized Coefficients		
		B	Std. Error	Beta	t	Sig.
1	(Constant)	-13.644	13.149		-1.038	.358
	TutorialTime	.011	.009	.665	1.237	.284
	FirstTime	.004	.006	.321	.648	.552
	FirstAngle	.079	.138	.783	.570	.599
	SecondTime	.018	.012	1.363	1.505	.207
	SecondAngle	-.043	.121	-.477	-.354	.741
	QuestionnaireTime	.035	.030	1.115	1.191	.299

a. Dependent Variable: PRF_ASQ

Residuals Statistics[a]

	Minimum	Maximum	Mean	Std. Deviation	N
Predicted Value	3.3452	6.4029	4.8788	.97983	11
Residual	-1.67855	1.97474	.00000	1.17444	11
Std. Predicted Value	-1.565	1.556	.000	1.000	11
Std. Residual	-.904	1.063	.000	.632	11

a. Dependent Variable: PRF_ASQ

Charts

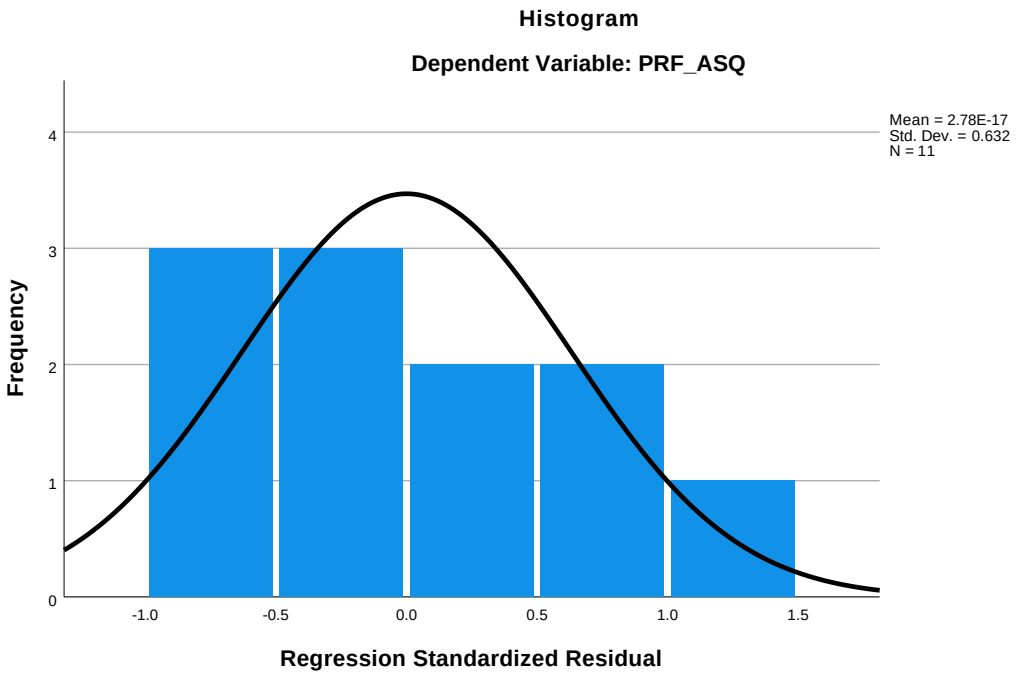

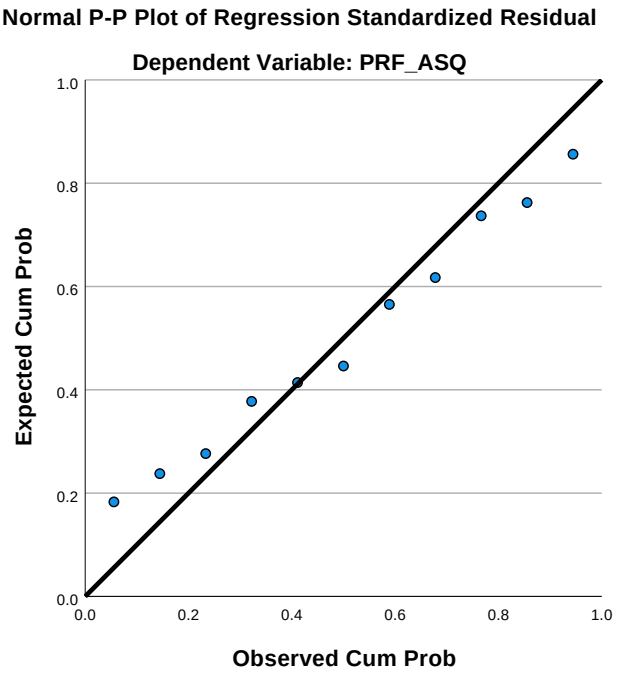

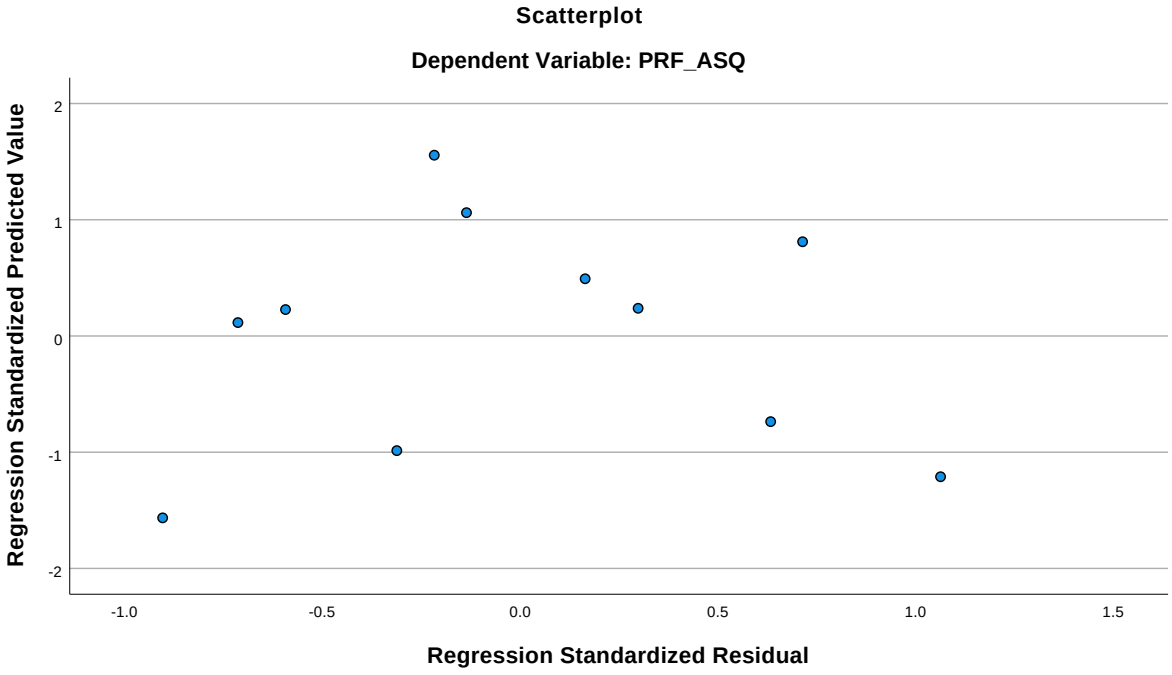

Regression: Angle ASQ determined by time spent on first attempt

Variables Entered/Removed[a]

Model	Variables Entered	Variables Removed	Method
1	FirstTime[b]	.	Enter

a. Dependent Variable: Angle_ASQ

b. All requested variables entered.

Model Summary[b]

Model	R	R Square	Adjusted R Square	Std. Error of the Estimate
1	.668[a]	.447	.400	1.12097

a. Predictors: (Constant), FirstTime

b. Dependent Variable: Angle_ASQ

ANOVA[a]

Model		Sum of Squares	df	Mean Square	F	Sig.
1	Regression	12.167	1	12.167	9.683	.009[b]
	Residual	15.079	12	1.257		
	Total	27.246	13			

a. Dependent Variable: Angle_ASQ

b. Predictors: (Constant), FirstTime

Coefficients[a]

Model		Unstandardized Coefficients		Standardized Coefficients		
		B	Std. Error	Beta	t	Sig.
1	(Constant)	7.346	.948		7.751	.000
	FirstTime	-.008	.003	-.668	-3.112	.009

a. Dependent Variable: Angle_ASQ

Residuals Statistics[a]

	Minimum	Maximum	Mean	Std. Deviation	N
Predicted Value	2.5876	5.4588	4.5476	.96744	14
Residual	-2.22307	1.89477	.00000	1.07699	14
Std. Predicted Value	-2.026	.942	.000	1.000	14
Std. Residual	-1.983	1.690	.000	.961	14

a. Dependent Variable: Angle_ASQ

Charts

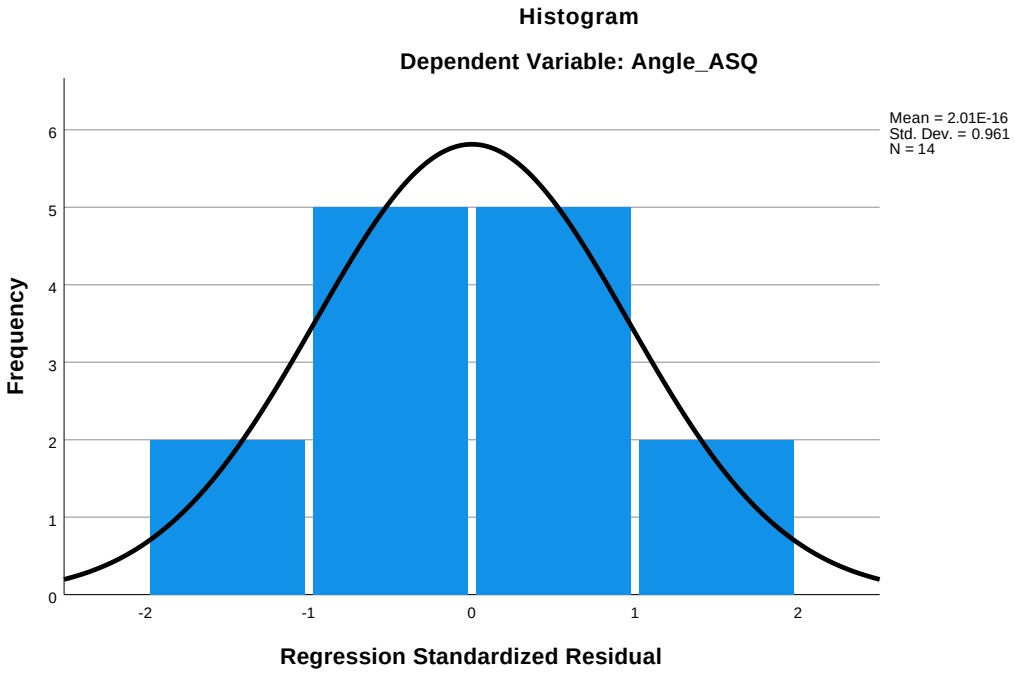

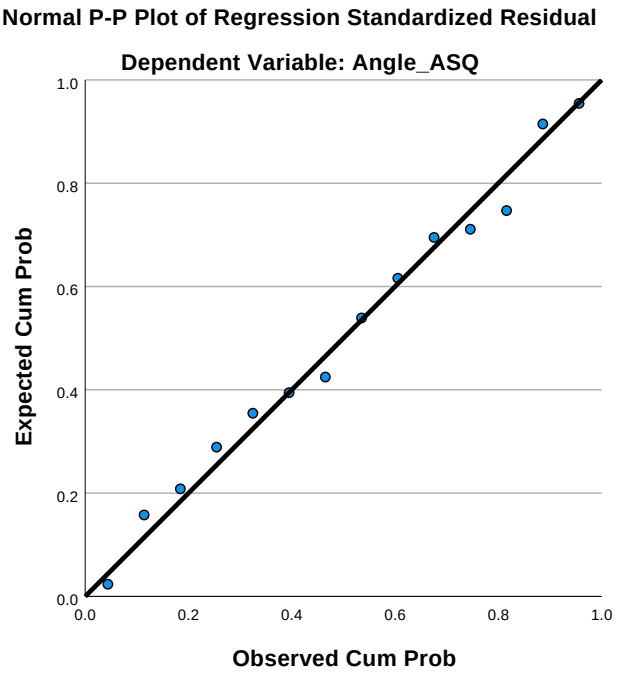

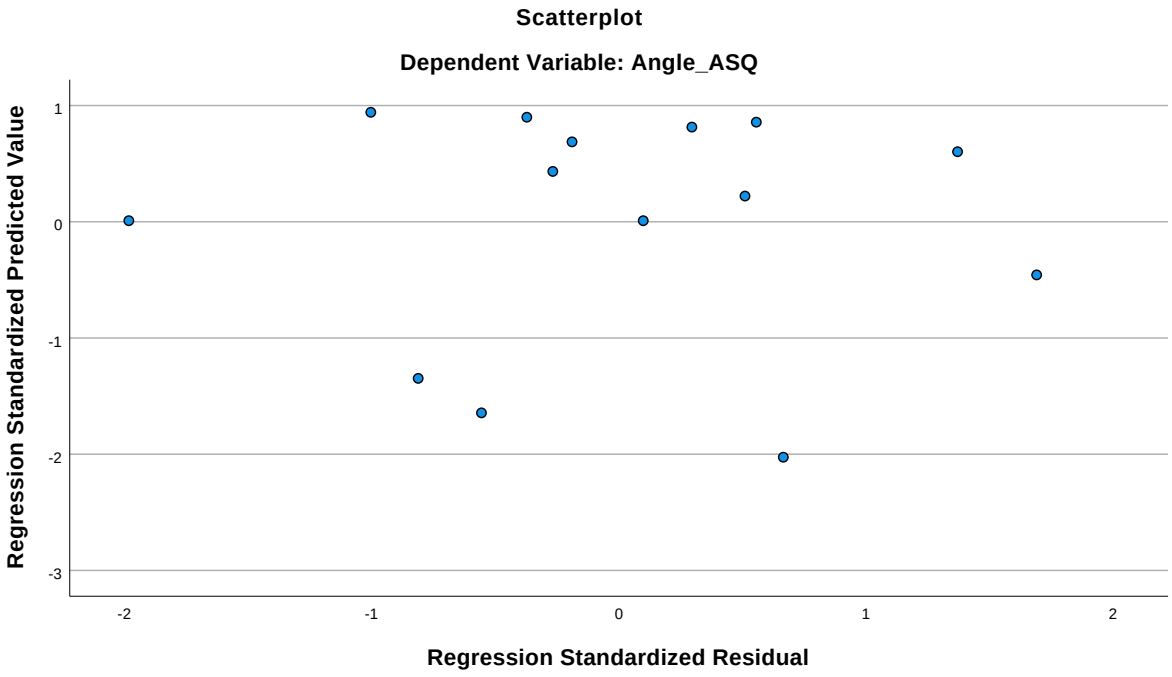

Regression: Second time

Variables Entered/Removed[a]

Model	Variables Entered	Variables Removed	Method
1	QuestionnaireTime, FirstTime, TutorialTime, FirstAngle, SecondAngle[b]	.	Enter

a. Dependent Variable: SecondTime

b. All requested variables entered.

Model Summary[b]

Model	R	R Square	Adjusted R Square	Std. Error of the Estimate
1	.906[a]	.820	.640	68.99810

a. Predictors: (Constant), QuestionnaireTime, FirstTime, TutorialTime, FirstAngle, SecondAngle

b. Dependent Variable: SecondTime

ANOVA[a]

Model		Sum of Squares	df	Mean Square	F	Sig.
1	Regression	108509.948	5	21701.990	4.559	.061[b]
	Residual	23803.688	5	4760.738		
	Total	132313.636	10			

a. Dependent Variable: SecondTime

b. Predictors: (Constant), QuestionnaireTime, FirstTime, TutorialTime, FirstAngle, SecondAngle

Coefficients[a]

Model		Unstandardized Coefficients		Standardized Coefficients		
		B	Std. Error	Beta	t	Sig.
1	(Constant)	985.779	210.561		4.682	.005
	TutorialTime	-.461	.249	-.379	-1.851	.123
	FirstTime	-.151	.224	-.158	-.677	.529
	FirstAngle	-6.387	4.264	-.845	-1.498	.194
	SecondAngle	4.973	3.891	.738	1.278	.257
	QuestionnaireTime	-2.187	.511	-.917	-4.285	.008

a. Dependent Variable: SecondTime

Residuals Statistics[a]

	Minimum	Maximum	Mean	Std. Deviation	N
Predicted Value	23.5433	401.9555	146.8182	104.16811	11
Residual	-81.84177	66.45670	.00000	48.78902	11
Std. Predicted Value	-1.183	2.449	.000	1.000	11
Std. Residual	-1.186	.963	.000	.707	11

a. Dependent Variable: SecondTime

Charts

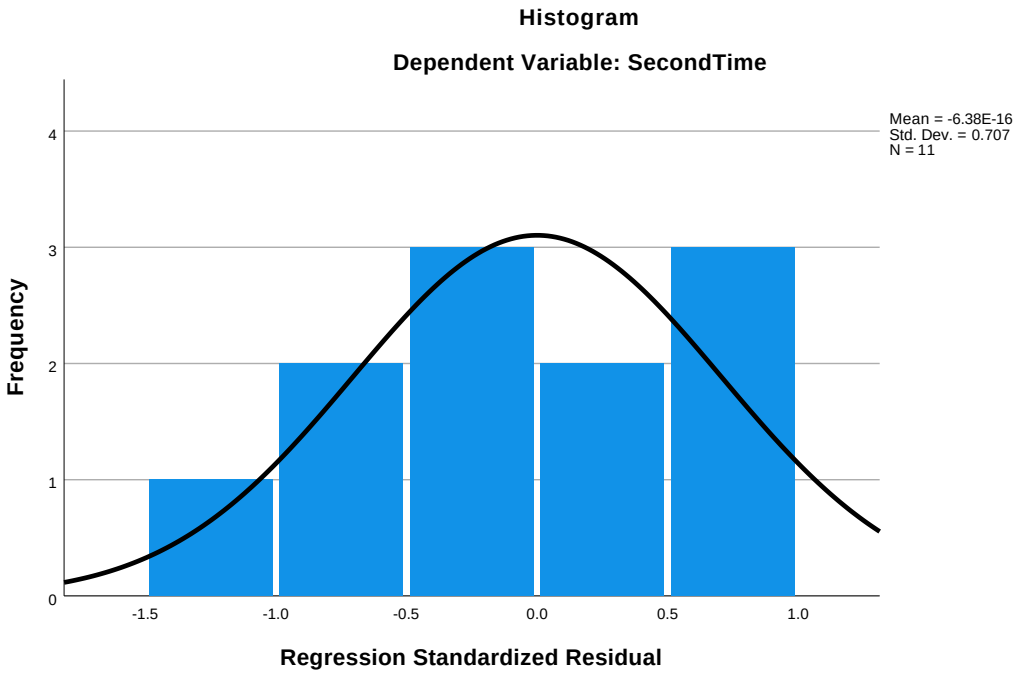

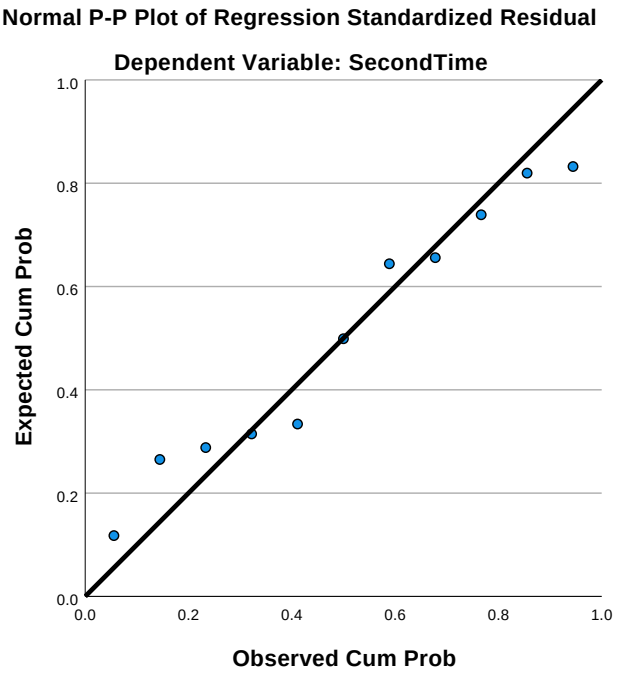

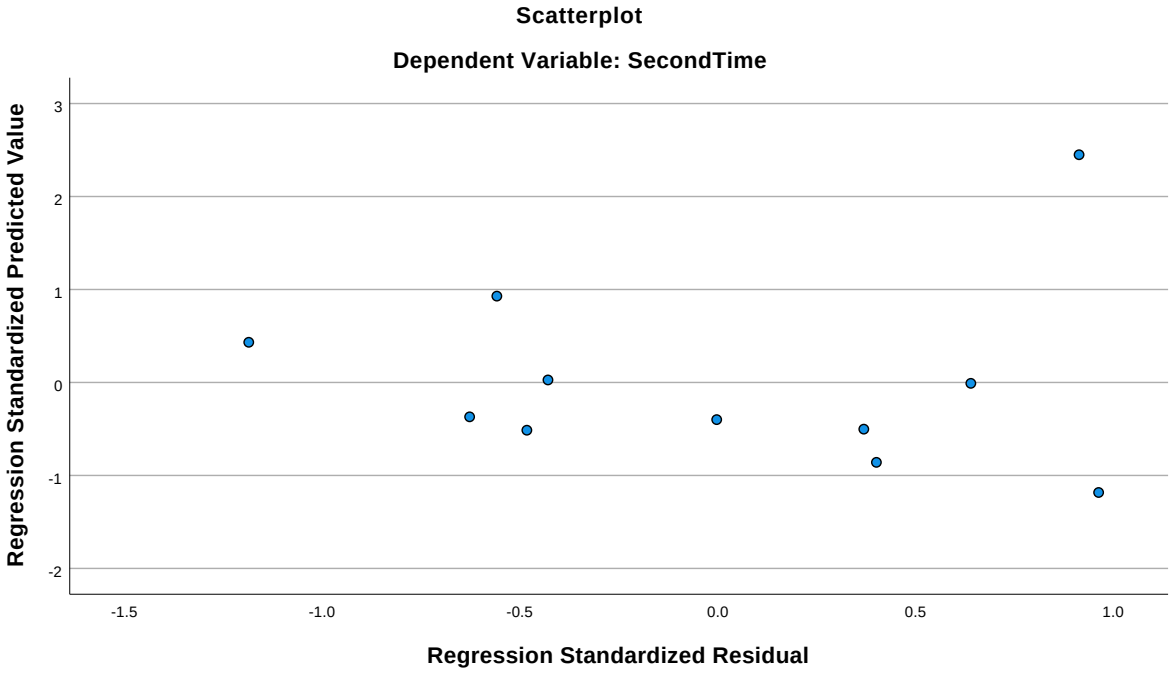

Regression: Questionnairetime

Variables Entered/Removed[a]

Model	Variables Entered	Variables Removed	Method
1	SecondTime, FirstTime, TutorialTime, SecondAngle, FirstAngle[b]	.	Enter

a. Dependent Variable: QuestionnaireTime

b. All requested variables entered.

Model Summary[b]

Model	R	R Square	Adjusted R Square	Std. Error of the Estimate
1	.912[a]	.832	.664	27.96453

a. Predictors: (Constant), SecondTime, FirstTime, TutorialTime, SecondAngle, FirstAngle

b. Dependent Variable: QuestionnaireTime

ANOVA[a]

Model		Sum of Squares	df	Mean Square	F	Sig.
1	Regression	19344.469	5	3868.894	4.947	.052[b]
	Residual	3910.076	5	782.015		
	Total	23254.545	10			

a. Dependent Variable: QuestionnaireTime

b. Predictors: (Constant), SecondTime, FirstTime, TutorialTime, SecondAngle, FirstAngle

Coefficients[a]

Model		Unstandardized Coefficients		Standardized Coefficients		
		B	Std. Error	Beta	t	Sig.
1	(Constant)	408.246	76.647		5.326	.003
	TutorialTime	-.194	.098	-.380	-1.973	.105
	FirstTime	-.047	.092	-.117	-.506	.634
	FirstAngle	-2.378	1.788	-.750	-1.330	.241
	SecondAngle	2.086	1.558	.738	1.339	.238
	SecondTime	-.359	.084	-.857	-4.285	.008

a. Dependent Variable: QuestionnaireTime

Residuals Statistics[a]

	Minimum	Maximum	Mean	Std. Deviation	N
Predicted Value	165.1927	324.8791	273.6364	43.98235	11
Residual	-30.79641	36.41802	.00000	19.77391	11
Std. Predicted Value	-2.466	1.165	.000	1.000	11
Std. Residual	-1.101	1.302	.000	.707	11

a. Dependent Variable: QuestionnaireTime

Charts

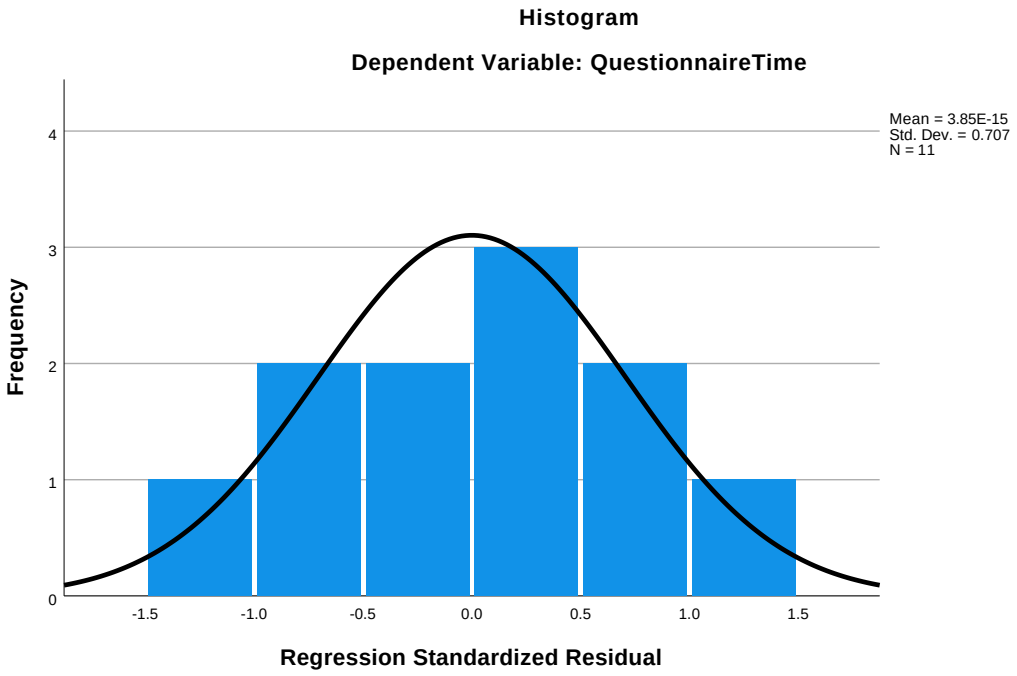

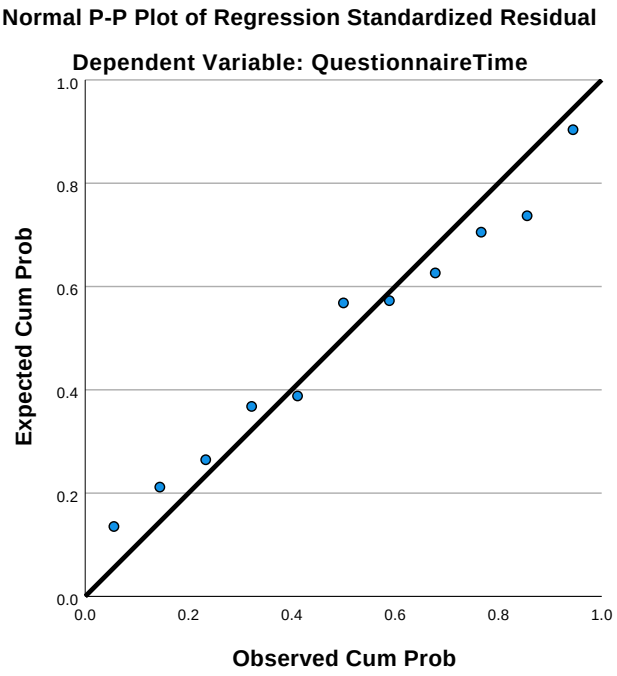

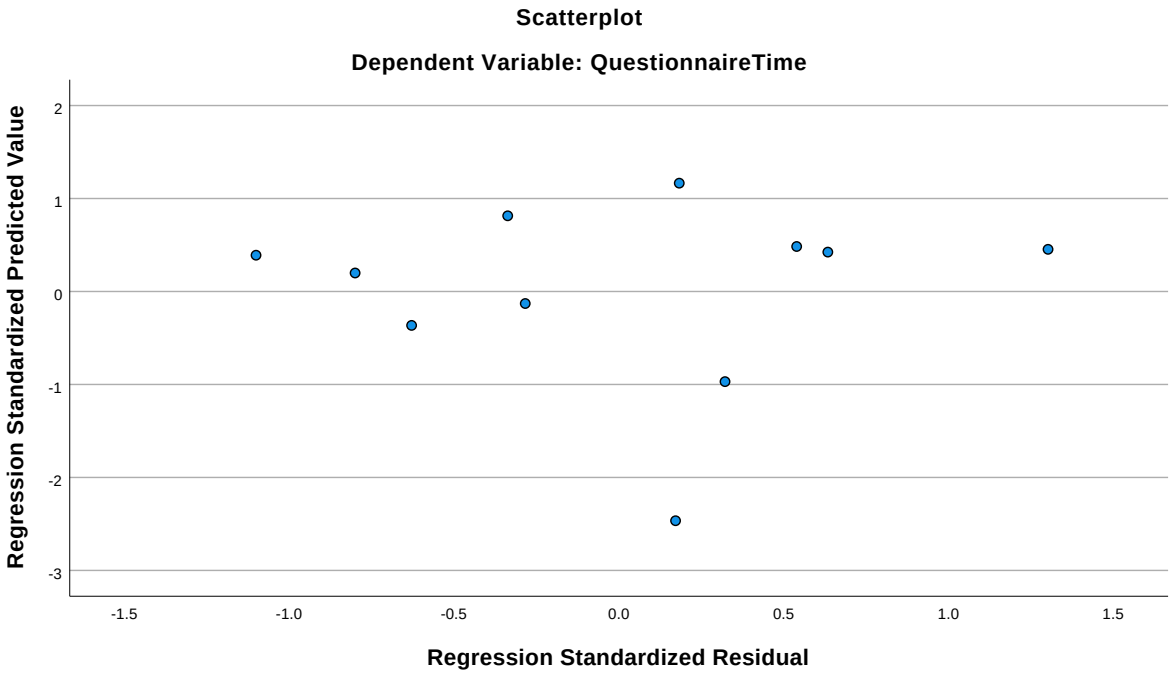

Regression: Time on second attempt determining questionnaire time

Variables Entered/Removed[a]

Model	Variables Entered	Variables Removed	Method
1	SecondTime[b]	.	Enter

a. Dependent Variable: QuestionnaireTime

b. All requested variables entered.

Model Summary[b]

Model	R	R Square	Adjusted R Square	Std. Error of the Estimate
1	.736[a]	.541	.495	40.45138

a. Predictors: (Constant), SecondTime

b. Dependent Variable: QuestionnaireTime

ANOVA[a]

Model		Sum of Squares	df	Mean Square	F	Sig.
1	Regression	19303.529	1	19303.529	11.797	.006[b]
	Residual	16363.138	10	1636.314		
	Total	35666.667	11			

a. Dependent Variable: QuestionnaireTime

b. Predictors: (Constant), SecondTime

Coefficients[a]

Model		Unstandardized Coefficients		Standardized Coefficients		
		B	Std. Error	Beta	t	Sig.
1	(Constant)	336.190	19.318		17.403	.000
	SecondTime	-.375	.109	-.736	-3.435	.006

a. Dependent Variable: QuestionnaireTime

Residuals Statistics[a]

	Minimum	Maximum	Mean	Std. Deviation	N
Predicted Value	161.6698	313.6710	283.3333	41.89112	12
Residual	-51.79447	81.95865	.00000	38.56887	12
Std. Predicted Value	-2.904	.724	.000	1.000	12
Std. Residual	-1.280	2.026	.000	.953	12

a. Dependent Variable: QuestionnaireTime

Charts

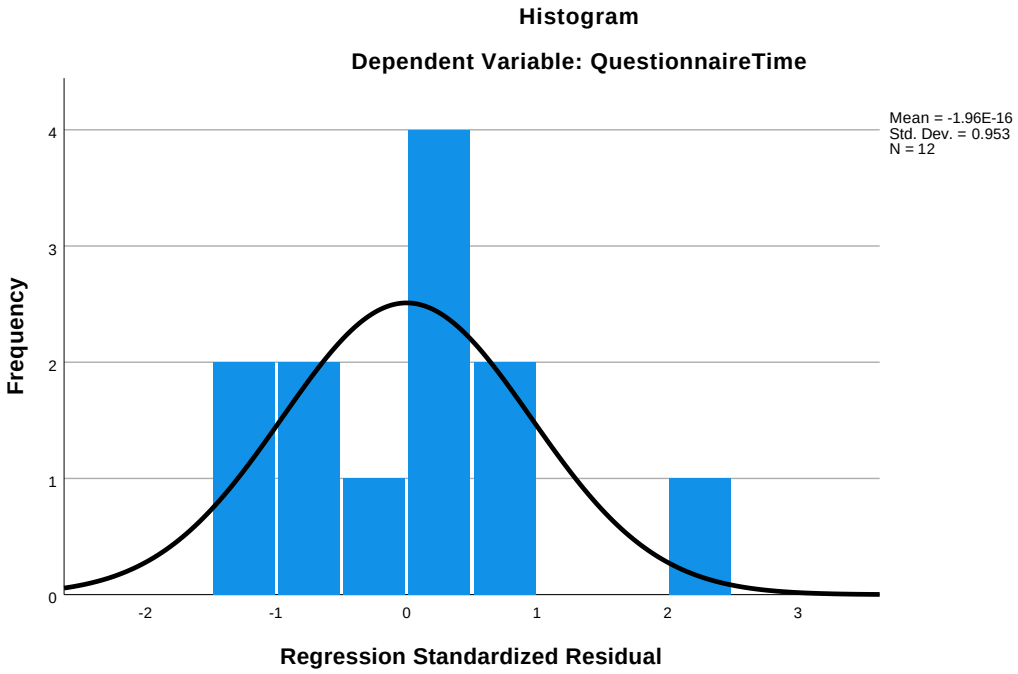

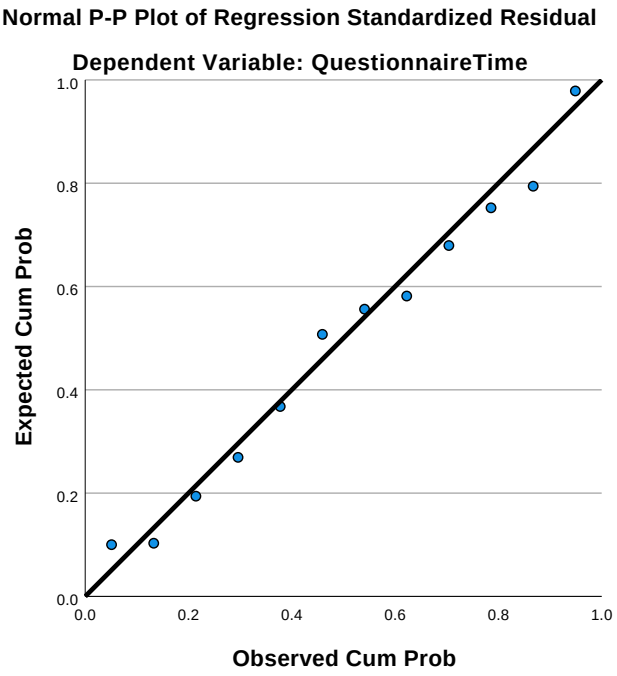
Normal P-P Plot of Regression Standardized Residual
Dependent Variable: QuestionnaireTime
Expected Cum Prob
Observed Cum Prob
0.0
0.2
0.4
0.6
0.8
1.0

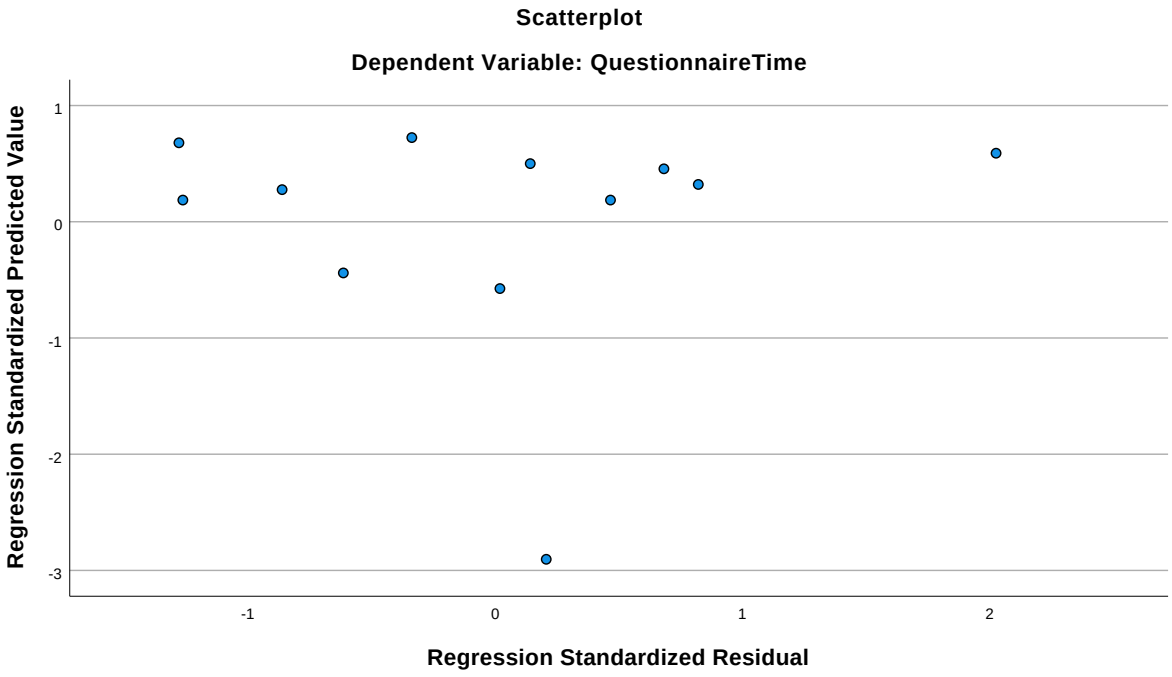
Scatterplot
Dependent Variable: QuestionnaireTime
Regression Standardized Predicted Value
Regression Standardized Residual
1
0
-1
-2
-3
-1
0
1
2

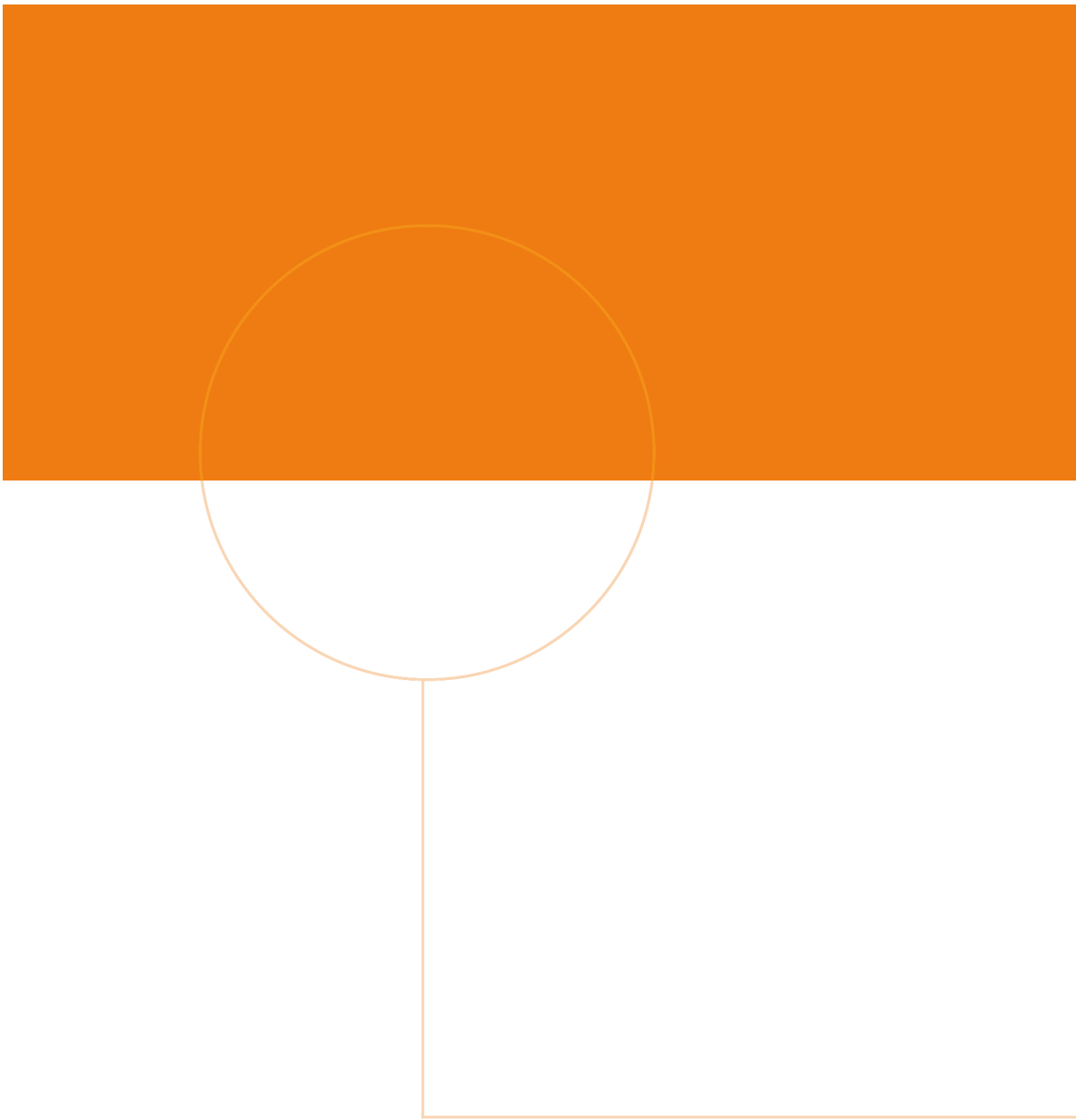

NTNU

Norwegian University of
Science and Technology